Study of Structural and Bonding Properties of Some Mixed Metal Clusters and Beta Zeolite using Density Functional Theory

Thesis submitted to the
University of Pune
for the degree of

Doctor of Philosophy
in
Chemistry

by

Sharankumar G. Shetty

Physical Chemistry Division
National Chemical Laboratory
Pune – 411 008, India.

July 2005

Certificate

Certified that the work done in the thesis

Study of structural and bonding properties of some mixed metal clusters and beta zeolite using density functional theory

submitted by **Sharankumar G. Shetty**, for the degree of Doctor of Philosophy, was carried out by the candidate under our supervision. Any material that has been obtained from other sources has been duly acknowledged in the thesis.

Date

Place

Dr. Sourav Pal
Thesis Supervisor

Prof. D. G. Kanhere
Thesis Co–Supervisor

. . . **to my family**

Acknowledgement

It is my great pleausre to thank my research supervisor, Dr. Sourav Pal for giving me the freedom to think and to express myself. He has been a fantastic advisor, who taught me how to do research and to think independently. I really appreciate his way of imagining things and his good sense of humor. I would especially like to mention the tea discussions, where we argued on the topics from sports to films to the ethics in science. I will always remember his quote, 'to do good science, first you need to be a good human being'.

I owe a special debt to my co–advisor Prof. D. G. Kanhere for introducing me to the field of *ab initio* molecular dynamics. I thank him for tolerating my chemistry, especially the anti–aromaticity concept. It has been really fun to do science under the guidance of Dr. Pal and Prof. Kanhere.

I take this opportunity to thank the Director of NCL for giving me the right place to pursue my research. I would also like to thank the NCL library, where I spent initial days of my research in reading those fascinating books. I also thank the Dept. of Physics for providing me the computational facilities for my research work. I cannot forget the Dept. of Chemistry, where I took my first lessons in the field of research. I acknowledge Prof. Gadre and Dr. Gejji for acquanting me to the field of computational chemistry.

I'm grateful to the Indo–French project for my research funding. I thank Dr. Annick Goursot for the useful discussions and advice on the work of zeolite modelling.

The present thesis work would have been difficult without the association of my labmates in NCL and Dept. of Physics. My thanks goes to Ajitha and Sham, for helping me with the basic quantum mechanics during the initial phase of my research. Special thanks goes to Chandra, Sailaja and Nayana, for making me very comfortable in the group and treating me more as a friend than as a junior. I would miss the delicious South–Indian food cooked by Chandra at many occasions. I thank my immediate juniors Prashant, Sajeev, Akhilesh and the 'most smiling' Sophy, for their help in other compuational techniques. I enjoyed the company of the new group which joined in the last phase of my work, Tuhina, Rahul, Sugata, Arijit, Nilanjan, Subrata and Sandeep. I also had a nice time with Rajshekar.

The same environment I experienced in the Dept. of Physics. First let me thank Chacko for inspiring me to write my thesis in Latex and all the help he made during my stay in the Dept. I thank Mrinal, Kavita, Ajitha and Ajay for the fruitful discussions on the physics related topics. I would like to acknowledge my juniors in the Dept., Lee,

Ghazal and Bhalchandra.

There are many, that from behind the scenes have inspired me and supported my work. My M.Sc. group needs a special acknowledgement with whom I have spent the best days of my life. Vishal is one of them who always stood by my side and encouraged me. I can never forget the moments I spend with Vishal, Selina, Ruchira and KP. I thank Vishwaseel for patiently listening to my science. It is worth mentioning Amita and Neetu, whom I met at IIT, Madras and became friends forever. I find myself fortunate to have friends like Amit, Chaitan and Vicky.

My parents made tremendous sacrifices to ensure that I had good education and freedom to choose my own field. For this and more, I am forever in their debt. I'm indebted to my cousin, Prakash, for his personal help. I also thank my parents–in–laws for their kind support. Vinci, you and Suhanee, have been my inspiration in whatever I have done and acheived till now.

July 2005 S.S.
Pune

Contents

Acronyms **iv**

Abstract **v**

List of Figures **vii**

List of Tables **xi**

1 Introduction **1**

1.1 **General Overview** 2

1.2 **Metal Clusters** 6

1.2.1 What are Metal Clusters?? 7

1.2.2 Homoatomic and Heteroatomic Metal Clusters 9

1.2.3 Experimental Techniques 11

1.2.4 Theory and Simulations 13

1.3 **Zeolites: An Overview** 17

1.3.1 Theoretical Models in Zeolites 21

1.4 Motivation and Purpose 23

1.5 Organization of the Thesis 24

2 Theoretical Methods and Computational Aspects **26**

2.1 The Schrödinger Equation 27

2.1.1 The Born – Oppenheimer Approximation 27

2.2 Density Functional Theory 28
2.2.1 Hohenberg–Kohn Theorems 28
2.2.2 Kohn–Sham Method 29
2.2.3 Plane Wave Basis Set and Periodic Boundary Condition 31
2.2.4 Pseudopotentials 32
2.3 Classical Molecular Dynamics 33
2.4 *Ab Initio* Molecular Dynamics 35
2.4.1 Car Parrinello Molecular Dynamics 35
2.4.2 Born Oppenheimer Molecular Dynamics 36
2.4.3 Comparison of CPMD and BOMD 37
2.4.4 Optimization Techniques 38
2.5 VASP Program 40
2.6 Interpretation of the Data 40
2.6.1 Structure 40
2.6.2 Bonding 41
2.7 Magnetic Ring Currents 43

3 Study of Electronic and Bonding Properties of Mixed Metal Clusters 45
3.1 Introduction 45
3.2 Computational Details 49
3.3 Results and Discussion 50
3.3.1 Structural Properties of Li_nSn 50
3.3.2 Bonding and Energetics of Li_nSn 51
3.3.3 Structural Properties of Al_4X_4 (X=Be, Mg, B, Si) 64
3.3.4 Bonding and Energetics of Al_4X_4 (X=Be, Mg, B, Si) 64
3.4 Conclusion and Scope 72

4 Structure, Bonding and Magnetic Properties of Metallo–anti–aromatic Compounds 73
4.1 Introduction 73

4.2 Computational Details 76
4.3 Results and Discussion 77
4.3.1 Structure and Energetics 77
4.3.2 Bonding 78
4.3.3 Magnetic Properties: Ring Current 83
4.4 Conclusion and Scope 86

5 A Periodic Density Functional Study of Sn Substituted Beta Zeolite 88
5.1 Introduction 88
5.2 Computational Details 92
5.3 Structural Properties 93
5.4 Energetics 95
5.5 Electronic and Bonding Properties 97
5.6 Conclusion and Scope 98

Epilogue 102

References 105

List of Publications 117

Abbreviations	Meaning
AIMD	*ab initio* Molecular Dynamics
BEA	Beta
BOMD	Born Oppenheimer Molecular Dynamics
CC	Coupled Cluster
CCD	Coupled Cluster Doubles
CI	Configuration Interaction
CPMD	Car Parrinello Molecular Dynamics
CTOCD–DZ	Continuous Transformation of Origin of Current Density–Diamagnetic
DFT	Density Functional Theory
ELF	Electron Localization Function
GAMESS	General Atomic Molecular and Electronic Structural System
GGA	Generalized Gradient Approximation
H–F	Hartree–Fock
HK	Hohenberg and Kohn
HOMO	Highest Occupied Molecular Orbital
IR	Infra Red
KS	Kohn Sham
LCAO	Linear Combination of Atomic Orbitals
LDA	Local Density Approximation
LUMO	Lowest Unoccupied Molecular Orbital
MAS	Magic Angle Spin
MC	Monte Carlo
MD	Molecular Dynamics
MOT	Molecular Orbital Theory
MP2	Möller–Plesset Second Order
NMR	Nuclear Magnetic Resonance
OLED	Organic Light Emitting Diodes
PBC	Periodic Boundary Condition
RHF	Restricted Hartree–Fock
UV	Ultra Violet
VASP	Vienna *Ab initio* Simulation Package
VBT	Valence Bond Theory
XRD	X-Ray Diffraction

Abstract of the Thesis

Recent advances in the field of nanotechnology has motivated researchers to understand and to fabricate new materials at the molecular level. The properties of these materials are completely goverened by the arrangement of the atoms at the molecular level. If we rearrange the atoms at the molecular level and allow the system to grow atom by atom, we would be able to design a new material. For e.g. depending upon the arrangement of the atoms in the carbon at the molecular level, we are able to distinguish between the three allotropes of carbon viz. diamond, graphite and fullerene. This has given a new dimension to build new experimental techniques and theoretical models to study these "nano" systems. The most difficult quest, which is still to be resovle, is to find the boundary between the atomic to nano to bulk.

Metal clusters play an important role in understanding the change of the chemical and physical properties as the systems grow from atomic level to a bulk. Hence, it bridges the atomic scale to a bulk scale through a nano scale and thus becomes a part of the nanoscience or nanotechnology. Several works are being carried out in this direction, to interpret the structural, electronic and bonding properties in metal clusters. Although experiments can provide useful information about the properties of clusters, it is very difficult to determine the structure of small atomic clusters by experimental means alone. Thus, theory helps in understanding the critical aspects of metal clusters structure, electronic and bonding properties.

The main goal of the present thesis is to investigate the structural, electronic and bonding properties of two different classes of systems using DFT. The first systems which we study belongs to the class of non–periodic mixed metal clusters such as Li–Sn, AlX, where X = Li, Na, Mg, B, etc. The other class is the crystal phase of a catalysis at the atomic level such as zeolite.

Chapter 1 starts with a brief history of the development of the VBT and MOT. Followed by the discussion on the new applications in the field of metal clusters and zeolites. We discuss the purpose and interest in studying metal clusters. We basically focus on th einteresting aspects such as magic clusters, metallo-anti-aromaticty etc. We describe the experimental and theoretical techniques employed in the study of metal clusters. We give an overview of zeolites nad the motivation behind studying the zeolites. The purpose of using the periodic approach to deal with zeolites is discussed. The chapter ends with the organization of the thesis.

Chapter 2 is devoted on the theoretical development and the computational details used in the present work. Initially we discuss the DFT approach. The details of the

AIMD technique is discussed along with CPMD and BOMD approach. The optimization techniques used in the present work such as simulated annealing and conjugate gradient is discussed. The ELF has been discussed in more detail, since it has been explicitly used.

Chapter 3 deals with the theoretical investigation of Sn doped Li_n ($n \leq 9$) clusters and Al based binary clusters. The study reveals that there is a transition from ionic to a metallic bond through ionic–metallic transition as we go on adding the Li atoms in the Li–Sn cluster. The Al based binary clusters show a different kinds of bonds in different systems for e.g. covalent bonding is observed in Al–Si clusters, a polar covalent bond is seen in Al–B system.

Chapter 4 is one of the most interesting chapter in the thesis. In this chapter for first time we give a theoretical proposition of anti–aromaticity in Al–Li metal clusters. This has been completely proposed on the basis of the basic criteria of anti–aromaticity. This was recently confirmed in an experimental work. We later show that the anti–aromaticity concept can be extended in Al–Na systems also. We have calculated the magntic ring currents in the Al–Li metallo–aromatic and anti–aromatic systems. Surprisingly we found that the magnetic properties do not support the anti–aromaticity criteria.

Chapter 5 is on the theoretical study of the crystalline phase Sn–BEA zeolite. This work has been completely motivated by a recent experimental work on the use of Sn–BEA in Baeyer–Villiger oxidation reaction. We investigate the structural, electronic and bonding properties of all the 9 active T–sites in BEA and show that the most active site for the activation and the reaction is the T1 site.

List of Figures

1.1 C_{60} fullerene 4

1.2 Growth sequence of a homoatomic gas cluster. (a)Microclusters (b)Small and Large clusters. (After H. Haberland, ed., Clusters of Atoms and Molecules, vol. 1, Springer-Verlag, 1994) 8

1.3 The three structural building units of a zeolite. (a)Primary, (b)Secondary and (c)Unit cell. 18

1.4 Extended structure of zeolite (MFI) consisting of several unit cells. . . . 19

1.5 Truncated cluster model from a zeolite. The central atom indicates the T–atom (Ge, Ti, Sn, etc). The dark grey spheres indicate the O atoms and the light grey and the white atoms indicate the Si and O atoms, respectively. 22

2.1 ELF of Methyl Acetate (left) and Benzene (right). (After references [105] and [108]). 43

3.1 Dark sphere represents the Sn atom and the white spheres represent the Li atoms. The equilibrium geometries of Li_nSn (n = 1 to 4). (a)Lowest energy structures. (b) and (c) Higher energy structures. 52

3.2 Dark sphere represents the Sn atom and the white spheres represent the Li atoms. The equilibrium geometries of Li_nSn (n = 5 to 7). (a)Lowest energy structures. (b) and (c) Higher energy structures. 53

3.3 Dark sphere represents the Sn atom and the white spheres represent the Li atoms. The equilibrium geometries of Li_nSn (n = 8 and 9). (a)Lowest energy structures. (b) Higher energy structures. 54

3.4 Dark spheres represent the Li atoms and the white spheres represent the Sn atom. Charge densities and ELF isosurfaces of Li_nSn (n = 1 to 4) First column: The charge density isosurfaces of LiSn(a) to Li_4Sn (m) at 1/3 of the maximum value. Second column: The ELF at 0.65 isosurface value of LiSn (b) to Li_4Sn (n). Third column: The ELF at 0.75 isosurface value of LiSn (c) to Li_4Sn (o). Fourth column: The ELF at 0.85 isosurface value of LiSn (d) to Li_4Sn (p). 57

3.5 HOMO isosurfaces of Li_4Sn and Li_5Sn clusters. (a), (b), (c) represent HOMO, HOMO–1, HOMO–2 of Li_4Sn, respectively. (d) and (e) represent HOMO, HOMO–1 of Li_5Sn, respectively. Dark sphere represents Li atoms and shaded atoms represent Sn atom. 58

3.6 Dark spheres represent the Li atoms and the white spheres represent the Sn atoms. Charge densities and ELF isosurfaces of Li_nSn (n = 5 to 7) First column: The charge density isosurfaces of Li_5Sn(a) to Li_7Sn (i) at 1/3 of the maximum value. Second column: The ELF at 0.65 isosurface value of Li_5Sn (b) to Li_7Sn (j). Third column: The ELF at 0.75 isosurface value of Li_5Sn (c) to Li_7Sn (k). Fourth column: The ELF at 0.85 isosurface value of Li_5Sn(d) to Li_7Sn (l). 59

3.7 Dark spheres represent the Li atoms and the white spheres represent the Sn atoms. Charge densities and ELF isosurfaces of Li_8Sn and Li_9Sn. First column: The charge density isosurfaces of Li_8Sn(a) and Li_9Sn (e) at 1/3 of the maximum value. Second column: The ELF at 0.65 isosurface value of Li_8Sn (b) and Li_9Sn (f). Third column: The ELF at 0.75 isosurface value of Li_8Sn (c) and Li_9Sn (g). Fourth column: The ELF at 0.85 isosurface value of Li_8Sn (d) and Li_9Sn (h). 60

3.8 HOMO isosurfaces of Li_7Sn and Li_9Sn clusters. (a), (b) represent HOMO, HOMO–1 of Li_7Sn, respectively. (c) and (d) represent HOMO, HOMO–1 of Li_9Sn, respectively. Dark sphere represents Li atoms and shaded atoms represent Sn atom. 63

3.9 Dark spheres represent the Al atoms and the white spheres represent the X (Be, Mg) atoms. The equilibrium geometries of Al_4X_4 (X = Be, Mg). (a) Lowest energy structures. (b) Higher energy structures. 65

3.10 Dark spheres represent the Al atoms and the white spheres represent the X (B, Si) atoms. The equilibrium geometries of Al_4X_4 (X = B, Si). (a) Lowest energy structures. (b) Higher energy structures. 66

3.11 Black spheres represent the Al atoms, while white spheres represent the X (Be, Mg) atoms. Charge densities and ELF isosurfaces of Al_4Be_4 and Al_4Mg_4 clusters. (a) Charge density isosurface at one third of its maximum isosurface value. (b) ELF at 0.85. (c) ELF at 0.83. (d) ELF at 0.78. (e) ELF at 0.76. (f) Charge density isosurface at 1/3 rd of its maximum isosurface value. (g) ELF at 0.78. (h) ELF at 0.77. (i) ELF at 0.77 at a different orientation. (j) ELF at 0.7. 68

3.12 Black spheres represent the Al atoms and the white spheres represent the Li atoms. Charge densities at 1/3 rd of their maximum isosurface values and ELF isosurfaces of Al4B4 and Al4Si4 cluster. (a) Charge density isosurface of Al_4B_4. ELF of Al_4B_4 are as follows: (b) ELF at 0.75. (c) ELF at 0.73. (d) ELF at 0.72. (e) ELF at 0.69. (f) Charge density isosurface. ELF of Al_4Si_4 are as follows: (g) ELF at 0.8. (h) ELF a 0.72. (i) ELF at 0.65. (j) ELF at 0.62 at a different orientation. 69

3.13 HOMO isosurfaces of Al_4Be_4 and Al_4Si_4 clusters. (a), (b) represent HOMO, HOMO–1 of Al_4Be_4, respectively. (c) and (d) represent HOMO, HOMO–1 of Al_4Si_4, respectively. Dark sphere represents Al atoms and shaded atoms represent X (Be, Si) atoms. 70

4.1 Ground state structure of (a)Al_4Li_4, (b)Al_4Na_4 and excited state structure of (c) Al_4Na_4. Ground state structure of (d)$Al_4Na_3^-$: Black spheres indicate the Al atoms and the white spheres indicate the X (Li and Na) atoms 77

4.2 Charge density, HOMO isodensities of Al_4Li_4. (a) Charge density, (b) HOMO, (c) HOMO–1, (d) HOMO–2, (e) HOMO–3 and (f) HOMO–4 : Black spheres indicate the Al atoms and the white spheres indicate the Li atoms. 80

4.3 Charge density, HOMO isodensities of Al_4Na_4. (a) Charge density, (b) HOMO, (c) HOMO–1, (d) HOMO–2, (e) HOMO–3 and (f) HOMO–4 : Black spheres indicate the Al atoms and the white spheres indicate the Na atoms. 81

4.4 The total induced current density, and the orbital contributions to the current density for Li_3Al_4 C_s , plotted at different heights above the Al_4 square. 85

4.5 The total induced current density, and the orbital contributions to the current density for Li_4Al_4 C_{2h}, plotted at different heights above the Al_4 square. 86

5.1 Unit cell of BEA consisting of 192 atoms. The 9 active sites are shown by the Sn atoms (orange spheres). The other are the Si (brown spheres) and the O (red spheres) atoms. 94

5.2 LUMO isodensity of Si–BEA. Blue and red spheres indicate the Si and O atoms, respectively. 99

5.3 LUMO isodensity of Sn–BEA. Blue sphere indicate the Sn atom, while red and green spheres indicate the Si and O atoms. 100

List of Tables

3.1 Calculated Binding energy (B.E.) and the HOMO–LUMO gap of Li_nSn ($n \leq 9$) are presented 61

3.2 Calculated Binding energy (B.E.) and the HOMO-LUMO gap of Al_4X_4 (X = Be, Mg, B, Si) are presented 67

4.1 The Al-Al bond lengths of the Al_4 unit of the optimized ground state of Al_4Li_4, Al_4Na_4, $Al_4Na_3^-$ clusters 78

4.2 The Energies and the Difference between the HOMO and the LUMO for Ground and Excited States of the Al_4Li_4 and Al_4Na_4 Cluster and the Ground State of the $Al_4Na_3^-$ Cluster obtained through Coupled-Cluster Calculations 78

5.1 Average Bond lengths (Å) and bond angles of Sn-O and Sn-O-Si and the next nearest neighbor Sn-Si distance (Å) of the optimized structures for the 9 different T-sites in Sn-BEA. 95

5.2 Cohesive energies, HOMO, energies the LUMO energies and the HOMO-LUMO gap of the 9 different T-sites 97

Chapter 1

Introduction

It does not matter how beautiful your theory is, it does not matter how smart you are. If it does not agree with experiment, it's wrong.
.....Richard Feynman

An understanding of the molecular structure, electronic properties and the nature of chemical bond is central to all fields of molecular sciences. The properties of a substance depend upon the type of bonds between the atoms of the substance and the atomic arrangement. The ways in which atoms are arranged in a material are determined primarily by the strength and directionality of the inter–atomic bonds. Qualitatively, we can understand why an atomic bond is strong or weak, localized or delocalized from the knowledge of the energies and the location of the bonding electrons with respect to the positively charged ion cores. The type of bond plays especially an important role in determining the configuration of molecules, clusters and crystals. Most of the qualitative and quantitative aspects, currently used to describe the nature of chemical bonds and its relation to the chemical structure, emerged in the earliest days of quantum mechanics. Indeed, one of the first succesful model to account the chemical bonding was proposed by G. N. Lewis in 1916. [1] He suggested two main types of bonds *viz.* ionic and covalent. The driving force for bond formation was identified as the pairing of electrons between atoms so as to attain a stable octet. The idea of electron pairing had an important influence on the earlier successful theories of the chemical structure and bonding.

1.1 General Overview

The first qunatum mechanical description of the electron pair bond was that given by Hietler and London for the hydrogen molecule in 1927. [2] This theory was further developed by Pauling and others in the 1930's, into a comprehensive theory of bonding called VBT. [3]–[6] This revolutionized the field of chemistry, encompassing all chemical structures from hydrogen molecule to DNA and to solids. In VBT the wavefunction is constructed in such a way that the two electrons can never be found on the same atom and hence their motion is correlated. Important chemical concepts of valence electrons such as resonance, octet rule and hybridization were first formulated as a part of VBT. However, in VBT the atomic orbitals are not orthogonal and hence the theory becomes more complicated as the number of atoms in the molecule increases. Moreover, Heitler and London wavefunction does not correspond to the virial theorem and is a poor approximation to the true wavefunction of the system. [4] Parallel with the development of VBT, a second type of qunatum mechanical approach, the MOT was developed. MOT is based on the concept of LCAO, which involves the assignment of electrons to molecular orbital, which are in general delocalized over the whole molecule and are uncorrelated, unlike the electrons in VBT. Most of the problems of VBT, such as the virial theorem, excited states, orthogonality, etc. were solved by MOT in a much simpler form. Nevertheless, due to the localized electrons, VBT becomes more useful in describing reactions and bond dissocitaion. [7] One can say that, VBT and MOT are two different but complementary models of the same phenomenon. However, nowadays most of the calculations are performed by MOT on account of its simplistic mathematical approach. Some of the theoretical models such as, H–F, CI, DFT, CC, etc., based on MOT, have been successfully applied to study the electronic properties of systems containing few electrons. [8] Along with this, the development of the present-day computer technology has made possible to apply the theory with ever greater accuracy to carry–out the simulations of more complex chemical systems. Hence, the results of the simulations are of great help to guide the experimental work. Among the theoretical

methods, DFT has emerged as one of the most successful method to investigate large systems. [9] In DFT, the electron density is the basic variable instead of the wave–function. This makes it computationally much more cheaper than the conventional *ab initio* methods, while retaining much of their accuracy. This feature is also a strong motivation to adopt DFT as a theoretical tool to study large molecules or clusters or even periodic solids.

The main aim of the present thesis is to apply the DFT to investigate the properties of two different classes of chemical systems. One of the aspects is to use a combined, DFT and MD approach basically known as AIMD, to study the structural and bonding properties of mixed metal clusters. The other aspect, is to deal with the structural and electronic properties of Sn-BEA zeolite in a crystalline phase by DFT with PBC.

In recent years, success of nanotechnology has made cluster science more interesting because large cluster sizes can eventually bridge with the nanosize materials in a more comprehensible way. [11, 12, 14, 15] Secondly, with the advent of new experimental techniques, it has now become possible to produce and analyze clusters consisting of several hundred atoms while the lower limit for the size of nanoscale particles has reached less than 1 nm. Experiments have demonstrated that the properties of clusters depend uniquley on their size and composition and that they evolve differently. [14] This aspect has made researchers to use clusters as building blocks for new materials. One of the most well–known 'new' clusters or nanostructures, belonging to the carbon family are the so called fullerenes, (Fig. 1.1) discovered in 1985 , which are symmetrical hollow carbon structures. [16] This discovery gave birth to a new field of carbon nanotubes and a new perspective to the study of cluster science. [17, 18] The exciting discovery of superconductivity at high temperature was acheived by doping K, Rb, Cs in C_{60} fullerenes. [19, 20] Other attempts of encapsulating atoms and molecules in C_{60} had been succesfully carried out. Moreover, clusters have been shown to have technological importance in catalysis, photographic films, magnetic recordings, etc. There are many

Fig. 1.1: C_{60} fullerene

different types of clusters, such as metallic clusters, molecular clusters, organic clusters, quantum dots, which all have their own features and properties.

Metal clusters are among the more complex and interesting ones from both, fundamental and technological points of view. Indeed, metal clusters provide a bridge between the limits of isolated atoms and bulk metal, and so much interest has focussed on the evolution of properties with size, particularly those, such as structural, electronic, magnetic and optical properties. [11, 14, 15] As the dimension of the metal clusters goes on decreasing quantum effects becomes much more prominent and affect the behavior of e.g. the B. E., ionization potentials, polarizabilities, optical spectra, etc. [21]–[23] Such changes in the electronic structure can affect the bonding and other physical and chemical properties of metal clusters. With the advance of computational power, in the last few years, it has been possible to apply the theory to larger clusters. Since the clusters do not have the periodicity as in crystals, the same theoretical tools that are used to study molecules in gas phase can be used to study them.

Lithium and sodium clusters are among the examples of metal clusters, which have been extensively studied in the last decade by experimental and theoretical methods. [21, 24, 25] The reason for this is obviously the less computational effort. However, recently Li has been very important in the applications of Li batteries. [26] It has been found

that some of the metal clusters are more abundant than the others due to exceptional stability as reflected in the mass spectra. These kinds of metal clusters have been referred to as 'magic' clusters. [12, 13] This was analogous to the shell filling in atoms and nuclei and the stability of these particular metal clusters was explained on the basis of electron shell filling. These kind of metal clusters were first observed in the mass spectra of Na. Pure boron is a large band-gap semiconductor. The allotropes of boron have been characterized on the different arrangment of the B_{12} icosahedra. Hence, one might be interested in the properties of boron clusters leading to different structural arrangement. Although, boron and carbon are neighbors in the periodic table, they vastly differ in their properties. Nevertheless, many studies have been carried out to show many chemical similarities between them. Recently Boron has been shown to form nanostructures similar to that of carbon nanostructures. [27, 28] Boron clusters have been widely studied by Hanley and Anderson. [27, 29] The other member belonging to the boron family is the Al. The important issue in the Al is that, unlike the alkali clusters the shell model does not hold for small Al clusters. Extensive experimental and theoretical studies have been focused on Al clusters to understand their electronic and structural properties. [30, 31] Al_7^+ and Al_{14}^+ appear as magic clusters in some mass spectra of Al clusters. Cox *et al* have investigated the reactions of neutral aluminum clusters with a number of different molecules. [32] Jarrold *et al* have measured the activation barrier of the adsorption of D_2 on the Al clusters. [33] It is believed that the transition metal atoms form the most reactive clusters, this is due to their unfilled d–orbitals, resulting in high coordination number. [23] The other way in which the metal clusters differ from their bulk is when they are alloyed. A single impurity in a metal cluster can create a drastic change in electronic and bonding properties. There are several reviews in which the stoichiometry of the different atoms have been related to the change in the chemical properties of the mixed metal clusters. [21, 34] Recently, Li *et al* showed that Al behaves as C of benzene in some Al-Li mixed clusters. [35]

The novelty of cluster physics has also been expanded in the field of catalysis such

as zeolites. [36] Zeolite is a crystalline material composed of Si, Al and O atoms. They have a wide range of industrial applications. Since they form pores and channels, they have been used as molecular sieves, ion exchangers and catalysts. [37] Zeolites have a long history of 100 years and still have been an active field of reserach. A full review of all applications in the area of zeolite is outside the scope of this thesis. [38] However, a more detailed description of the uses of zeolites studies are given in the next sections.

Small and large clusters, truncated out of the crystal structure of zeolites, have been used as models to study the role of the active sites and reaction mechanisms of certain organic molecules within the zeolites. [36] It is still difficult to use the conventional *ab initio* methods to investigate the properties of catalysis in solid state. Relatively cheap cluster calculations can give reasonably accurate results especially for bond lengths. However, it has been debated that the cluster does not account for the long–range interactions as in a crystal and hence the cluster approximation would not be a realistic approximation. [39] In these cases, for theoretical calculations, it is usually advised to adapt PBC within the quantum mechanical framework for e.g. periodic H–F or Periodic DFT. [40, 41] These theories account for the long–range interactions and treat the active sites within the zeolites in a much more accurate way. Therefore, in the present thesis, we have explicitly used periodic DFT to treat the zeolite problem rather than the zeolite cluster approach.

1.2 Metal Clusters

One of the fundamental goals of nanotechnology is to understand and characterize the properties at the atomic–scale. The study of metal clusters enables us to interpret such fundamental aspects and to explain the behavior of the nanoscale systems as their sizes and compositions are changed atom by atom.

1.2.1 What are Metal Clusters??

Clusters are aggregates of atoms or molecules, intermediate in size between individual atom and bulk. Clusters are different from both molecules and solids, and for this reason can have very different properties. Molecules are characterized by having definite and unique structure and specific composition. On the other hand clusters may be composed of any number of particles and have a tendency to grow. As the number of particles of the cluster becomes larger, the number of locally stable structures (isomers) of the cluster grows rapidly. Some fundamental questions which can be raised about the clusters are, for e.g. (1) how does the physical property of a cluster change as the size of the cluster is evolved ?; (2) When does a transition from atomistic scale to a bulk scale take place ?; (3) Does the stability of the cluster increase monotonically with the size ?; (4) Does the cluster property suddenly change when it is doped with an impurity ? For the last few years, an extensive experimental and theoretical research has been carried out to answer the above questions. The most inetersting are the metal clusters where the transition from a localized (covalent or ionic) to a delocalized (metallic like) bonding occurs as the size of the cluster increases. [11, 12, 14] Growth sequence of a neutral gas cluster is shown in Fig. 1.2. Metal clusters are therefore expected to exhibit many unusual and interesting properties that are distinct from those of discrete molecules or extended solids. Structure and stability are the most important properties of the metal clusters, which can be correlated with the type of atom–atom bonds formed in the metal cluster. In general there are four types of bonds which can be distinguished within the metal clusters *viz.* covalent, ionic, metallic and van der Waal. [14]

Among these clusters, covalent and ionic clusters are supposed to be the most stable clusters due to strong interatomic bonds.

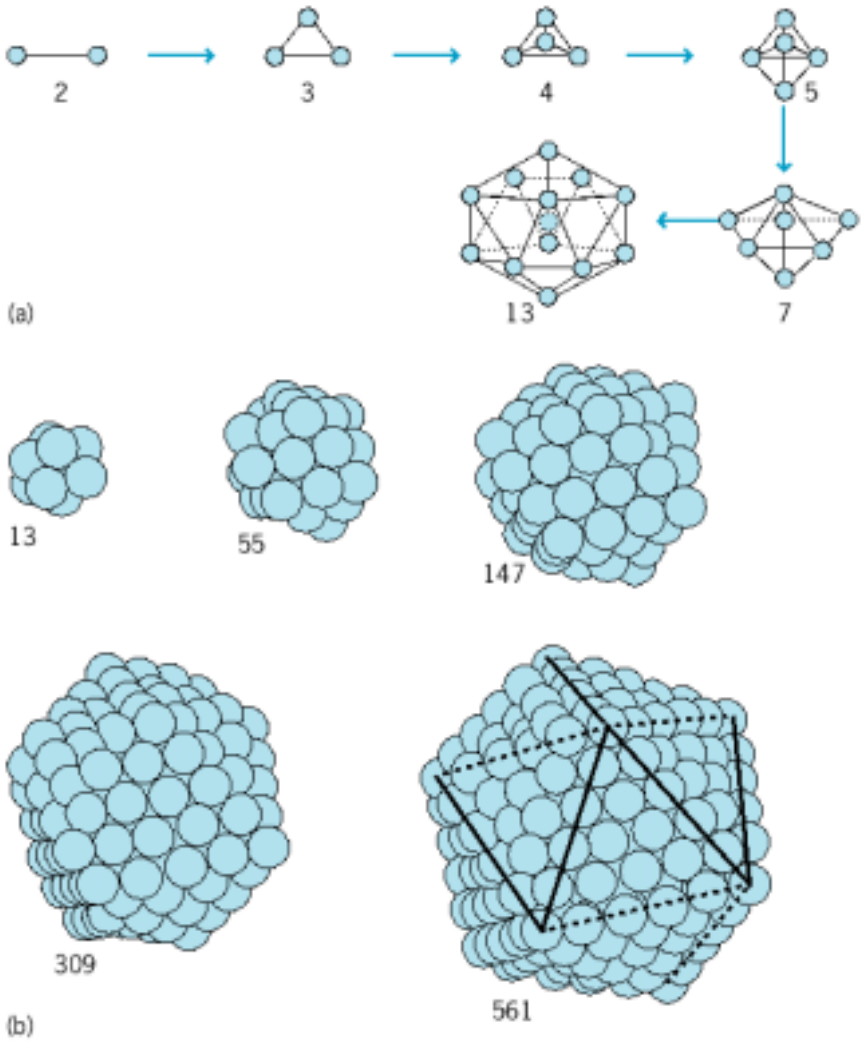

Fig. 1.2: Growth sequence of a homoatomic gas cluster. (a)Microclusters (b)Small and Large clusters. (After H. Haberland, ed., Clusters of Atoms and Molecules, vol. 1, Springer-Verlag, 1994)

1.2.2 Homoatomic and Heteroatomic Metal Clusters

Metal clusters can be classified as homoatomic and heteroatomic (or mixed) clusters according to their composition *i.e.* homoatomic metal clusters contain same type of atomic species, on the otherhand heteroatomic clusters are made up of different type of atomic species. Extensive theoretical and experimental studies have been carried out on the structural and electronic properties of homoatomic metal clusters such as Li, Na, K, Al, Sn etc. [21, 42] Generally, the bonding in homoatomic clusters containing less than 10 atoms can be characterized as covalent. Thus, in these clusters the possibility of isomerization at a relatively low temperature is expected to be less. However, as the number of atoms increases, the delocalization of electrons within the cluster grows eventually, converting it into a metallic like behavior. It is worth mentioning that the delocalization occuring in the homoatomic covalent clusters such as carbon, resulting into graphite, is different from the delocalization due to metallic bonding in metals (Group Ia and IIb). The delocalization in the graphite is more directional than the delocalization in the Li or Na bulk. Among the elements of group 13, less work has been carried out on Ga, In and Th clusters. [44] Relatively, more detailed study has been done on Al and B clusters. [29, 31, 33] Some of the homoatomic metal clusters that have been studied are Be, Mg, Al, Sn, Si and transition metals. [14, 22, 23, 43] In the last decade, similar investigations have been extended to study the heteroatomic clusters, but comparatively to a lesser extent than the homoatomic metal clusters. One of the reasons for this would be the complexity produced by the additional interactions of the unlike atoms (heterointeractions) within the heteroatomic clusters. Due to this reason, heteroatomic clusters are shown to have interesting properties. In small clusters, even a single impurity is expected to influence the structural and electronic properties. For example, an unstable homoatomic metal cluster can be converted to a stable 'magic' cluster by doping with a single impurity. [45, 46, 47] Zhao *et al* have recently studied carbon doped aluminium clusters using mass spectrometric and ab initio methods. [47] They showed Al_7C^- cluster to be magic with extremely high stability. Kumar and

Sundararajan have shown that the substitutional doping of Al_{13} cluster by a tetravalent atom leads to a more stable cluster. [48] Joshi *et al* have studied the structural and electronic properties of Sn doped Li_n clusters using AIMD simulations. [49]

Binary clusters such as A_xB_y also belong to the class of mixed clusters. Different kinds of alloys can be formed by changing the proportion of A and B of these binary clusters. [34, 50] Changing the stoichiometry of different kinds of atoms provides another interesting way of improving the reactivity and selectivity of clusters possibly in the context of catalysis. Bonačić-Koutecký *et al* have discussed the structural stability and ionization potential of some Ia-IIa mixed metal binary clusters. [21] Chacko *et al* have worked on some Al_4X_4 mixed clusters where (X=Li, Na, K, Be, Mg, B and Si). [51] Recently, in some interesting works, aluminum based alkali clusters were shown to exhibit aromaticity properties. [35] The other interesting works on mixed–metal clusters are on GaAs, AlAs, [52], AuIn [53] .

Metallo-aromatic and metallo-anti-aromatic compounds

Aromaticity and anti–aromaticity are among the most historically important properties exhibited by the organic compounds. [54] The criteria to define aromatictiy in the organic molecules are as follows: (1) The system should have a cyclic π conjugation. (2) The system should be planar. (3) The system has a special stabilisation due to the π electron delocalization. (4) It should follow the Hückel's (4n+2) π–electron rule. (5) The system is mostly unreactive and its ground state is a singlet state. (6) It has a diamagnetic ring current. On the other hand, the anti–aromatictity is said to exist, if the system has following properties: (1) The system is unstable due to the π electron delocalization (2) It is planar (3) The system should have 4n π electrons (4) The system in its ground state has alternate single and double bonds in a cyclic conjugation. (5) It is highly reactive and has a triplet state. (6) It has a paramagnetic ring current The cyclic conjugation in these compounds allows an external magnetic field to create a ring current which in turn induces a magnetic field. The aromatic and the anti–

aromatic compounds show diamagnetic and paramagnetic ring currents, respectively. This has motivated researchers to study the magnetic properties in these systems. Benzene and cyclobutadiene are the prototypical molecules to study the aromaticity and anti–aromaticity in organic compounds. [54, 55] In recent years studies have been carried out to show the existence of aromaticity in the organometallic compounds.. [56] Recently, in a combined experimental and theoretical work, Li *et al* [35] for the first time showed the existence of aromaticity in XAl_4^- (where, X=Li, Na, Cu) clusters.

This work motivated researchers to investigate the magnetic properties in these metal clusters using the ring current maps. Interestingly, Fowler *et al* showed that the current density induced by the external magnetic field supports a diamagnetic ring current in the Al_4^{2-} species of XAl_4^- cluster where, X=Li, Na and Cu. [57] This diamagnetic ring current was shown to arise from the σ electron delocalization rather than the π electron delocalization, as seen in benzene molecule. Surprisingly, a mixed dimagnetic and a paramagnetic ring currents were observed and hence the total current was seen to be zero. The work on the metallo-aromaticity and anti-aromaticity would give a new insight into the field of metal clusters.

1.2.3 Experimental Techniques

Cluster production is one of the most important steps in cluster studies. To produce them, one can either aggregate the particles or break them directly from a solid or in liquid. These can be produced in the form of colloidal particles. Mostly, the studies have been focused on the formation of clusters in the gaseous phase by using cluster sources. One of the most popular sources to produce metal cluster is the supersonic jet. In these sources the clusters are formed by condensation of an expanding gas of atoms. A highly compressed gas (P $\sim$ 10 bar) of the material whose clusters are to be aggregated is allowed to expand through a small nozzle (0.03 to 1 mm). As a consequence of this adiabatic expansion, thermal motion of this expanding gas slows down, resulting in a succesive aggregation of the atoms in the cluster. The other two sources to produce

clusters are the gas aggregation and the surface source. In gas aggregation source, the atoms are injected on the rare gas and are slowed down by the collision with the rare gas atoms, ultimately forming atomic clusters. However, in laser vaporization technique the clusters are produced from a surface of a solid material by particle or photon impact or by a high electric field. Smalley and coworkers were the first to combine a laser ablation method and a supersonic beam. In this source, metal vapor is produced by the pulsed-laser ablation of a rod of the material to be investigated. This source can be considered as the hybrid of the supersonic jet and the gas aggregation source. [58]

Once these clusters are formed, these can be further differentiated as unsupported (free) clusters produced in molecular beams or special ion traps and supported (trapped in a matrix) clusters. Free clusters are isolated and are easy to study than the supported clusters, since in the latter case we have to account the cluster-matrix interaction. On the other hand it is difficult to produce large sized free clusters, unlike the supported clusters and it is hard to study the structural properties of free clusters. Charged clusters are easy to sort by electrostatic or time-of-flight mass spectra to yield a beam of free clusters. This is the reason the charged clusters are studied more thoroughly than the neutral clusters. [58] Recently, structures of silver and gold cluster ions have been studied by collision cross section. [59] All known spectroscopic techniques such as optical, [60] infrared, photoelectron, [58] have been applied to study the poperties of clusters. Photodetachement and photodissociation techniques have allowed us to gain insight into the electronic properties of charged clusters. Jarrold *et al*, have investigated the photodissociation of aluminum cluster ions. [62] The first attempt to measure the ionization energies of aluminium clusters by laser vaporization was by Cox *et al.* [32] In photoionization experiments, it it is important that the temperature of the clusters should be less, since the the photoionization threshold will be shifted to lower energy and the ionization energies would be affected. They showed that the smaller cluster ions (n < 8) dissociate to give Al_n^+ and the larger ones (n > 13) give Al_{n-1}^+. [62] Information on the structural and bonding properties can be obtained through vibrational spectroscopy.

Very recently, Fielicke *et al* used far-infrared spectroscopy to determine the structures of cationic vanadium clusters containing 6 to 23 atoms. [63]

Magic clusters

During the study of the structural properties of metal clusters, it has been found that some clusters have unusual stability than others and were termed to be 'magic clusters'. The stability of these magic clusters was analogous to the stability seen in atoms and nuclei due to shell closing. Magic clusters show significant peaks in the mass spectra and are easily distinguishable via mass spectrometry techniques. Knight *et al* used a mass spectra of the alkali clusters to show that the most stable clusters consist of 2, 8, 20, 40,... atoms, which interestingly coincides with the magic numbers observed in nuclei with 2, 8, 20, 40,... nucleons. [24] Magic numbers are different for different clusters and depend on the electronic structure and the geometry of the cluster. The interactions between the rare gas atoms is of van der Waal's type and hence the stability of the magic clusters in these systems is due to the atomic packing and atomic shell closure. These clusters correspond to an icosahedral geometry. However, in simple alkali or alkaline earth metals the atoms interact more strongly and hence the formation of magic clusters is due to the electronic shell closure. [24, 62, 31, 64]

1.2.4 Theory and Simulations

In section 1.2.3, we focused on the experimental methods used to study the metal clusters. In what follows, we will discuss the role of theory and simulations in the field of metal clusters. In the last two decades, computational cluster science has become a rapidly expanding field of study, as theoretical techniques have advanced and computational power has increased. This has led to novel way of doing science that combines both theory and experiments, namely computer simulations. The finite number of atoms considered in the metal clusters makes these systems ideal for theoretical studies. They can also help and guide the experimental work.

Classical and Other Approximate Approaches

Theoretical approaches developed for studying the molecules and now used in the cluster science are based on either first principle approaches, such as the H–F approximation, CI and DFT or other pproximate (eg. jellium, tight binding), methods based on the classical equation of motion called MD and statistical sampling methods called MC methods.

In order to study a system, one must have a knowledge of the interaction of potential within that system. Once the potential in the system is defined, one can search for the stable configurations of that system on the potential energy surface. Clusters do not possess translational symmetry and hence the number of degrees of freedom of a cluster scales linearly with the cluster size and the number of minima on the potential energy surface scales exponentially. Many techniques, such as simulated annealing, conjugate gradient, Newton-Raphson have been employed for searching the potential energy surface to find the lowest energy configuration. Simulated annealing technique begins by heating the cluster at a very high temperature and then cooling or quenching it slowly, hence probing the thermally accesible regions of the phase space. [65] This technique also helps in studying the melting of clusters. Simulated annealing is carried out by using two kinds of simulations which have dominated the research on thermodynamical/statistical ideas and concepts such as temperature, equipartition, phase transition, [66] conformational search of clusters. [67] Some have been on the statistical approach carried out by MC methods and others by MD, which is simply a succesive solution of the equations of motion from an assumed potential of interaction among the particles. These simulations are carried out in a microcanonical ensemble (constant energy) or in a canonical ensemble (constant temperature). [68] The canonical ensemble, introduced by Nosé and Hoover, allows the system to interact with a heat bath represented by an additional degree of freedom in the system. The kinetic energy is allowed to flow dynamically from the heat bath to the system and back. Thousands of atoms can be simulated if one uses a simple classical pair potentials such as Lennard–Jones

potential, Morse potential, Buckingham potential etc. [68] Pair potential accounts only for the interactions between a pair of atoms and the functional form of the potential depends on the interatomic separation. However, these classical potentials fail to consider the nature of bonding and also the aspects like the forming and making of bonds during a reaction, which arise due to the quantum mechanical effects. These failings of pair potentials have led to the development of potentials for metals where the local environment of an atom is incorporated into the potential through many body effects to produce a more faithful description of the interatomic interactions.

Jellium model is one of the simplest and widely used theoretical model to study the electronic properties of metal clusters. It is simple enough to be applied to spherical metal clusters ranging upto few thousand atoms. Jellium model completely ignores the ionic core structure and replaces it by an uniform positive charge as being smeared out over the entire volume of the cluster, while the valence electrons are free to move within this homogeneously distributed positively charged background. The electronic energies are calculated self-consistently to obtain the energy levels. [12, 14, 69] This approach is thus particularly suitable for systems with rather delocalized valence electrons such as bulk metal. According to the jellium model clusters with closed electronic shells have the spherical shapes, while clusters with partially filled or opened electron shells are deformed. Hence, the background of the jellium model can be modified according to the shape of the cluster. The initial work by Ekardt have succesfully shown that the jellium model can account for the experimentally observed properties. [70] A number of characteristic properties of metal clusters such as static polarizabilities, collective electronic excitations (plasmons), ionization potentials as well as the so called 'magic numbers' can be explained in terms of jellium model and its extensions. [69, 70]

The limitation of using the jellium model is obvious since it neglects the ionic perturbation. It fails to understand the properties of covalent and ionic solids, where the electrons are localized in the bonding region. Thus jellium model has a limited range of applications which include the group Ia metals, alkaline earth metals and to

some extent the transition metals. Nevertheless, the model cannot compete with the conventional *ab initio* quantum chemical methods to study the properties of less than 20 atoms cluster. For the detailed study of the jellium model and its applications, we refer the reader to the reviews independently by Brack [71] and W. de Heer [22] .

*A*b initio methods

Classical and semiclassical approaches have been widely succesful in cluster research to evaluate the structural properties and stability of large clusters. However, these methods are not based on quantum mechanical methods, little information about the electronic structure can be obtained. In particularly electronic properties such as polarizabilities, optical spectra and ionization potentials of small clusters are less accurately described by the semiclassical models. More importantly, the hybridization taking place within the atoms cannot be explained on the grounds of classical and semiclassical theories. The most widely used *ab initio* method to calculate the ground state properties are the H–F and DFT. The post–H–F method such as CI, CC have been used to calculate the excited state properties of metal clusters. [21] In a series of papers the electronic structure of the clusters composed of Ia–group metal atoms and of only one IIa–group atom have been investigated at the *ab initio* level. [72] Other studies on mixed metal clusters have also been carried out at the *ab initio* levels. [73]

In the last decade combined approach of DFT and MD has been employed to study the ground state and dynamical properties of metal clusters. [74, 75, 76] In this approach the electronic potential derived from the DFT is combined with the classical MD equation, during the motion of nuclei to develop an efficient combined electron–ion minimization. This approach was first proposd by Car and Parrinello. [77]

1.3 Zeolites: An Overview

Zeolites are highly crystalline, hydrated aluminosilicates of group IA and IIA elements. Chemically they are represented by the empirical formula $M_{2/n}.Al_2O_3.ySiO_2.wH_2O$, where y is 2 to 10, M is the metal cation or proton, n is the cation valence and w represents the water contained in the voids of the zeolite. [37, 38] The structure of a zeolite consists of a three dimensional framework of SiO_4 and AlO_4 tetrahedra, each of which contains a silicon or an aluminum atom in the center. They are termed as TO_4 tetrahedron (Fig. 1.3(a)), where T is Si or Al. The oxygen atoms are shared between the adjoining tetrahedra units which can be present in various ratios and arranged in different ways. The conbination of several aluminosilicate rings then leads to the formation of structural channels and cavities. The diameter of these channels or pores range from 0.3 to 1.0 nm. The smallest pore size is formed by a eight ring pore with diameters 0.3 to 0.4 nm e.g. zeolite A, a medium pore zeolite, is a ten ring pore with a 0.4 to 0.6 nm in diameter, such as ZSM-5. Large pore zeolites are with twelve ring pores with 0.8 nm, e.g. zeolite beta. [78] A zeolite with a two or three dimensional channel system can have a better catalytic activity invoving physical or chemical adsorption. Diffusion of molecules also depends on the number of channels. [37, 38]

The structural formula of a zeolite is based on the crystallographic unit cell formula $M_{x/n}.[(Al_2O_3)_x.(SiO_2)_y].wH_2O$, where x and y are total number of tetrahedra per unit cell and y/x is usually 1 to 5, and w is the number of water molecules in the unit cell, M is the metal cation or proton of valence n, to produce electrical neutrality, since for each Al tetrahedron in the lattice there is an overall charge of -1. The sum x+y is the total number of tetrahedra in the unit cell. The portion [ ] above represents framework composition. In most zeolite structures the primary structural TO_4 tetrahedra (Fig. 1.3(a)) are assembled into secondary building units (Fig. 1.3(b)), which may be simple polyhedras such as cubes, hexagons and octahedra. [78] The final structure framework (unit cell) consists of assemblies of these secondary units. The framework may be considered in terms of large polyhedra building blocks forming characteristic cages. For example,

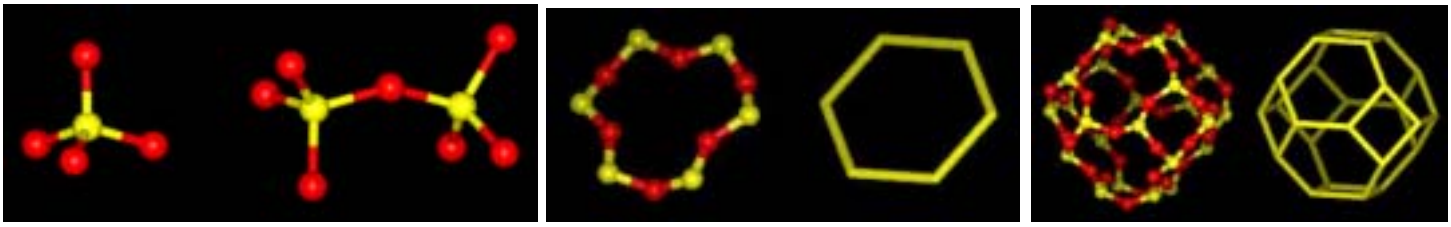

(a) **(b)** **(c)**

Fig. 1.3: The three structural building units of a zeolite. (a)Primary, (b)Secondary and (c)Unit cell.

sodalite and sodalite Y can both be generated by the truncated octahedron known as beta-cage. Extended structure of zeolite MFI with pores and channels formed from several unit cells is shown in Fig. 1.4.

Zeolites either occur naturally as minerals or are synthesized in the laboratory. They selectively adsorb or reject different molecules and hence, act as a molecular sieve. The molecular sieve action may be total or partial, depending upon the conditions, such as the pore size of the zeolite, size of the diffusing molecule and moreover, the activation energy of the molecule to pass through the channels. Zeolites are microporous materials widely used as heterogeneous catalysts, where the shape and selectivity of the zeolites plays an important role. Dimension of the pore is crucial for the selectivity of a molecule. The above properties of zeolites are responsible for widespread industrial applications of zeolites, as ion exchangers, selective adsorbents. [79] More importantly, they have been used in oil and petrochemical industries as oxidation or reduction catalyst in many processes such as cracking, isomerization and alkylation. [80, 81, 82] Recently, they have been shown to have applications in optical switching, microwave absorption, optical data storage, etc.

Zeolites have very good catalytic property, because they can act as solid acids. The acidity of zeolites is mainly due to the presence of Brönsted and Lewis acid sites. [37, 38] The Brönsted acidity in the zeolites arises from the protons present in the zeolite for compensating the negative charge from the substitution of the trivalent Al atoms in the place of tetravalent Si atoms. Alternatively, extra–framework cations, either

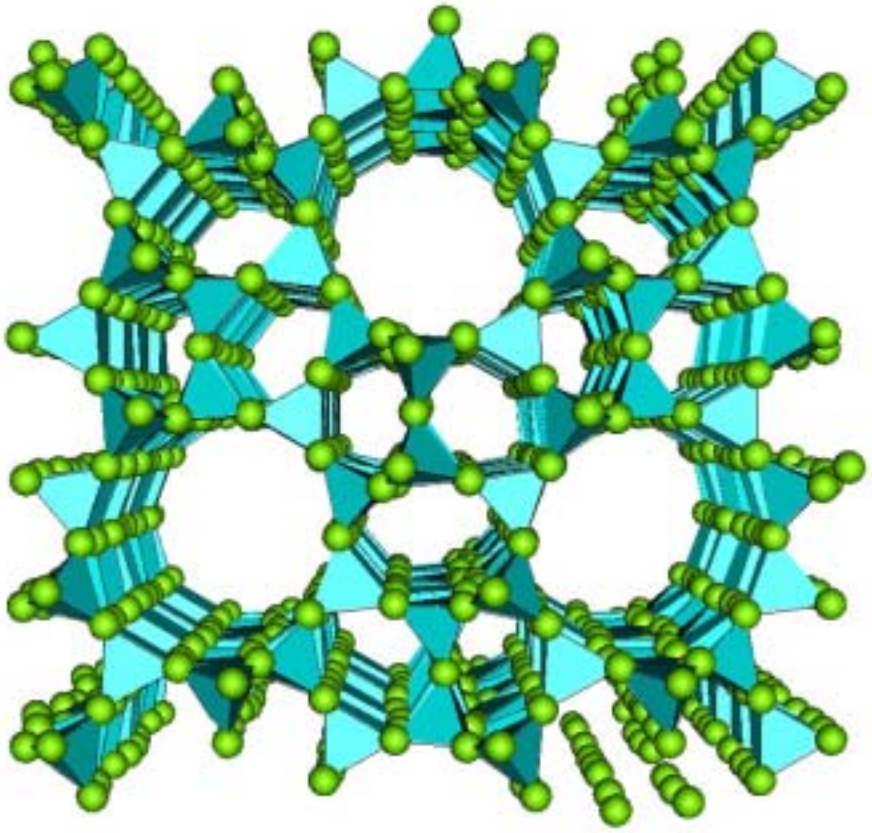

Fig. 1.4: Extended structure of zeolite (MFI) consisting of several unit cells.

monovalent (e.g. Na^+ or K^+), or divalent (e.g. Ca^{2+}, Sr^{2+}) are incorporated into the extra–framework sites. [37, 38, 82] Experiments have shown that there are some 'free' hydroxyl groups present on the zeolite framework, which are also responsible for acidity. Lewis acid sites arise from the isomorphous substitution of more electronegative atom such as Ti, Sn, etc, at the active sites. Due to the high electronegativity, they have ability to accept a pair of electrons and are probable sites for oxidation reactions. [83, 84]

In the present thesis we have characterized such Lewis acid site in Sn substituted BEA zeolite. One of the important postulate in siting the Al atoms is the Löwenstein's rule which forbids Al–O–Al bridges. [37, 38, 82] Another interesting feature of zeolites is their flexibility.

The chemical substitution of Si by some other atoms like Ge, Sn, Ti, etc., can relax the zeolite framework and can affect a certain chemical reactions taking place within the zeolite. [85, 86] Hence, the characterization of these substituted sites is important. Various experimental techniques such as EXAFS-XANES, IR, UV, NMR spectroscopies and XRD methods have been implemented to understand these sites. [87] However, accurate characterization of these sites, which act as an active sites, by the means of experiments is still difficult. XRD methods have improved greatly in recent years and are still more accurate methods to determine the crystal structure of a new material. [87] In zeolites the number of inequivalent T–sites within a zeolite can definitely be distinguished by using XRD. It also provides the fractional coordinates and the unit cell parameters which are necessary for a particular theoretical calculations. However, determination of zeolite structure is not as simple as the other crystal structures. The crystallographic problems in the zeolite structure analysis are: The effect of framework flexibility on the structure analysis, disorder of the non-framework species and its effect on the structure solution, defects within the framework, problems caused by isomorphous substitution. In addition, the structure factors obtained from XRD are averaged all over the crystal and hence, it is difficult to obtain information about the local active sites of interest. One of the ways of investigating the local active site is with the help of quantum chem-

ical calculations, since such properties are not always easily quantified by experimental means. Thus a better understanding on the structural and electronic properties at the microscopic level can be achieved from theoretical calculations.

1.3.1 Theoretical Models in Zeolites

The conventional quantum mechanical methods such as H–F, CI, DFT, etc, which have been formulated to study metal clusters, as discussed in 1.2.4, also have been applied to investigate the chemical and physical properties of zeolites. One of the earlier approximations to investigate the active sites in zeolites was the cluster model approach. The main difference between the metal cluster and the zeolite cluster is that, the metal clusters have completely different characteristics than their bulk. Whereas, zeolite cluster is a hypothetical model to approximate the active sites present in the crystalline phase of the zeolite.

In the following section we discuss some of the aspects of cluster model approach, followed by the necessity of the periodic approach to study zeolites in a crystalline phase.

Cluster Approach

The active sites of the zeolite crystal, which are difficult to treat quantum mechanically, can thus be represented by a fragment of that zeolite crystal. These fragments are cutouts of the sites of interest and are called cluster models. In the case of metals, these clusters are cutouts of a particular metal and are refereed to as metal clusters (as discussed in the previous section). The dangling bonds resulting from the cutouts are saturated by hydrogen atoms. [82, 36, 88] Larger is the size of the cluster better it represents the solid. Cluster approach is computationally cheap approximation to understand the properties of the solid phase that have local character. One of the truncated cluster models is shown in Fig. 1.5. It reduces the problem of electronic structure and local geometry of the solid to the common problem of determining the geometry and electronic structure of molecules, it also reduces the problem of the reactions or

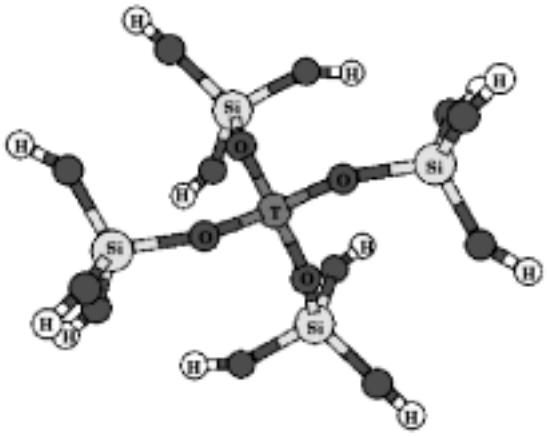

Fig. 1.5: Truncated cluster model from a zeolite. The central atom indicates the T–atom (Ge, Ti, Sn, etc). The dark grey spheres indicate the O atoms and the light grey and the white atoms indicate the Si and O atoms, respectively.

adsorption of molecules on the surfaces by just cluster–molecule interaction. Krishnamurty *et al* have used cluster models for studying the adsorption of guest molecules in zeolites. [89] The bridging hydroxyl group is a well studied site to understand the acidity, using quantum chemical methods in a cluster model. The simplest model to represent a cluster in zeolite is shown in Fig. 1.5, in which the central T atom can be substituted by Ge, Sn, Ti or Al. In the case of Al, the proton would be located on one of the O atoms. For more detailed study of zeolite cluster models, one should refer to the papers by Sauer. [36, 90]

There are some limitations of the cluster model. Due to the breaking of the Si–O covalent bonds some artificial surface states, located in the forbidden zone are introduced. Moreover, the cluster model does not consider the long–range interaction resulting from the crystal structure. This becomes very crucial when the active sites are located within the cages of the zeolite and not on the surfaces. However, in the periodic calculations such as periodic DFT, all the short-comings of the cluster model are taken care, but at a larger computational expense. To understand the limitations of the cluster model, it is necessary to compare the results with the periodic calculations. In recent investigations regarding the comparison of cluster and periodc calculations of zeolites have been

carried out. [39, 91]

Periodic Approach

As discussed above that the cluster model is an artificial and an insufficient model to approximate the active sites in the zeolites. In last two–three years it has been a practice to use the PBC in combination with DFT or H–F to deal with the crystal phase systems. For crystals such as zeolites, PBC corresponds to one or more unit cells replicated to form an infinite lattice. If the system contains dynamic processes such as adsorption or diffusion, the translated images move exactly in the same way. The PBC ensures that the density of the system remains constant throughout the simulation, and thus the surface effects are absent.[1] Considering the limitations of the cluster model,*in the present thesis, we have only used the periodic approach for studying the properties of the active sites in Sn-BEA zeolite.*

1.4 Motivation and Purpose

The progress of naotechnology in the field of molecular electronics, catalysis, quantum computations and molecualr biology, has made possible to develop new experimental techniques and theortical models to study the properties of nanoscale systems. One such theoretical method which has been extensively used and modified in the last few years, is the DFT. New theoretical methods such as AIMD, time–dependent DFT, periodic DFT, which use the basic principles of DFT, has brought theory very close to experiments.

Motivation of the present thesis is to apply the advanced DFT techniques to study the physical and chemical properties of metal clusters and catalysis at a microscopic level. Recent advances in the field of metal clusters has helped in understanding the evolution of the physical and chemical properties from an atomistic scale to nano and to a bulk scale. In addition to this, by mixing different kinds of metal atoms, new materials

[1]The technical details and the implementation of the PBC in DFT has been discussed in Section 2.2.3

can be formed. One of the purposes of the present work is to use AIMD simulations to obatin the ground state properties of some mixed metal clusters such as Sn doped lithium and aluminum based binary clusters.

The other purpose of the work is to use periodic approach of DFT for understanding the local properties of the active sites within the BEA zeolite for the substitution of Sn atom in a solid phase. Motivation to this study was the recent experimental study of the Baeyer–Villiger oxidation reaction in the Sn–BEA zeolite.[2]

1.5 Organization of the Thesis

Chapter 2: This chapter discuss the necessary theoretical background that has been used for the present calculations. The chapter begins with the introduction to the basics of DFT which forms the theoretical foundation of the present thesis. We then discuss the use of PBC and the details of plane wave basis set and pseudopotentials. This is followed by the discussion on classical MD. The combined approach of DFT and classical MD, known as AIMD is presented. The two approaches based on AIMD, CPMD and BOMD has been described. Later, we explain the optimization techniques used in the present work. The chapter ends with the analysis of the data obtained from the theoretical calculations.

Chapter 3: In this chapter we discuss the structural and bonding properties of two different kinds of mixed clusters. One is the single impurity based Li_nSn ($n \leq 9$) and the other is the mixed aluminum based binary clusters, Al_4X_4 (X=Be, Mg, B, Si). BOMD technique has been adopted to obtain the ground state structural properties of both the classes of mixed clusters. used to study the structural properties of the metal clusters. The bonding characteristics of the metal clusters have been investigated using the ELF along with the charge density and valence molecular orbital isodensity maps. Several different kinds of bonding has been investigated in these metal clusters. From

[2]Applications of these systems have been explained in the earlier sections of this chapter

the bonding analysis, we show that there is a transition from ionic bond to a metallic bond through an intermediate ionic-metallic bond in Li_nSn ($n \leq 9$), as the cluster size grows. In the aluminum based binary clusters, it has been shown that there are different trends of bonding such as lone pairs, multi-center bonding etc.

Chapter 4: This chapter deals with one of the most important concepts of organic chemistry *viz.* anti–aromaticity in metal clusters. We discuss the anti–aromaticity concept in metal clusters such as Al_4Li_4, Al_4Na_4 and anionic $Al_4Na_3^-$, on the basis of their structural, bonding, electronic and magnetic properties. It is shown that the Al_4 in all the above clusters has 4 π–electrons and has a rectangular structure with alternate π bonds. Hence, they satisfy the basic criteria of anti–aromaticity and are called as metallo–anti–aromatic compounds. However, the magnetic properties show that in addition to the π–anti–aromaticity, they also have σ aromaticity.

Chapter 5: In the last two chapters the theory has been used to deal with gas phase clusters. In this chapter we show the application of the DFT to solid phase. To do this we have chosen a crystal structure of Sn substituted BEA zeolite. The translational symmetry of the crystal has been taken care by PBC using plane wave and pseudopotentials. We investigate the structural and electronic properties of all the active sites for the substitution of Sn in the crytals structure of BEA. The work concludes that the T2 site, out of the 9T sites, is the most favorable for the substitution of Sn in the BEA.

Chapter 2

Theoretical Methods and Computational Aspects

Abstract:

This chapter is devoted to some of the theoretical approaches used for the description of non-periodic systems, such as metal clusters and periodic systems, such as zeolites. We shall discuss the AIMD technique based on the DFT, to study the ground state properties of metal clusters. Later, we also discuss the use of DFT to study the ground state properties of periodic solids such as zeolites.

Finding the ground state geometry and the properties associated with it has been a central goal of many researchers. In the last decade, various quantum mechanical methods have been implemented to treat the electronic structure of molecules, clusters and solids. In the present chapter we give a brief overview of the DFT and its implementation in the AIMD technique and the use of PBC to investigate the ground state properties of Sn-substituted Beta zeolite. We also discuss the optimization techniques such as simulated annealing and conjugate gradient used for obtaining the ground state structures. It is difficult to discuss all the theoretical methods in this chapter. In the last section of this chapter, we discuss the interpretation of the data obtained from these theoretical calculations. For more detailed information the interested reader is referred to the review by Payne *et al.* [92]

2.1 The Schrödinger Equation

The time independent non-relativistic Schrödinger equation

$$\hat{H}\Psi = E\Psi \tag{2.1}$$

provides a theoretical foundation for the solution of virtually all problems in chemistry. H is the Hamiltonian operator, Ψ is a many–particle wave function, and E is the energy of the system. The set of wave functions Ψ_i , (i = 1, 2,...) , which are the solutions of this equation, represent the set of possible quantum states of the system with the wave function Ψ_i containing all information for the state i. However, the analytic solution of the Schrödinger equation has only been possible to date for atoms and molecules with only one electron.

In atomic units the Hamiltonian for N electrons and M nuclei is

$$\begin{aligned} \hat{H} &= -\sum_{i}^{N}\frac{1}{2}\nabla_i^2 - \sum_{A}^{M}\frac{1}{2M_A}\nabla_A^2 - \sum_{i=1}^{N}\sum_{A=1}^{M}\frac{Z_A}{r_{iA}} \\ &+ \sum_{i=1}^{N}\sum_{j>i}^{N}\frac{1}{r_{ij}} + \sum_{A=1}^{M}\sum_{B>A}^{M}\frac{Z_A Z_B}{R_{AB}} \end{aligned} \tag{2.2}$$

In the above equation M_A and Z_A are the mass and the charge of the nucleus A, $r_{iA} = \mid \vec{r}_i - \vec{R}_A \mid$ is the distance between the ith and the Ath nucleus, $r_{ij} = \mid \vec{r}_i - \vec{r}_j \mid$ is the distance between the ith and the jth electron and $R_{AB} = \mid \vec{R}_A - \vec{R}_B \mid$ is the distance between the Ath and the Bth nucleus. For molecules, the first approximation made in all the calculations is the Born–Oppenheimer approximation, in which the nuclear and the electronic wave functions are considered separately.

2.1.1 The Born – Oppenheimer Approximation

Since nuclei are much heavier than electrons, they move more slowly. Hence, to a good approximation, one can consider the electrons in a molecule to be moving in the field of

fixed nuclei. Within the approximation, the kinetic energy of the nuclei is neglected and the repulsion between the nuclei is taken to be constant. Hence, electronic Hamiltonian describing the motion of N electrons in the field of M nuclei, is given as, [8]

$$\hat{H} = -\sum_{i}^{N}\frac{1}{2}\nabla_i^2 - \sum_{i=1}^{N}\sum_{A=1}^{M}\frac{Z_A}{r_{iA}} + \sum_{i=1}^{N}\sum_{j>i}^{N}\frac{1}{r_{ij}} + \sum_{A=1}^{M}\sum_{B>A}^{M}\frac{Z_A Z_B}{R_{AB}} \tag{2.3}$$

Electronic structure methods solve the eigenvalue equations of the electronic Hamiltonian and th etotal energy is obtained as a sum of the electronic energy and the constant nuclear repulsion. There are many theoretical methods which can be used to solve the Schrödinger equation such as H–F, CI, CC, etc. [8] One such method is the DFT which uses the electron density instead of the wavefunction. This method is not only easy to derive but also computationally cheaper than the other *ab initio* methods. Moreover, DFT considers the electron–electron correlation unlike the H–F. DFT has been explicitly used in the present thesis.

2.2 Density Functional Theory

DFT has long been an extremely useful method for the electronic structure calculations in quantum chemistry. It has been successfully applied to calculate the ground state properties of atoms, molecules, metals, semiconductors, etc. DFT is a rigourous way of circumventing the interacting problem of ground state by a more trivial non-interacting problem. The main idea of DFT is to describe an interacting system of N-electrons through its electron density and not via its many-body wave function. The fact that the ground state properties are functionals of the electron density, ρ(r), was proved by HK and it provides the basic framework for modern DFT. [9]

2.2.1 Hohenberg–Kohn Theorems

The first HK theorem states that the external potential v(r) (second term in the eqn 2.3) is determined, within a trivial additive constant, by the electron density ρ(r). [9] Since

ρ determines the number of electrons, it follows that ρ(r) also determines the ground state wave function Ψ and all other electronic properties of the system.

$$\rho(r) \longrightarrow N \longrightarrow \{\Psi_i\} \longrightarrow \text{all properties}$$

The second HK theorem provides the energy variational principle. It states that, for a trial density ρ'(r) such that $\rho'(\mathrm{r}) \geq 0$ and $\int \rho'(r)dr = N$

$$E_0 \leq E_v[\rho'] \tag{2.4}$$

E_0 is the energy which corresponds to the ground state electron density. The above equation presents a search for the ground state electron density and corresponding ground state energy through the minimization of the energy functional $E_0[\rho]$. However, the trial densities should satisfy the necessary criteria of *N*–representability, i.e. the trial density should be associated with an anti–symmetric wavefunction. More importantly, the density should also have *some* external potential and satisfying the *v*–representability condition. The *N*–representability condition is necessary for the *v*–representabiliy condition. Levy has shown that there are some densities which are not *v*–representable i.e. the densities do not map to any external potential. [10] Therefore, such non–*v*–representable densities would not correspond to any ground state.

2.2.2 Kohn–Sham Method

KS introduced a method based on the HK theorem that enables minimization of E[ρ(r)] by varying ρ(r) over all densities containing N electrons. [9]

The total electronic energy in the KS approach, E[ρ(r)] can be partitioned as follows

$$\begin{aligned} E_{\text{total}}\left[\rho(\mathbf{r}), \{\mathbf{R}_I\}\right] &= -\frac{1}{2}\sum_i \langle \psi_i(\mathbf{r}) \mid \nabla_i^2 \mid \psi_i(\mathbf{r})\rangle + \frac{1}{2}\int\int \frac{\rho(\mathbf{r})\rho(\mathbf{r}')}{\mid \mathbf{r}-\mathbf{r}' \mid} d\mathbf{r}d\mathbf{r}' \\ &+ E_{\text{xc}}[\rho(\mathbf{r})] + \int V_{\text{nuc}}(\mathbf{r})\rho(\mathbf{r})d\mathbf{r} \end{aligned} \tag{2.5}$$

In the above Eqn 2.5, the first term is the kinetic energy of electrons in a model non–interacting system which has the same electron density as the real system. The second term is the pure Coulomb interaction between the electrons. The third term is the exchange-correlation energy, which includes the electron exchange, the difference of the non-interacting and the interacting kinetic energy and the correction for the self interaction due to the Coulomb potential, and the last term is the external potential, i.e., potential coming from nuclei. The minimum of the KS functional is obtained by varying the energy functional (Eqn. 2.5) with respect to the electron density. This leads to the KS orbital equations

$$\left[-\frac{1}{2}\nabla_i^2 + v_{eff}\right]\psi_i = \epsilon_i\psi_i \tag{2.6}$$

$$v_{eff}(\mathbf{r}) = v(\mathbf{r}) + \int \frac{\rho(\mathbf{r}')}{\mid (\mathbf{r}) - (\mathbf{r}') \mid} d(\mathbf{r}') + V_{xc}(\mathbf{r}) \tag{2.7}$$

$$\rho(r) = \sum_i^n \mid \psi_i(r) \mid^2 \tag{2.8}$$

Eqn. 2.8 is the electron desnity. Since the sum of the orbital energies is not equal to the total electronic energy. Hence, the total electronic energy can be derived as

$$E = \sum_i^n \epsilon_i - \frac{1}{2}\int \frac{\rho(\mathbf{r})\rho(\mathbf{r}')}{\mid \mathbf{r} - \mathbf{r}' \mid} d\mathbf{r}d\mathbf{r}' + E_{xc}[\rho(\mathbf{r})] - \int V_{xc}\rho(\mathbf{r})d\mathbf{r} \tag{2.9}$$

The exchange-correlation functional as defined by KS remains unknown However, there exist several approximations. LDA is the simplest possible density functional approximation where the exchange and correlation of an interacting but homogeneous electron gas at the density given by the local density ρ(r) at space point r in the inhomogeneous system. [9] It is defined as

$$E_{xc}^{LDA}[\rho(\mathbf{r})] = \int \rho(\mathbf{r})\epsilon_{xc}(\rho(\mathbf{r})d\mathbf{r} \tag{2.10}$$

More sophisticated is the GGA approximation, where the unknown functional is approximated by an integral over a function that depends only on the density and its

gradient at a given point in space. [103]

$$E_{xc}^{GGA}[\rho(\mathbf{r})] = \int d(\mathbf{r})\rho(\mathbf{r})\epsilon_{xc}^{GGA}(\rho(\mathbf{r}); \nabla\rho(\mathbf{r})) \tag{2.11}$$

Some of the GGA functional for example, are the BLYP, [102] the PW91, [103] or the PBE exchange–correlation density functionals. The PW91 is extensively used throughout this thesis.

2.2.3 Plane Wave Basis Set and Periodic Boundary Condition

In molecular applications of DFT, atomic centered Gaussian basis functions are used. However, in solid–state theory, periodicity introduced by the PBC of the underlying lattice produces a periodic potential and thus imposes the same periodicity on the density. Hence, the single particle orbitals satisfy the Bloch theorem and can be expanded in plane wave basis set. [93]

$$\psi_i^{\mathbf{k}}(\mathbf{r}) = e^{i\mathbf{k}.\mathbf{r}} \sum_{\mathbf{g}} c_i^{\mathbf{k}}(\mathbf{g}) \mathbf{e}^{\mathbf{ig}.\mathbf{r}} \tag{2.12}$$

where g is the reciprocal lattice vector of the cell and the wave vector k lies within the Brillouin Zone of the reciprocal lattice of the cell. The computation of the electron density is

$$\rho(\mathbf{r}) = \sum_{\mathbf{k}} \sum_{i} \mid \psi_i^{\mathbf{k}}(\mathbf{r}) \mid^2 \tag{2.13}$$

The choice of plane wave expansions for the single particle orbitals have many advantages. Plane waves are independent of the atomic positions and therefore, atomic forces can be easily computed. This also makes them free of basis set superposition errors. This is particularly useful in molecular dynamic simulations, where different atomic configurations are explored. It allows the use of fast Fourier transform techniques which are computationally very efficient. The disadvantage of plane wave expansion is the large number of of basis functions needed to represent the orbitals, compared to the localized Gaussian like orbitals. Hence, pseudopotentials are used in conjunction with the plane waves to describe the more localized core electrons. [94]

In simulation of solids, PBC is introduced by repeating the simulation box infinitely. Hence, application of plane wave is very useful. In the present thesis, we have used this approach to investigate the properties of zeolites. For the non-periodic systems, such as amorphous material or clusters, PBC can still be adopted. This can be done by using a supercell (large simulation box), so that the interaction of the adjacent cells does not affect the properties of the system. [92] As a non-periodic system, in the present work we study the structural and bonding properties of mixed metal clusters with the help of supercell.

2.2.4 Pseudopotentials

In most of the chemical systems, it is possible to separate atomic states in valence state and core state. The latter are much deeper in energy and can therefore be considered as chemically inert. These inert states can be eliminated by replacing the true atomic Coulomb potential by pseudopotentials, such that the effect of the core states on the valence states is effectively reproduced. Pseudopotential is required to correctly represent the long range interactions of the core and to produce pseudowavefunction solutions that approach the full wavefunction outside a core radius. Inside this radius, the pseudopotential and the wavefunction should be as smooth as possible, in order to allow for a small plane wave cutoff. For the pseudo–wavefunction, this requires that the nodal structure of the valence wavefunction is replaced by a smooth function. [122] In addition, it is desired that a pseudopotential is transferable, which means that one and the same pseudopotential can be used in calculation of different chemical environment. The properties that depend crucially on the wavefunction close to the core cannot be obtained directly from the pseudo–wavefunction and pseudopotential calculations.

One of the important steps in the field of pseudopotential was to introduce the norm–conserving pseudopotentials. [96] They have a semi–local form

$$v_{ps}(\mathbf{r}) = \sum_{l=0}^{\infty} v_l(\mathbf{r})\hat{P}_l \tag{2.14}$$

where $\hat{P}_l$ is a projection operator onto the l^{th} angular momentum.

Recently, Vanderbilt proposed new pseudopotentials by relaxing the norm-conserving condition on the pseudo wavefunctions and hence, were termed to be ultra-soft pseudopotentials. [97] In this the pseudo wavefunctions are not required to have the same charge as the all-electron wave functions, and can therefore be as smooth as possible in the core region. This approach leads to a powerful technique of plane–wave pseudopotential electronic structure calculations in the framework of DFT. In the present thesis, we have used only the ultra–soft pseudopotentials.

2.3 Classical Molecular Dynamics

In classical MD, the nuclear motion in a molecular system is treated by the classical equations of motion interacting via a potential. The potential used to derive the forces on the atoms are classical such as Lennard–Jones, Buckhingham, etc. These potentials do not account the electronic motion and hence, classical MD becomes computationally much cheap. In MD, successive configurations of the system are generated by integrating the Newton's equation of motion. The result is the trajectory that specifies how the positions and velocities of the atoms in the system vary with respect to time. Hence, MD is a deterministic approach, in which the state of the system at any future time can be predicted from its current state. [68]

The trajectory is obtained by solving the differential equations involved in the Newton's second law. Given a set of atoms of masses M_I at position $\mathbf{R}_I$, one can write

$$F_I = M_I\ddot{\mathbf{R}}_I \tag{2.15}$$

where the force on the atom I is given by F_I, which can be related to the potential

E(R_I)as

$$F_I = -\frac{\partial E(\mathbf{R}_I)}{\partial \mathbf{R}_I} \tag{2.16}$$

Various algorithms have been devised to solve the above equations. Perhaps the most widely used method is the Verlet algorithm.[68] The method is based on the atomic positions $\mathbf{R}_I$(t), accelerations $\mathbf{A}_I$(t) and the atomic positions of the previous step $\mathbf{R}_I$(t + $\triangle$t). The equation for the next step is calculated from the Taylor expansion

$$\mathbf{R}_I(t+\triangle t) = \mathbf{R}_I(t) + \triangle t\mathbf{V}_I(t) + \frac{1}{2}\triangle t^2\mathbf{A}_I(t) + \cdots \tag{2.17}$$

$$\mathbf{R}_I(t-\triangle t) = \mathbf{R}_I(t) - \triangle t\mathbf{V}_I(t) + \frac{1}{2}\triangle t^2\mathbf{A}_I(t) - \cdots \tag{2.18}$$

Adding 2.17 and 2.18 we have

$$\mathbf{R}_I(t+\triangle t) = 2\mathbf{R}_I(t) - \mathbf{R}_I(t-\triangle t) + \frac{\triangle t^2}{M_I}F_I \tag{2.19}$$

where F_I is given by Eqn 2.16

The velocities are not needed to compute the trajectories, but they are useful to calculate the kinetic energy. They may be obtained as

$$\mathbf{V}_I(t) = \frac{\mathbf{R}_I(t+\triangle t) - \mathbf{R}_I(t-\triangle t)}{2\triangle t} \tag{2.20}$$

In MD simulations, it is very important to store the information of the system after every $\triangle$t step, such as, velocities, forces and the instantaneous values of all the calculated properties. The information stored in an MD simulation is time ordered and can be used to calculate time correlation function, and thus, can be used to calculate the transport properties such as diffusion coefficient, viscosity coefficient, etc. Moreover, the temperature dependent properties can also be calculated from the equipartition law

$$\frac{3}{2}NK_BT = \langle \sum_{i=1,N} \frac{1}{2}m_i v_i^2 \rangle$$

Although many systems have successfully been investigated with model potentials like for eg. Lennard-Jones potentials. In classical MD it is difficult to account for the local atomic properties such as, chemical bonding, including the chemical reactions which form and break bonds in a quantum mechanical fashion. On the other hand, quantum dynamics of the nuclear motion of a large molecular system becomes highly computationally expensive. These difficulties can be accomplished by the use of AIMD.

2.4 *Ab Initio* Molecular Dynamics

AIMD method allows to simulate the motion of the individual atoms based on forces which are calculated quantum mechanically. [92, 98] The basic idea behind AIMD is that, since the nuclei are much heavier than the electrons should be moved classically using the Newton's equation of motion under the electronic potential derived from quantum mechanical approach. In 1985, in a seminal paper, Car and Parrinello initiated the field of AIMD by combining the conventional MD technique with the DFT and were termed to be CPMD. [77] This allows one to study, formation and breaking of chemical bonds in contrast to the conventional MD. A number of other techniques have been developed which are based on minimization of the electronic orbitals to their ground state at each time step. These techniques were referred to as BOMD. [99]

2.4.1 Car Parrinello Molecular Dynamics

Car and Parrinello proposed a scheme based on MD and DFT. [77] They postulated the following Lagrangian

$$\begin{aligned}\mathcal{L}_{CP} &= \frac{1}{2}\sum_i \mu \int |\, \dot{\psi}_i(\mathbf{r})\,|^2\, d\mathbf{r} + \frac{1}{2}\sum_I M_I \dot{\mathbf{R}}_I^2 - E_{\text{total}}\left[\{\psi_i\},\{\mathbf{R}_I\}\right] \\ &\quad + \sum_{ij}\Lambda_{ij}\left(\int d\mathbf{r}\psi_i^*(\mathbf{r})\psi_j(\mathbf{r}) - \delta_{ij}\right) \end{aligned} \tag{2.21}$$

$\mathcal{L}$ does not depend explicitly on time, and is a functional of two states of classical degrees of freedom, the ψ_i and the $\mathbf{R}_I$, which depend on time. The μ_i are arbitrary

parameters which play the generalized masses for the electronic degrees of freedom. The first and the second term in Eqn. 2.21 are the kinetic energy of the electronic (K_e) and ionic degrees of freedom (K_I), respectively. E is the potential energy of the coupled electron-ion fictitious system. The Lagrangian multipliers Λ_{ij} are used to impose orthonormality conditions on the ψ_i.

The Euler equations associated with the Eqn. 2.21 are

$$\mu\ddot{\psi}_i = -\frac{\delta E}{\delta \psi_i^*} + \sum_j \Lambda_{ij}\psi_j \tag{2.22}$$

$$M_I\ddot{\mathbf{R}}_I = -\frac{\partial E}{\partial \mathbf{R}_I} \tag{2.23}$$

According to the Car-Parrinello equations of motion, the nuclei evolve in time at a certain physical temperature $\propto K_I$, whereas a fictitious temperature $\propto K_e$ is associated to the electronic degrees of freedom. Thus, a groundstate wavefunction optimized for the initial configuration of the nuclei will stay close to its ground state also during time evolution if it is kept at a sufficiently low temperature and need not be optimized after each time step.

2.4.2 Born Oppenheimer Molecular Dynamics

An alternative approach to include the electronic structure in molecular dynamics simulations consists in straightforwardly solving the static electronic structure problem in each molecular dynamics step, given the set of fixed nuclear positions at that instance of time. [99] Thus, the electronic structure part is reduced to solving a time independent quantum problem, e.g. by solving the time independent Schrödinger equation, concurrently to propagating the nuclei via classical molecular dynamics. Thus, the BOMD equation is given by

$$\mathcal{L}_{BO} = \frac{1}{2}\sum_I M_I\dot{\mathbf{R}}_I^2 - min_{\{\psi_i\}}E_{\text{total}}\left[\{\psi_i\},\{\mathbf{R}_I\}\right] \tag{2.24}$$

and the minimization is constraint to orthogonal sets of $\{\phi_i\}$. The equations of motion are

$$M_I \ddot{\mathbf{R}}_I = -\nabla_I \left[min_{\{\psi_i\}} E\left[\{\psi_i\}; \{\mathbf{R}_I\}\right] \right] \tag{2.25}$$

The above Eqn. ensures that the minimization of the electronic energy is done at each MD step.

2.4.3 Comparison of CPMD and BOMD

It is very important to ask which AIMD method would be the most computationally efficient? One of the advantage of CPMD over BOMD is that no diagonalization of the Hamiltonian (or the equivalent minimization of an energy functional) is necessary, except at the very first step in order to obtain the initial wavefunction. In CPMD, the explicitly treated electron dynamics does not allow one to take a larger time-step that can be used in order to integrate the coupled equations of motion for nuclei and electrons. Since, in BOMD there is no explicit dependence on the electronic motion the maximum time-step is given by the nuclear motion only. However, the time gained in BOMD due to the larger time step is lost in the orthogonalization. But it is seen that BOMD is an order of magnitude faster than the CPMD. For a more detailed comparison between the CPMD and BOMD, one can refer to [100].

In the present thesis we have used the BOMD approach for obtaining the ground state structures of mixed metal clusters. The BOMD method has been used to drive the system in a minimum energy configuration by using the simulated annealing technique (subsection 2.4.4). The details of BOMD and CPMD are discussed in several reviews and thesis. [75, 76, 94, 99, 92]

2.4.4 Optimization Techniques

Optimization techniques are used to drive the system in the minimum energy configuration. Once the initial configuration is defined the next step is to find its minimum energy structure. A variety of optimization techniques have been suggested. Basically, there are two kinds of optimizations, one is the electronic energy optimizations at a fixed nuclei and the other is the geometrical optimization. The final ground state geometry is considered only when the ions and the electrons are in their minimum energy configurations.

Conjugate gradient

The conjugate gradient method provides simple and efficient way to locate the minimum of a particular system. [92] The initial direction is taken to be the negative of the gradient at the starting point. A subsequent conjugate direction is then constructed from a linear combination of the new gradient and the previous direction that minimized the function. It should be noted that at each point the gradients are orthogonal but the directions are conjugate. Since the minimization along the conjugate directions are independent, the dimensionality of the vector space explored in this technique reduces by one at each iterations. When the dimensionality of the function has been reduced to zero, there are no directions left in which to minimize the function, so the trial vector must be at the minimum. In this technique, the search direction is generated using the information from all the sampling points along the conjugate gradient path. This method works very well for the systems lying close to the minima.

Simulated Annealing

Annealing is the process in which the temperature of a system is increased till it melts and then it is slowly reduced until the material crystallizes. Simulated annealing is a computational method which uses the same approach as this, in order to find the minimum of a particular system. [65]

For a system containing many ions will have several ionic configurations that are minimas. The simulated annealing procedure has to explore all these minimas to locate the lowest energy minima. At a given temperature the system is allowed to reach thermal equilibrium using a AIMD technique. At high temperatures, the system is able to occupy high energy regions of conformational space and to pass over high energy barriers. As the temperature is lowered, the lower energy becomes more probable in accordance with the Boltzmann distribution. At absolute zero the system should occupy the lowest energy state(i.e. the global energy conformation). Simulated annealing is ideal for the systems having small difference between the local and the global minima. This is often difficult to acheive in practice. Thus, simulated annealing cannot guarantee to find the global minimum. This technique has been very useful in obtaining the ground state geometries of metal clusters and to study their thermodynamical properties. [75]

In the present thesis we use the simulated annealing technique to obtain the lowest energy state structures of the metal clusters.

Finding the Minimum using AIMD

Initially the charge density is obtained from Eqn. 2.8 to calculate the KS energy functional (Eqn. 2.9) by solving the KS equations (Eqn. 2.6) self-consistently as discussed in the section 2.2.2. Reaching the minimum of the energy is only the first step in an AIMD simulation. In the next step, the force on the ions are computed according to the Hellman–Feynman theorem. The ions are then moved by solving the Newton's equation of motion (Eqn. 2.23) by Eqn. 2.19. As the ions are moved, the KS energy functional is minimized again, in order to calculate the Hellman-Feynman forces at every point in the MD trajectory.

2.5 VASP Program

VASP is a package for performing AIMD simulations with the use of DFT potential and PBC . [101] It is a useful package for simulating periodic solids and hence uses plane wave basis set in conjunction with Vanderbilt's ultra–soft pseudopotentials. However, finite cluster or molecules can be simulated by using a supercell. Its an all–purpose code for carrying out AIMD simulations. The AIMD approach implemented in VASP is based on BOMD concept, where an exact evaluation of the instantaneous electronic ground state is obtained from DFT at each MD step using efficient matrix diagonalization schemes. The optimization techniques discussed in the earlier section are efficiently implemented in VASP.

2.6 Interpretation of the Data

2.6.1 Structure

To study the ground state properties of a system it is necessary to obtain the ground state geometry of the system. Location of global minimum of any system is a complicated problem. The geometry optimization belongs to the problem of minimizing a N-dimensional function with respect to a set of coordinates. Hence the problem becomes much more complicated as the dimension of the system increases. None of the optimization schemes discussed in the earlier section can guarantee for the search of global minimum. The only way to find the global minimum is to find same minimum energy configuration in a number of different calculations. When subsequent calculations do not locate any new low energy configurations found previously or a configuration of significantly higher energy, then there is a high probability that all the low energy configurations of the system have been located and, hence, one can say that the global energy minimum has been located.

Moreover, the search for a transition state structure is more difficult than the

location of an equilibrium geometry. In a chemical reaction locating the transition state is as important as finding the equilibrium geometry of a particular isolated system. Transition state structure are mostly unknown. The energy difference between the energy of the reactants and the transition state which is also called as the activaton barrier, decides the stability of the reaction.

In the present thesis we discuss only the ground state structures and not their transition states.

2.6.2 Bonding

Bonding in chemical systems can be described either as localized or delocalized. The covalent, ionic, hydrogen and polar bonds belong to the localized bonding character, while metallic bonding belongs to the other class. The characterization of chemical bonds is a qualitative rather than a quantitative exercise. Bader used the topological description of electron density ρ(r) as a tool to understand the bonding in various chemical systems. However, it is known that, electron density alone does not easily reveal the consequences of the Pauli exclusion principle on the bonding.

Electrom Localization Function

Becke and Edgecombe proposed ELF, [104] which has been used to examine electron localization in atoms, molecules and solids. The idea was based on the measure of the probability of finding an electron in the neighborhood of another electron with the same spin. Several reviews have discussed in depth the application of ELF. [105]– [108] ELF can be viewed as a local measure of the Pauli repulsion between electrons owing to the exclusion in three dimensional space. It therefore makes it possible to define regions of space that are associated with different electron pairs in a molecular or a solid. The ELF is defined as

$$\eta(\mathbf{r}) = \frac{1}{1+(\frac{D_p}{D_h})^2} \tag{2.26}$$

$$D_p = \frac{1}{2}\sum_{i=1}^{N} \mid \nabla\psi_i \mid^2 - \frac{1}{8}\frac{\mid \nabla\rho \mid^2}{\rho} \tag{2.27}$$

$$D_h = \frac{3}{10}(3\pi^2)^{\frac{2}{3}}\rho^{\frac{5}{3}} \tag{2.28}$$

$$\rho = \sum_{i=1}^{N} \mid \psi_i(\mathbf{r}) \mid^2 \tag{2.29}$$

where the sum in Eqn. 2.29 is over all the occupied orbitals. D_h is the kinetic energy of the electron gas having the same density or one can say its the value of D_p in a homogeneous electron gas. This clearly shows that for a homogeneous electron distribution the value of ELF will be equal to 0.5. According to the definition, the ELF values lie between zero and one. Chemical systems in which, in the vicinity of one elctron, no other electron with the same spin may be found, that is, where electrons are alone, or form pairs of antiparallel spins, for instance as occurs in bonding pairs or lone pairs. In this case, the Pauli principle has little influence on their behavior and the ELF value tends to 1. However, if the probability of finding the electron in the vicinity of other electron is high than the ELF value decreases.

Examination of each term in the Eqn. 2.27 is quite revealing. First term is the total kinetic energy of N noninteracting fermions in the ground state, whereas the second term is what the kinetic energy density at a point in space would be if only one occupied orbital contributed to the electron density at the point. The latter term is a lower bound for the former. Eqn. 2.27 quantifies the amount of Pauli repulsion at a given point $\mathbf{r}$ in space. As a result the 'excess' Pauli kinetic energy is small in region where the electrons are localized as discussed above.

Fig. 2.1 shows the ELF pictures of two different molecular systems *viz* methyl acetate and benzene. Region (a) of the methyl acetate shows a loclaization region at the center of C–C bond, indicating a covalent bond. The double bond character is shown by the region (b). Region (d) and (e) indicate a lone pair of electrons on the O

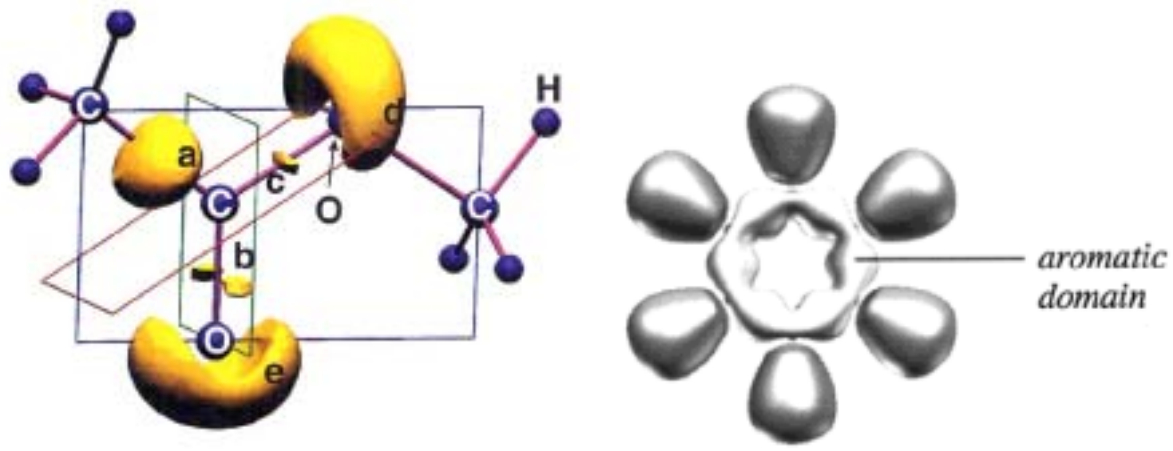

Fig. 2.1: ELF of Methyl Acetate (left) and Benzene (right). (After references [105] and [108]).

atoms. ELF of benzene clearly shows a symmetric electron localization pattern. Hence, indicating a resonance or delocalized state.

In the present work ELF has been used to understand the interplay between the localized and delocalized electrons as the metal cluster grow and eventually show a bulk characteristics. Later, it has been used to analyze the localized bonding in Sn–Beta zeolite.

2.7 Magnetic Ring Currents

In diamagnetic molecules an external magnetic field induces a current whose magnetic field lies in the opposite direction to the applied field. In cyclic unsaturated molecules where the π–electrons are delocalized, the external magnetic field creates a ring current. This ring current induces a secondary magnetic field perpendicular to the current loop and opposite to the applied magnetic field. On this basis the aromaticity and anti-aromaticity of a monocyclic conjugated molecule can be characterized. It has been proved that four electrons produce the whole of the induced diatropic current in an aromatic system with (4n+2) π electrons, and just two are responsible for the induced paratropic current of a 4n-πelectron anti-aromatic systems. [109]

In the present thesis, investigation of the magnetic response of a conjugated molecule to an external magnetic field i.e. to understand the presence or absence of ring currents, current-density maps were computed via coupled H–F theory in the CTOCD-DZ formulation implemented in the SYSMO program. [57] This method yields the first-order response of the current density to an external field, by taking a distributed origin such that the induced current density at any point is calculated with that point as origin. This approach has been used to give a qualitative picture of currents in many conjugated ring systems. In practice, for a planar conjugated system (aromatic or anti–aromatic), a uniform magnetic field perpendicular to the molecular plane is applied and the induced current density is plotted in slices parallel to the plane. For more detalis one should refer to [57].

Chapter 3

Study of Electronic and Bonding Properties of Mixed Metal Clusters

Abstract:

Bonding and electronic properties of two different classes of heteroatomic (mixed) metal clusters *viz.* single impurity based Li_nSn (n$\leq$ 9) and mixed aluminum based binary clusters, Al_4X_4 (X=Be, Mg, B, Si) have been investigated. BOMD within the framework of DFT has been used to study the structural properties of the metal clusters. The bonding characteristics of the metal clusters have been investigated using the ELF along with the charge density and valence molecular orbital isodensity maps. The bonding analysis of Li_nSn (n$\leq$ 9) cluster reveals that, there is a transition from ionic bond to a metallic bond through an intermediate ionic–metallic bond. However, it is found that Al_4X_4 (X=Be, Mg, B, Si) clusters show interesting features, such as lone pair of electrons on Al, polar covalent bonding and a multi-centerbonding. In this chapter, the role of electron localization function has been shown to play an important role in analyzing the bonding characteristics.

3.1 Introduction

In recent years, extensive theoretical and experimental investigations have been carried out in understanding the stability and electronic properties of small homogeneous metal clusters ranging between 2 to 100 atoms. The theoretical study was mostly limited for alkali metal atoms, [21] due to the less number of valence electrons. However, in last

decade, the theory has been extended to study the structural and electronic properties of transition metals and also group III A and IV A elements. [14, 23, 110] Jellium model has been one of the most widely used methods to describe the delocalized electrons in various metal clusters. A large variety of phenomena in metal clusters, such as optical properties, static polarizabilities, ionization potentials and the stability of the magic numbered clusters, can be explained in terms of jellium model. [22, 71] In the last decade similar studies have also been extended to investigate the properties of mixed clusters. The studies on mixed clusters have brought out some interesting properties. In small mixed clusters even a single impurity is expected to influence the electronic and bonding properties. [34]

Lithium has a single s-valence electron with electronic configuration $1s^2 2s^1$. Hence, it serves as one of the prototypical elements to study the metallic properties using various theoretical methods. It is known that lithium exists as diatomic molecule, with two lithium atoms held together by a single covalent bond. However, in lithium metal each atom has eight nearest neighbors and one valence elctron in the s-orbital, which permits the formation of electron-pair bond for each pair of atoms. This configuration allows the bonds to resonate within the Li atoms. This resonance would require the use of an additional orbital on the atom receiving an extra bond. [4] The additional orbital formed arising from the resonance is the metallic orbital. Consequently, giving rise to a metallic bond. Hence, it is of fundamental interest to understand the change in structural and electronic properties of such systems, as the bonding changes from a localized covalent to a delocalized metallic bond, as the number of atoms grow from a molecular regime to the bulk scale. Boustani and co-workers have done an extensive study of neutral and anionic Li_n ($n \leq 9$) using H–F based methods. [72, 111] They showed that the Li clusters prefer a planar stucture until n=6 and then change to a three dimensional structure. Jones and coworkers did structural and bonding analysis of Li_n and Li_nO ($n \leq 10$) systems. [112] In this study it was shown that Li clusters have a weaker tendency to form directional bonds. Earlier work on understanding the bonding

in planar Li clusters were carried out by using charge density analysis. [113] In this study the three centered bonding was predicted. Savin *et al* later showed the existence of three centered bonding in Li clusters on the basis of ELF. [105] Rousseau and Marx used the same approach of Savin *et al* and did an extensive work on the bonding of Li clusters from Li_4 to Li_{40}. [114] Interestingly, they found out that large Li p π-type contribution in the electronic wave function causes the electrons to localize in interstitial regions. This leads to multicenter bonding for both, the clusters and the solids. [114]

In recent years, use of Li have brought out some inetersting applications in the field of Li and Li–ion batteries, which are currently the best energy storage devices for the electronic materials. [26, 115] It has been shown that the utilization of the carbonaceous materials as the host for the Li ions has improved the efficiency of the Li ion batteries by $\sim$1.7 times. However, Li-metal alloys are more advantageous, due to the high packing density of Li that can be acheived in Li-metal alloys. One of the disadvantage of the formation of Li-metal alloy, is that it undergoes a drastic three-dimensional structural rearrangement. Consequently, the matrix cracks and eventually disintegrates. Li alloys with Sn forming various Li_xSn_y type compounds, [116] giving rise to a discharge capacity of 991 mAh/g. Previously it has been shown that the Li/Sn ratio of 4.4 gives a dishcarge capacity of 790 mAh/g. However, if the ratio is decreased to 2.0 the discharge capacity also decreases to 405 mAh/g. [26] This clearly shows that the Li/Sn ratio plays a crucial role in the efficiency of the Li–Sn alloyed batteries. Moreover, the phase diagram of Li-Sn alloy indicate that the stable compound concentrates around Li_4Sn composition. This behavior has been interpreted as octet composition, due to eight valence electrons. According to the octet rule, the Li_4Sn composition should have a tetrahedral structure. [117] Hence, it is interesting to understand the effect of the stoichiometry on the structural and bonding properties of the Sn doped Li clusters. In the last decade, more work has been carried out on understanding the behvior of clusters and their applications in the alloys. The other class of mixed clusters are, the binary clusters with an atomic ratio of 1:1. Several investigations on the mixing of various

alkali clusters has been carried out. Wang *et al* have studied A_4Pb_4, where A=Li or Na. [118] They showed tha the A_4Pb_4 clusters have a very high stability. The reason for this was given, to be the formation of stable $Pb_4{}^{-4}$ tetrahedral species. The most interesting alloys belonging to this class, are the aluminum based binary clusters.

Aluminum clusters have been widely used as one of the model systems for studying the physical and chemical properties of metal clusters. [14] Although bulk Al is known to be a free electron metal, several experimental and theoretical studies have shown that, small Al clusters do not display the well known magic behavior. The dissociation of Al cluster ions have been investigated by several groups. Begemann *et al.*, have studied the dissociation of aluminum cluster ions through sputtering technique. [30] Broyer *et al*, [11] and Jarrold *et al*, [62] have examined the photodissociation of Al cluster ions. From these studies it was found that Al_7 and Al_{13} clusters were more stable than their neighbors. Experimentally, Al_7^+ and Al_{14}^+ clusters appeared as "magic numbers" . Rao and Jena carried out theoretical investigation of these Al clusters using DFT. [119] They confirmed the above experimental results from the B.E., fragmentation channels, ionization potential, and vertical and adiabatic electron affinities, obatined from the DFT calculations. However, the application of the shell model to study the Al clusters has not been well defined. One of the reasons for this is the 3.6 eV gap between the filled 3s and the partially filled 3p orbitals in the Al atom. Recently, Rao and Jena showed that the application of shell model failed to predict the stability of Al_5X_m (X = Li, Na; $1 \leq m \leq 4$). [120] This was due to the s-p hybridization in the Al atom, which the shell model failed to explain. [120] They also showed that, alkalization lowers the ionization potential of the Al clusters. Moreover, it was shown by others that the bonding in these systems is ionic. [51] Hence, these systems were supposed to be very stable. It should be noted that Al forms stable alloys with the other elements such as Be, Mg, Si, etc. Thus, it is very interesting to understand the change in the structural and the bonding properties of the Al clusters when it is mixed with the other clusters in 1:1 proportion i.e. binary clusters.

The present work has been divided in two parts. Initially, we discuss the evolution of the structural and bonding properties of Sn doped Li_n (n=1 to 9) clusters. Later, we investigate the structural and bonding properties of several aluminum based binary clusters, such as Al_4X_4 (where X = Be, Mg, B and Si). We propose here an investigation of the bonding in these clusters using a combination of ELF, charge density and valence molecular orbitals.

3.2 Computational Details

We have performed BOMD based on the KS formulation of DFT using damped equations of motion to calculate the ground–state geometries of the Li_nSn ($n \leq 9$) and Al_4X_4 (where X = Be, Mg, B and Si) clusters. [121] In order to get reliable equilibrium geometries, we have used simulated annealing technique. Starting with random configurations in the Li_nSn ($n \leq 9$) clusters were heated up to 500–700 K, while the Al_4X_4 clusters were heated from 600–900 K and in certain cases up to 1800–1900 K followed by slow cooling. The lowest energy confirmations have been confirmed by reheating the clusters with different geometries. In many cases the equilibrium geometries were also obtained by using steepest descent on expected configurations. For example, in the Li_nSn clusters, the Li_4Sn cluster is expected to have a tetrahedral structure with the Sn atom at the center and the 4 Li atoms taking the corner positions of the tetrahedron, hence minimizing the Coulomb interactions between the Li atoms. Considering this geometry, we repeated the above procedure and found that the Li_4Sn cluster is not tetrahedral. In Al_4X_4 clusters, the low energy structures have been verified by interchanging the positions of Al and X atoms and repeating the above procedure. We have used the norm-conserving pseudopotential of Bachelet*et al.*, [122] in Kliennam and Bylander [123] form in conjunction with PW91 exchange–correlation potential [103]. A cubic supercell of 15 with an energy cutoff of 16.5 Ry was found to provide a sufficient convergence of the total energy. The structures were considered to be converged when the forces on all the atoms were less than 10^{-5} eV/. ELF and charge density have been

computed to study the ground-state electronic and bonding properties. The technical details of the ELF has beed discussed in the earlier chapter.

3.3 Results and Discussion

We begin this section by making some pertinent comments on the effect of using GGA on exchange-correlation potentials as compared to LDA results. It turns out that the GGA binding energies are higher by about 8%–10%. However, the effect on the HOMO–LUMO gap is very small, less than 3%. In Li_nSn structures the bond lengths obtained through GGA are 10%–15% higher than the LDA results. However, in Al_4X_4 systems the increase in the bond length is about 4%–5%. Except in the case of Li_5Sn, the ground and first excited state separated by 0.02 eV in LDA becomes nearly degenerate within GGA. In all other clusters the ordering of the isomers remains unaltered. In what follows, we present the systematic analysis of the bonding characteristics as revealed through ELF and molecular orbital analysis of the single impurity clusters Li_nSn for n$\leq$9 and several aluminum-based binary clusters viz. Al_4X_4 (where X = Be, Mg, B and Si). We also present a brief discussion on the B.E. and the gap between the HOMO and the LUMO . We begin the discussion of the results with a brief introduction to the ground state structural properties. For more details on stability of the above clusters, refer to the studies by Joshi *et al.* [49] and by Chacko *et al* [51].

3.3.1 Structural Properties of Li_nSn

Calculated ground-state geometries of Li_nSn (n $\leq$ 9) are shown in Fig. 3.1, 3.2 and 3.3 where the impurity Sn is shown in a black sphere. The ground state geometry of Li_2Sn (a) as shown in Fig. 3.1 is an isosceles triangle where the Li–Sn bond length is 2.48 Å. The ground-state structure of Li_3Sn (a), Fig. 3.1, is a trigonal pyramidal (C_{3v} symmetry). The excited state structure of Li_3Sn (b), Fig. 3.1, which is 0.18 eV higher in energy, is a planar geometry. Generally, the ground-state Li_4Sn structure is expected

to be tetrahedral with 4 Li atoms sharing the corners of the tetrahedron with the Sn atom at the center. Surprisingly, we see that the ground-state Li_4Sn (a), Fig. 3.1, is a slightly distorted trigonal bipyramidal and is 0.5 eV lower in energy than the expected tetrahedral Li_4Sn (c) structure. The reason for this is given in the next section.

The ground-state structure of Li_5Sn (a), Fig. 3.2, is a rectangular bipyramid. The excited state structure of Li_5Sn (b), Fig. 3.2, is a bicapped tetrahedron 0.013 eV higher in energy than the ground state. We expect a transition from Li_5Sn (a) to Li_5Sn (b) at room temperature. Investigation of the remaining structures reveals that after Li_6Sn, the Li atom does not form a direct bond with Sn atom. Instead, in all cases from Li_7Sn to Li_9Sn the added Li atom prefers to bond with Li atoms only. From Fig. 3.1, it is also evident that the pyramidal structure of Li_3Sn is retained from Li_3Sn to Li_6Sn. The sudden structural change from Li_6Sn (a) (Fig. 3.2) to Li_7Sn (a) (Fig. 3.2) reveals that there is a considerable change in the energetics and the bonding of Li_7Sn, which will be discussed in detail in the next section. In the excited state structure of Li_6Sn (b), which is 0.2 eV higher in energy than the ground state, it is seen that the Sn atom takes the interstitial position. This shows that the Sn atom is not trapped within the Li atoms and remains on the surface as seen in Li_6Sn (a) .

The ground state of Li_8Sn (a) (Fig. 3.3) is a pentagonal bipyramid, which is also observed in Li_9Sn (a) (Fig. 3.3) without much change in the geometry, except the capping of Li atom on the surface. It is very interesting to note that the Sn atom prefers to remain outside the Li cluster from Li_2Sn to Li_4Sn cluster. From Li_5Sn onwards the Sn atom tries to diffuse within the Li clusters. In Li_8Sn and Li_9Sn clusters the Sn takes the interstitial position.

3.3.2 Bonding and Energetics of Li_nSn

In the present section, we discuss the change in the bonding characteristics of the Li_nSn ($n \leq 9$) clusters by the use of ELF at different isosurface values, the charge density isosurface at one third of its maximum isosurface value, and the valence molecular

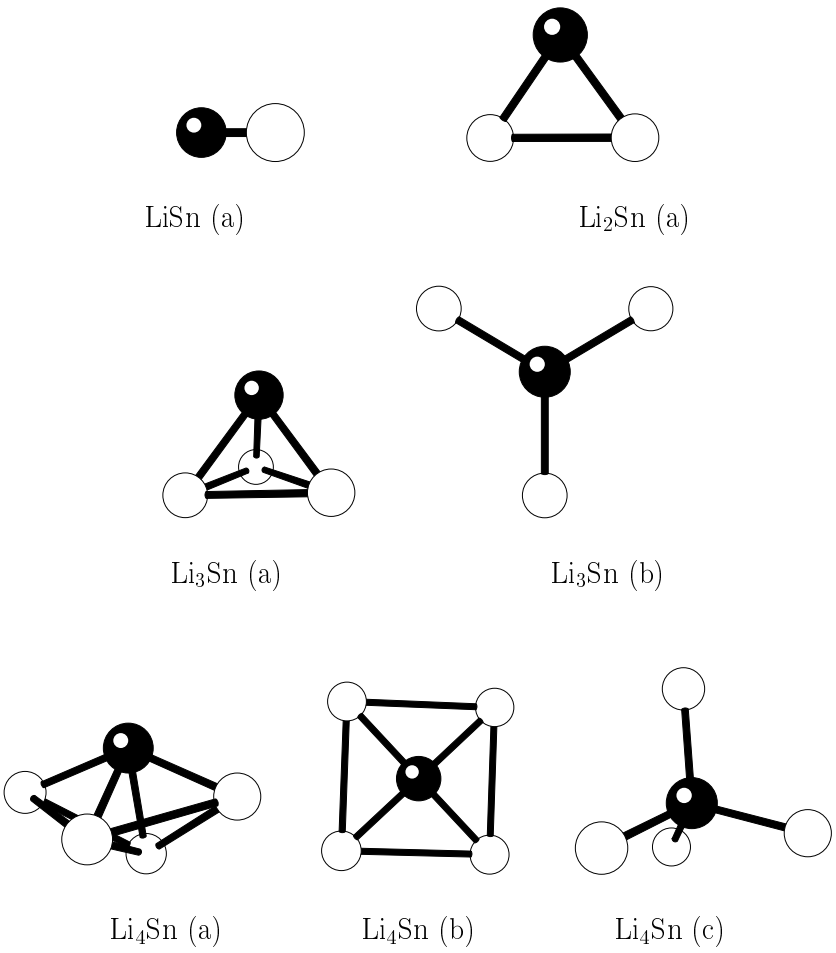

Fig. 3.1: Dark sphere represents the Sn atom and the white spheres represent the Li atoms. The equilibrium geometries of Li_nSn (n = 1 to 4). (a)Lowest energy structures. (b) and (c) Higher energy structures.

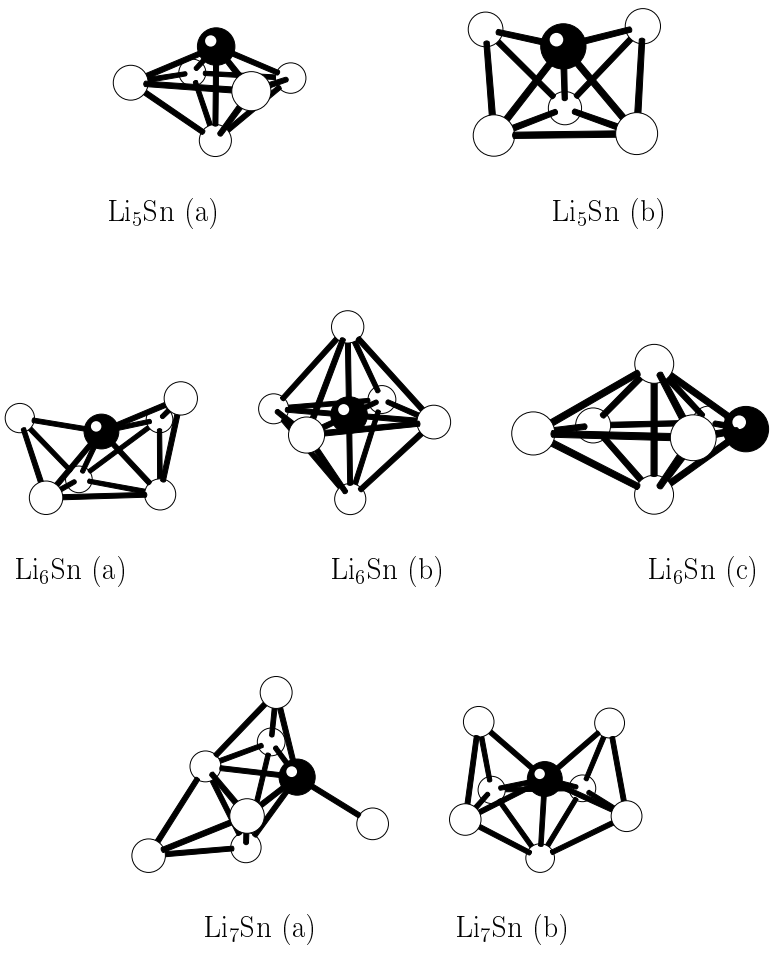

Fig. 3.2: Dark sphere represents the Sn atom and the white spheres represent the Li atoms. The equilibrium geometries of Li_nSn (n = 5 to 7). (a)Lowest energy structures. (b) and (c) Higher energy structures.

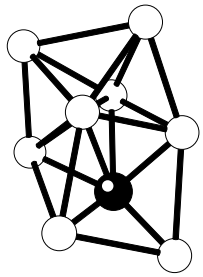

Li_8Sn (a)

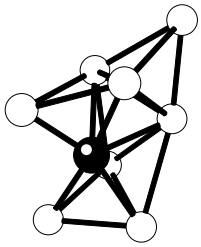

Li_8Sn (b)

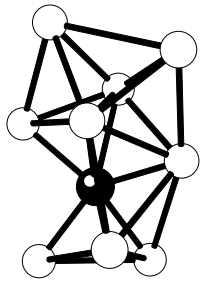

Li_9Sn (a)

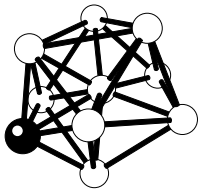

Li_9Sn (b)

Fig. 3.3: Dark sphere represents the Sn atom and the white spheres represent the Li atoms. The equilibrium geometries of Li_nSn (n = 8 and 9). (a)Lowest energy structures. (b) Higher energy structures.

orbital isosurfaces of some specific clusters. We see from the charge density isosurface of LiSn (Fig. 3.4 (a)) cluster that there is an almost complete charge transfer from Li to Sn showing an ionic bond between Li and Sn. However, ELF at 0.65 isosurface value of LiSn (Fig. 3.4 (b)) shows a localization domain between the Li-Sn bond and the localization region extends towards the Sn atom. At a higher isosurface value of ELF 0.75 (Fig. 3.4(c)), a localization region is seen between Li and Sn atoms, which reveals that Li strongly polarizes the p orbital of Sn atom and thus localization on the Sn atom becomes deformed. This is also due to the small electronegativity difference between the Li and Sn atom. In Li_2Sn cluster, the ELF at 0.65 isosurface value (Fig. 3.4(f)) shows a localization region between the two Li atoms, indicating a strong polarization of the p orbital of Sn atom by the two Li ions. Even at higher ELF values of 0.75 and 0.85 (Fig. 3.4 (g)) and (Fig. 3.4(h)) , respectively, the localization between the two Li atoms is clearly seen. This reveals that the charge is shared between the Li atoms and the Sn atom. Li_3Sn shows the same trend as Li_2Sn with the only difference that at ELF=0.65 (Fig. 3.4(j)) a strong localization region is identified at the center of the three Li atoms, indicating a three-centered bonding region. There is a sudden increase in the HOMO–LUMO gap (Table. 3.1) from Li_2Sn to Li_3Sn, showing stabilization in the Li_3Sn cluster which can be attributed to the participation of the p orbital of Sn atom. This indicates that the bonding in Li_3Sn is ionic. This gives rise to a three-dimensional structure. At ELF value of 0.85 (Fig. 3.4(l)). we see a bell-shaped localization over the Sn atom which is due to the polarization by the Li ions. It should be noted that although the Li_3Sn cluster is three-dimensional, the three Li atoms lie in one plane. This proves that the p orbital of Li atom does not participate in bonding. The change in the B.E. and the HOMO-LUMO gap are given in Table. 3.1.

As expected, the charge density isosurface of Li_4Sn shows a charge transfer from Li atoms to the Sn atom (Fig. 3.4 (m)). This can be understood from the ELF isosurface at 0.85 (Fig. 3.4 (p)) of Li_4Sn, where a semispherical localization region is seen on the Sn atom, indicating a higher localization region on the Sn atom. No localization region

is seen between the four Li ions and the Sn ion. This shows that an ionic bond exists between the four Li atoms and the Sn atom. We also see a localization region between the Li bonds, which also indicates that the charge on the Sn atom is strongly polarized by the four Li ions. Figure 3.5 shows the last three HOMO's of Li_4Sn. These HOMO isodensities reveal that the HOMO, HOMO-1, HOMO-2, are p_x, p_y , p_z orbitals of Sn atom, respectively. Thus, the charge transfer from Li to Sn is accompanied by a strong polarization of Sn-based orbitals by the electropositive Li atoms.

Due to the charge transfer from the 4 Li atoms to the Sn atom, the p_y and the p_z orbitals of Sn are filled and hence there is no hybridization of s and p orbitals. This is the reason that the Li_4Sn do not obey the octet rule and hence do not have tetrahedral geometry. This is in contrast to the earlier work, where it was shown that the Li_4 Sn obeys the octet rule. [117] Moreover, ELF of Li_4Sn reveals that Li atoms strongly polarize the charge on the Sn atom. From Table. 3.1, it is clear that the B.E. of Li_4Sn (1.693 eV/atom) is higher compared to the other clusters. Consequently, the HOMO–LUMO gap is also more compared to the other clusters. Hence, Li_4Sn proves to be the most stable cluster. Moreover, it should be noted that, there are 8 valence electrons in the Li_4Sn. Hence, indicating a "magic" cluster. From the bonding analysis it is clear that the bonding in Li_nSn ($n \leq 4$) is dominantly ionic. As the number of monovalent lithium atoms becomes more than 4, the interference with the resonance of the bond between the Li atoms is expected to increase, leading to an increase in the metallicity of the system.

The interesting bonding characteristic is seen in the clusters from Li_5Sn to Li_7Sn, where an intermediate bond between an ionic bond and a metallic bond is expected. Introduction of another Li atom in Li_4Sn will allow the Li_5Sn cluster to have an unpaired electron. The unpaired electron, which is free to move within the Li atoms, will give rise to a resonance showing metallicity within the Li atoms. Indeed, ELF 0.65 (Fig. 3.6 (b)) of Li_5Sn shows a delocalization cloud around the Li atoms which was not seen in the earlier clusters for Li_nSn ($n \leq 4$). However, ELF at 0.75 (Fig. 3.6 (c)) shows two

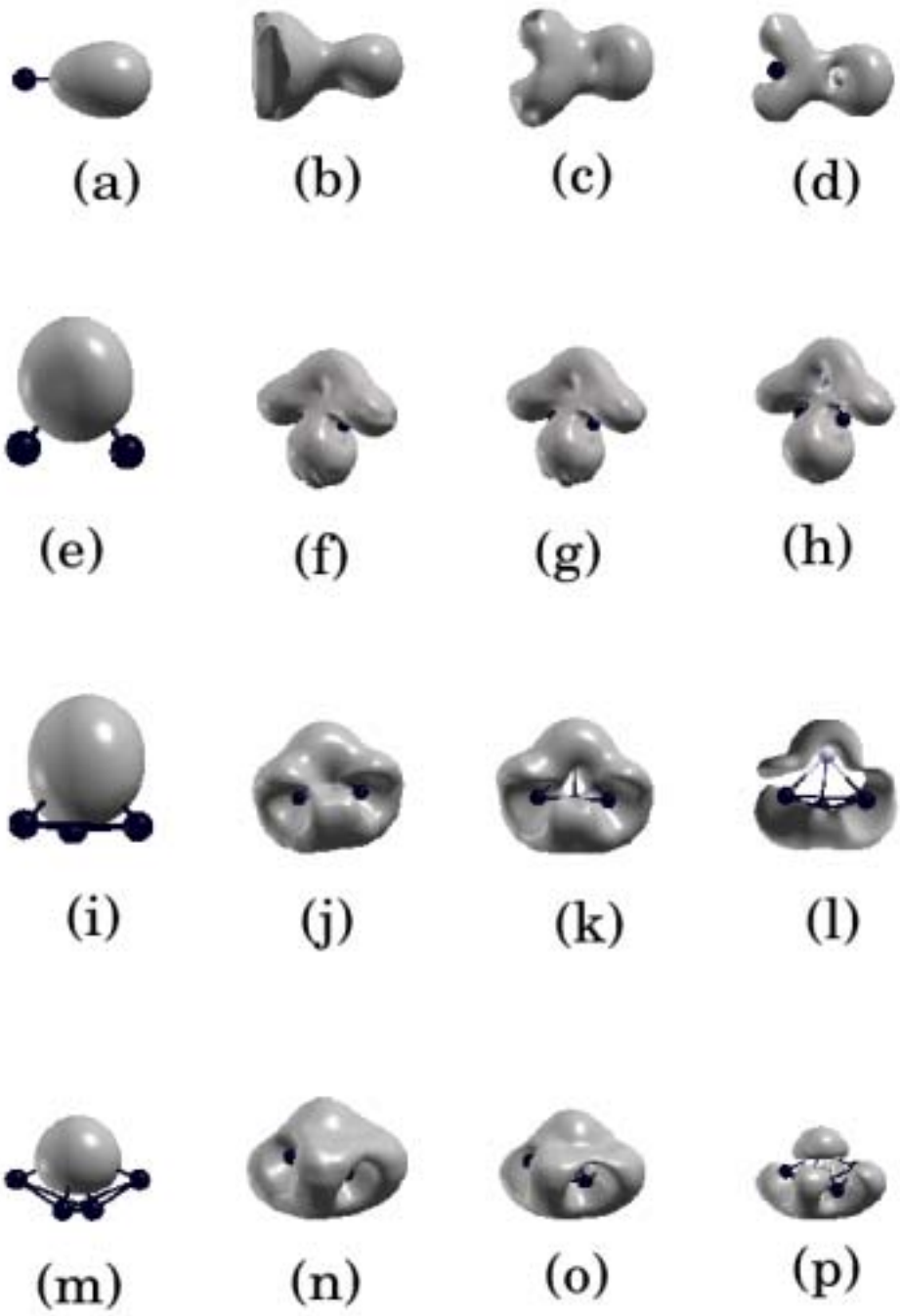

Fig. 3.4: Dark spheres represent the Li atoms and the white spheres represent the Sn atom. Charge densities and ELF isosurfaces of Li_nSn (n = 1 to 4) First column: The charge density isosurfaces of LiSn(a) to Li_4Sn (m) at 1/3 of the maximum value. Second column: The ELF at 0.65 isosurface value of LiSn (b) to Li_4Sn (n). Third column: The ELF at 0.75 isosurface value of LiSn (c) to Li_4Sn (o). Fourth column: The ELF at 0.85 isosurface value of LiSn (d) to Li_4Sn (p).

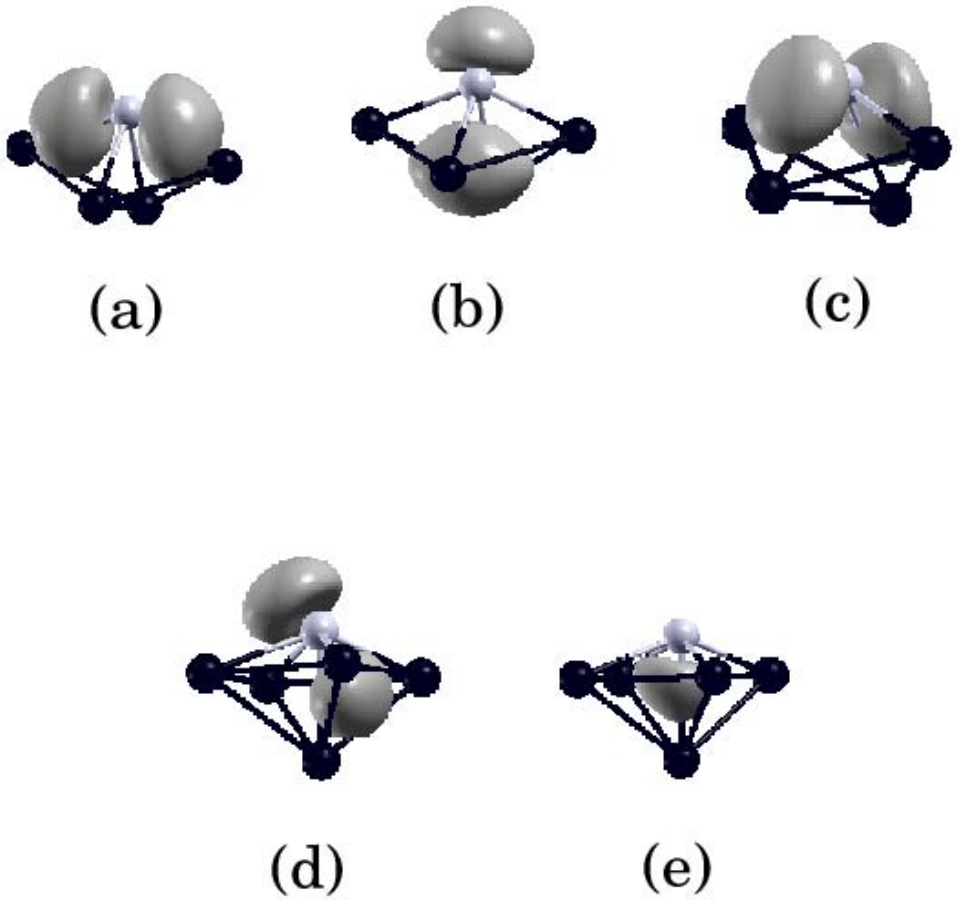

Fig. 3.5: HOMO isosurfaces of Li_4Sn and Li_5Sn clusters. (a), (b), (c) represent HOMO, HOMO–1, HOMO–2 of Li_4Sn, respectively. (d) and (e) represent HOMO, HOMO–1 of Li_5Sn, respectively. Dark sphere represents Li atoms and shaded atoms represent Sn atom.

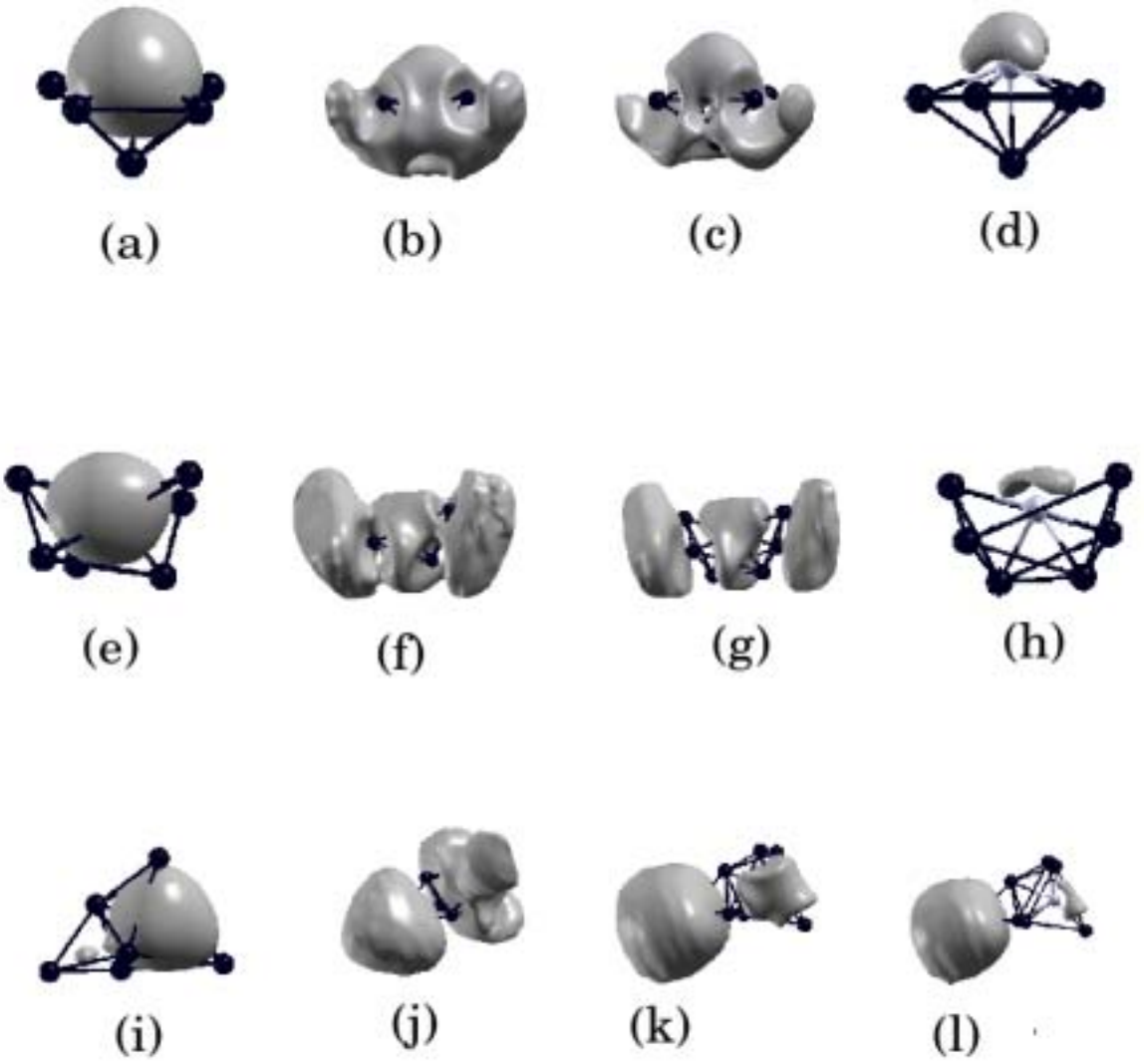

Fig. 3.6: Dark spheres represent the Li atoms and the white spheres represent the Sn atoms. Charge densities and ELF isosurfaces of Li_nSn (n = 5 to 7) First column: The charge density isosurfaces of Li_5Sn(a) to Li_7Sn (i) at 1/3 of the maximum value. Second column: The ELF at 0.65 isosurface value of Li_5Sn (b) to Li_7Sn (j). Third column: The ELF at 0.75 isosurface value of Li_5Sn (c) to Li_7Sn (k). Fourth column: The ELF at 0.85 isosurface value of Li_5Sn(d) to Li_7Sn (l).

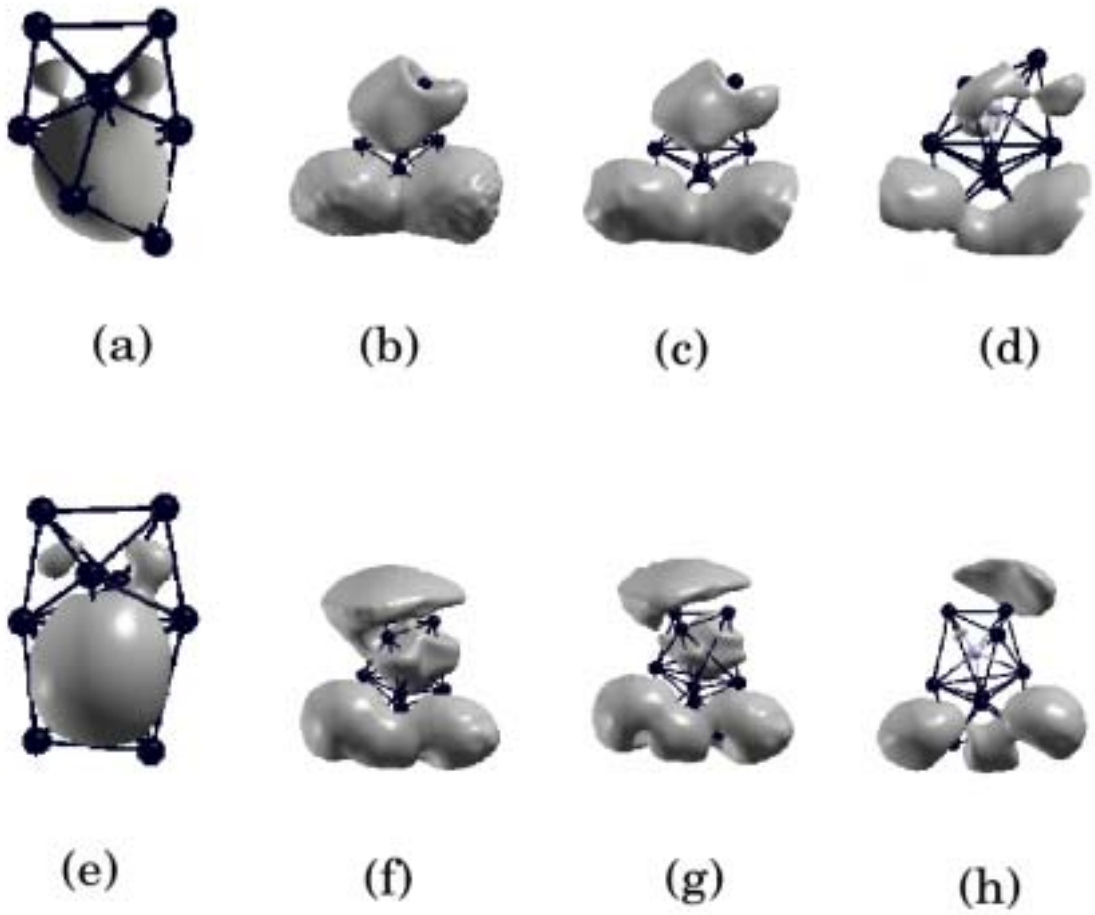

Fig. 3.7: Dark spheres represent the Li atoms and the white spheres represent the Sn atoms. Charge densities and ELF isosurfaces of Li_8Sn and Li_9Sn. First column: The charge density isosurfaces of Li_8Sn(a) and Li_9Sn (e) at 1/3 of the maximum value. Second column: The ELF at 0.65 isosurface value of Li_8Sn (b) and Li_9Sn (f). Third column: The ELF at 0.75 isosurface value of Li_8Sn (c) and Li_9Sn (g). Fourth column: The ELF at 0.85 isosurface value of Li_8Sn (d) and Li_9Sn (h).

Table 3.1: Calculated Binding energy (B.E.) and the HOMO–LUMO gap of Li_nSn (n≤9) are presented

Li_nSn	B.E. (eV/atom)	HOMO-LUMO GAP (eV)
LiSn	0.993	0.022
Li_2Sn	1.333	0.132
Li_3Sn	1.495	1.179
Li_4Sn	1.693	1.039
Li_5Sn	1.662	0.538
Li_6Sn	1.668	0.732
Li_7Sn	1.596	0.410
Li_8Sn	1.612	0.508
Li_9Sn	1.602	0.331

different regions of Li_5Sn system, a delocalization region around the Li atoms and a symmetric localized domain on the Sn atom. This shows a metallic bond between the Li atoms and an ionic bond between Li–Sn. An examination of ELF at 0.85 (Fig. 3.6 (d)) indeed shows a semispherical localization around the Sn atom, confirming the above observation. Deformation of the charge is clearly seen in the last HOMO (Fig. 3.5 (d)) of Li_5Sn cluster. The penultimate HOMO-1 (Fig. 3.5 (e)) shows a p-type orbital. This indicates that the Sn atom is behaving like a metal due to the high coordination of Li atoms around the Sn atom. It is interesting to note that although the B.E. does not change much in going from Li_4Sn to Li_5Sn (Table 3.1) there is a significant reduction in the HOMO-LUMO gap. This is consistent with the change in bonding character as a fifth lithium atom is added to the system. ELF of Li_6Sn (Fig. 3.6 (f) to (h)), shows the same trend as Li_5Sn, showing two regions of localization which are electron gas like and a region of localization on Sn atom. However, (Fig. 3.6 (h)) , depicting an ELF isostructure of 0.85, shows that the localization region on the Sn atom is deformed from its semispherical localization, which was seen for the Li_5Sn cluster (Fig. 3.6 (d)). In Li_7Sn cluster, Li atoms form a bond with the other Li atoms instead of bonding with the Sn atom, which is reflected in the structural behavior of Li_7Sn cluster, as discussed earlier. The spherical localization seen on one of the Li atom clusters (Fig. 3.6 (j))

shows that it remains isolated from the cluster and does not participate in bonding. The molecular orbital picture of Li_7Sn agrees with the ELF. In the last HOMO, Fig. 3.8 (a), we also see electron cloud on three Li atoms showing a metallic characteristic, and also the lower HOMO-1, Fig. 3.8 (b), shows a delocalization in some of the Li atoms. The low B.E. and the HOMO–LUMO gap (Table 3.1) shows high instability in the system. This is due to the formation of an ionic-metallic intermediate bond in the cluster. The ELF isosurface at 0.65 for Li_8Sn (Fig. 3.7 (b)) and Li_9Sn (Fig. 3.7 (f)), shows a high delocalization characteristic over the Li atoms, indicating a high metallicity in the system.

In Li_8Sn and Li_9Sn clusters, the localization in the interstitial region of Li atoms is due to the maximum participation of p orbitals and gives rise to p-π interactions between the Li atoms, leading to a multicenter bonding between the Li atoms. HOMO (Fig. 3.8 (c)) clearly shows that the Li atoms are participating in multicenter bonding and the delocalization cloud seen below the Li atoms is due to the participation of p orbitals in bonding. We also see two to three center bonding in HOMO-1 (Fig. 3.8(d)). The p-π interaction in Li_n ($n \leq 4$) clusters have been studied and it has been proven that the multicenter bonding arises due to the p-π interactions. The B.E. and the HOMO–LUMO gap of Li_8Sn and Li_9Sn are given in Table 3.1, which shows characteristics of a metallic system. We have also performed spin-polarized calculations on clusters from Li_5Sn to Li_9Sn to understand the change in the HOMO–LUMO gap. We found that the Li_6Sn and Li_8Sn clusters show pairing of electrons and hence a stability in the system with a higher HOMO–LUMO gap, whereas Li_nSn (n=5, 7, 9) has an unpaired electron and shows less stability in the system (Table 3.1). This is evident from the fact that the even electron clusters are more stable than the odd electron clusters. In the above clusters we see three types of bonding characteristics. LiSn to Li_4Sn shows a dominantly ionic bond in the system. Li_5Sn to Li_7Sn shows an intermediate bond between an ionic and a metallic bond in the system, while Li_8Sn and Li_9Sn show a metallic characteristic due to a multiple bonding in the Li atoms. We show from the above description that

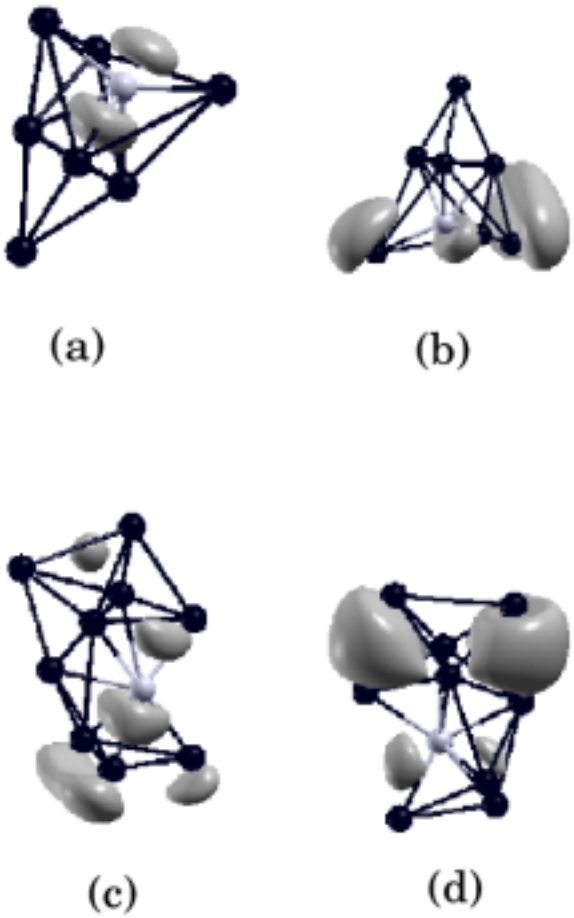

Fig. 3.8: HOMO isosurfaces of Li_7Sn and Li_9Sn clusters. (a), (b) represent HOMO, HOMO–1 of Li_7Sn, respectively. (c) and (d) represent HOMO, HOMO–1 of Li_9Sn, respectively. Dark sphere represents Li atoms and shaded atoms represent Sn atom.

ELF plays a significant role in studying the different types of bonding features in a chemical system, which cannot be explained by charge density alone.

3.3.3 Structural Properties of Al_4X_4 (X=Be, Mg, B, Si)

The ground state and the excited state geometries of aluminum based binary clusters are shown in Fig. 3.9 and Fig. 3.10. The ground-state geometries of Al_4Be_4 (a), (Fig. 3.9) and Al_4Mg_4 (a), (Fig. 3.9) have a similar structure with a capped quinted roof. The excited state structures of Al_4Be_4 (b), (Fig. 3.9) and Al_4Mg_4 (b), (Fig. 3.9) are 0.17 and 0.15 eV higher in energy than their respective ground states. The ground-state structure of Al_4B_4 (a) (Fig. 3.10), is also a quinted roof with only the difference that the inner core of Al atoms is replaced by the B atoms. The excited state structure of Al_4B_4 (b), (Fig. 3.10), is just 0.01 eV higher in energy than its ground-state structure. Substitution of a semiconductor atom such as Si to form Al_4Si_4 (Fig. 3.10) shows an interesting structure, with a distorted hexagon having D_{3d} symmetry with symmetrically capped by the other two Si atoms. The excited state structure of Al_4Si_4 (b), shows a different capping, and also the geometry is asymmetric compared to the ground state.

3.3.4 Bonding and Energetics of Al_4X_4 (X=Be, Mg, B, Si)

Fig. 3.11 and Fig. 3.12 shows the ELF and the charge density isosurfaces of the aluminum based binary clusters. We can clearly see that the ELF isosurface of Al_4Be_4 at 0.85 isovalue (Fig. 3.11(b)) shows a horse-shoe like extended localization region indicating a lone pair of electrons on the Al atoms. In earlier studies this kind of localization was detected for the lone pairs on the oxygen atoms in organic compounds. [105] ELF plots of Al_4Be_4 show a charge transfer from Be to Al, which can also be predicted from the large HOMO–LUMO gap of 2.018 eV (Table 3.2). ELF isosurface of 0.85 clearly shows that the lone pair has p character. At a smaller ELF value (0.78, 0.76) the electron density gets delocalized around the Al atoms. Even the molecular orbital pictures of Al_4Be_4 show the same trend. The last HOMO (Fig. 3.13(a)) shows a lone

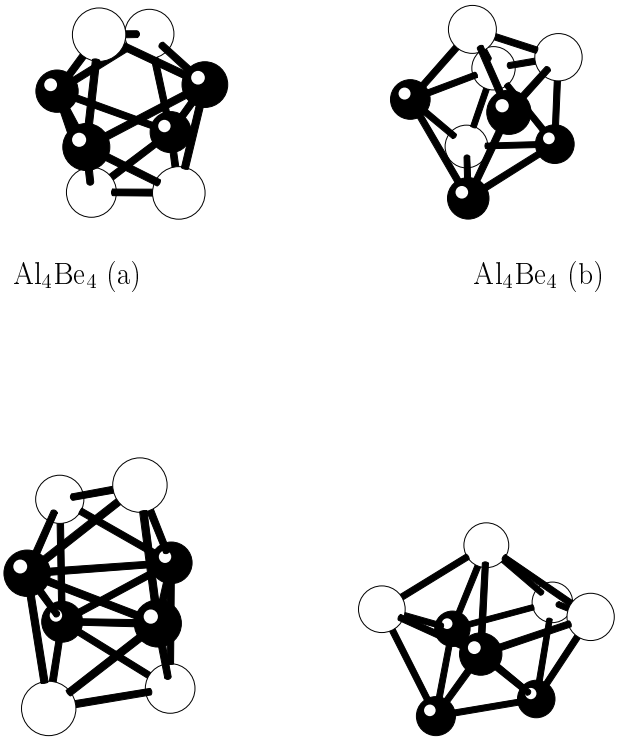

Fig. 3.9: Dark spheres represent the Al atoms and the white spheres represent the X (Be, Mg) atoms. The equilibrium geometries of Al_4X_4 (X = Be, Mg). (a) Lowest energy structures. (b) Higher energy structures.

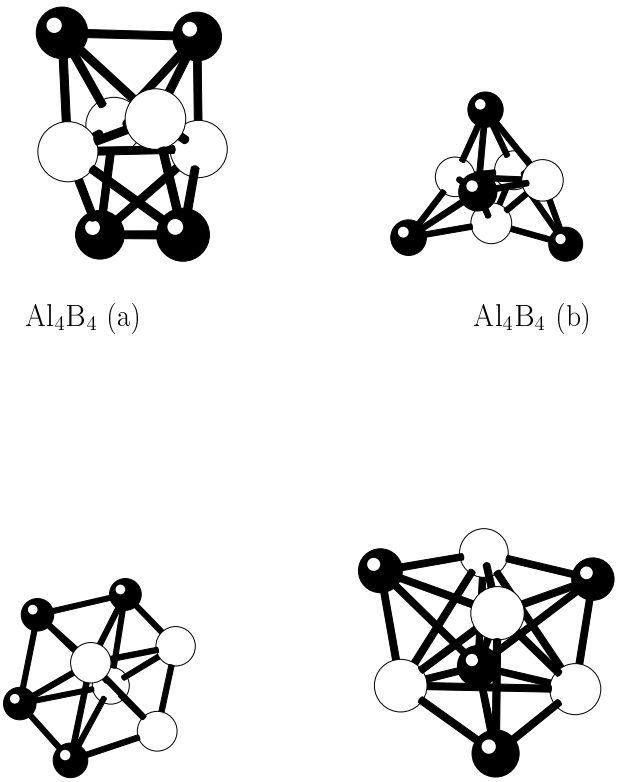

Fig. 3.10: Dark spheres represent the Al atoms and the white spheres represent the X (B, Si) atoms. The equilibrium geometries of Al_4X_4 (X = B, Si). (a) Lowest energy structures. (b) Higher energy structures.

Table 3.2: Calculated Binding energy (B.E.) and the HOMO-LUMO gap of Al_4X_4 (X = Be, Mg, B, Si) are presented

Al_4X_4	B. E.(eV/atom)	HOMO-LUMO gap(eV)
Al_4Be_4	1.921	2.018
Al_4Mg_4	1.328	1.358
Al_4B_4	3.056	0.930
Al_4Si_4	2.893	2.145

pair of electrons on the Al atoms of p characteristic. In addition, at 0.83 isovalue (Fig. 3.11(c)) there is a localization region found between the two Al pairs, indicating a covalent bond between them. As the ELF isovalue is decreased ELF 0.78 (Fig. 3.11(d)), the localization region of the lone pair starts to interact with the covalent bond of the Al. This leads to the deformation of the ELF distribution around the Al atoms (Fig. 3.11(e)). Interaction of such lone pair of electrons with the covalent bond has been seen for methyl acetate compounds. At ELF isovalue of 0.78, (Fig. 3.11(g)), there is a build-up of localization between the Mg–Mg and Al–Mg atoms showing a covalent bond. Surprisingly, no localization region is seen between the Al atoms. At ELF 0.77 (Fig. 3.11(h)), Al form bonds with the other pair of Mg atoms, showing a multiple bonding characteristic. At a different orientation of the cluster (Fig. 3.11(i)) we still see that there is no bond between the Al atoms. Unexpectedly, at 0.7 isovalue of ELF (Fig. 3.11(j)) very weak bonds crossing each other are seen between the Al atoms. This may be due to the contribution of p orbitals of Al, which cause the electrons to localize in the interstitial region. This shows that there exists a multicenter bonding in the cluster. The decrease in the B.E. and the HOMO–LUMO gap, (Table 3.2), of Al_4Mg_4 can be attributed to the p-orbital contribution of Al atoms leading to a localization in the interstitial region. It is seen from the above discussion that, although Al_4Be_4 and Al_4Mg_4 cluster show similarity in their structures, they differ in their bonding.

Figures 3.11 and 3.12 show the ELF isosurfaces for Al_4B_4 and Al_4Si_4 clusters. ELF of Al_4B_4 at 0.75 isosurface value (Fig. 3.12 (b)) shows a strong covalent bond between the Al–Al. The bond between Al–B is clearly polarized in the direction of the

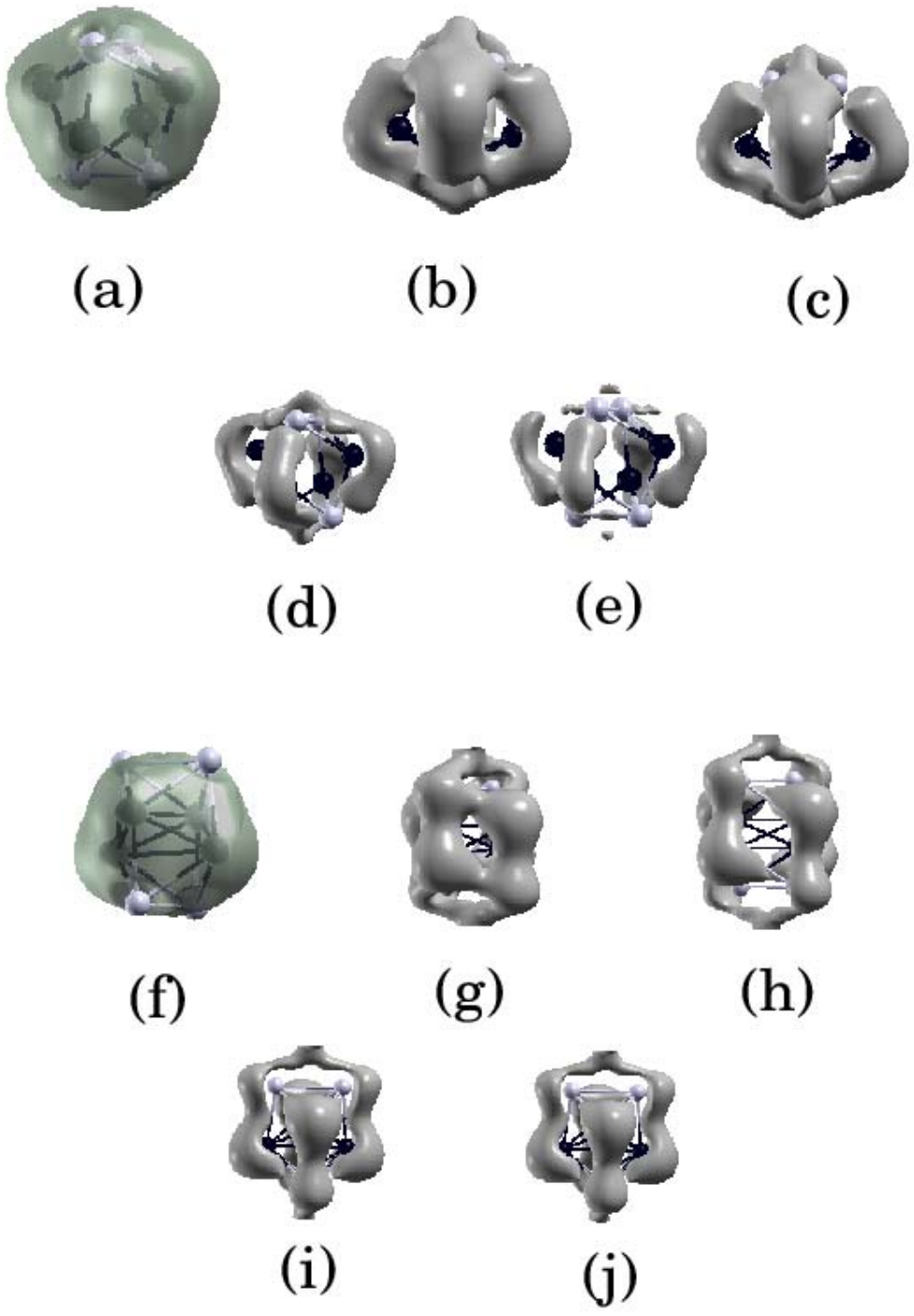

Fig. 3.11: Black spheres represent the Al atoms, while white spheres represent the X (Be, Mg) atoms. Charge densities and ELF isosurfaces of Al_4Be_4 and Al_4Mg_4 clusters. (a) Charge density isosurface at one third of its maximum isosurface value. (b) ELF at 0.85. (c) ELF at 0.83. (d) ELF at 0.78. (e) ELF at 0.76. (f) Charge density isosurface at 1/3 rd of its maximum isosurface value. (g) ELF at 0.78. (h) ELF at 0.77. (i) ELF

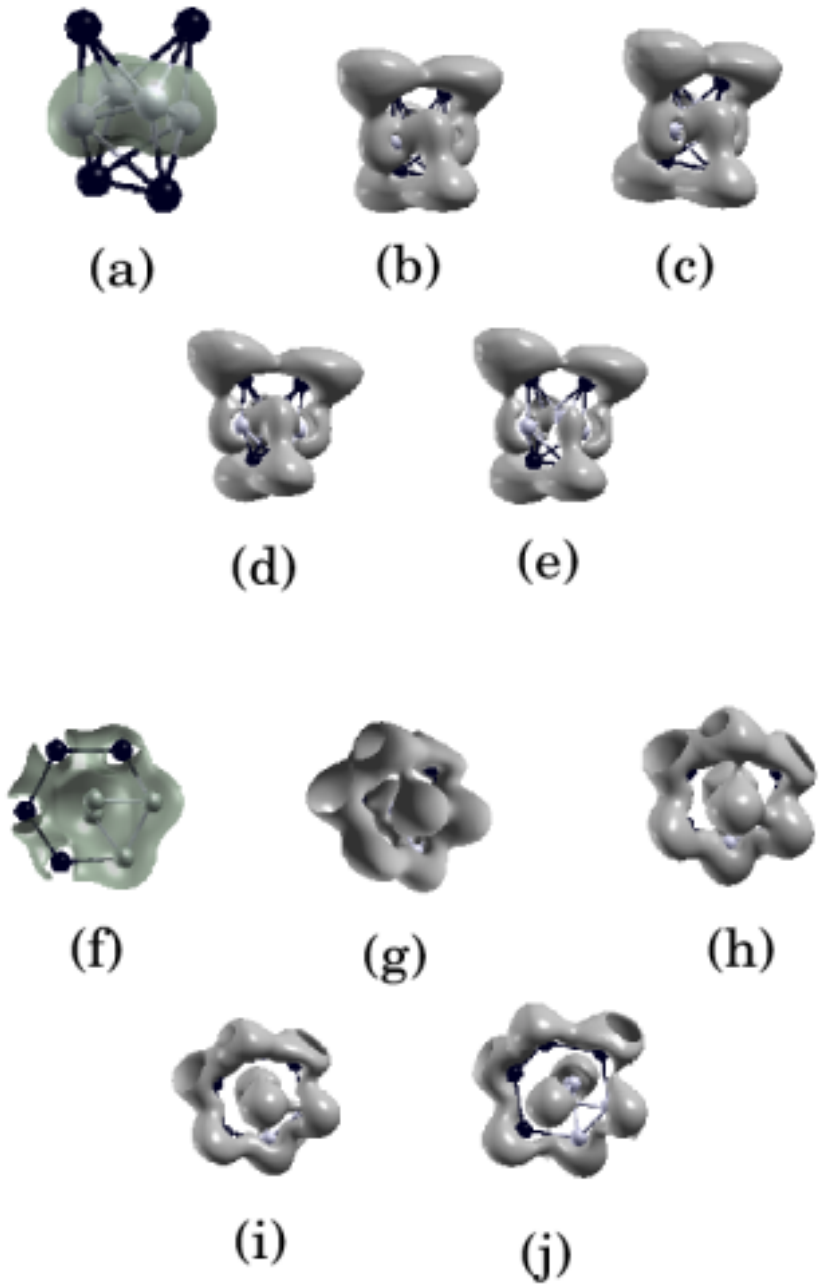

Fig. 3.12: Black spheres represent the Al atoms and the white spheres represent the Li atoms. Charge densities at 1/3 rd of their maximum isosurface values and ELF isosurfaces of Al4B4 and Al4Si4 cluster. (a) Charge density isosurface of Al_4B_4. ELF of Al_4B_4 are as follows: (b) ELF at 0.75. (c) ELF at 0.73. (d) ELF at 0.72. (e) ELF at 0.69. (f) Charge density isosurface. ELF of Al_4Si_4 are as follows: (g) ELF at 0.8. (h) ELF a 0.72. (i) ELF at 0.65. (j) ELF at 0.62 at a different orientation.

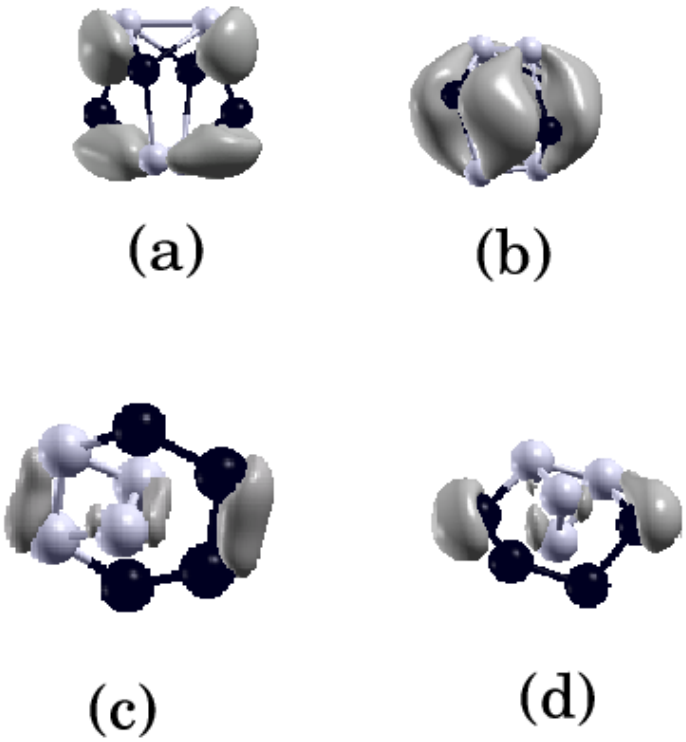

Fig. 3.13: HOMO isosurfaces of Al_4Be_4 and Al_4Si_4 clusters. (a), (b) represent HOMO, HOMO–1 of Al_4Be_4, respectively. (c) and (d) represent HOMO, HOMO–1 of Al_4Si_4, respectively. Dark sphere represents Al atoms and shaded atoms represent X (Be, Si) atoms.

electronegative B atoms, hence indicating a polar bond between Al–B. This arises due to the higher percentage of ionicity in the intermediate ionic–covalent bond. Electronegative boron atoms occupy the inner core of the Al_4B_4 cluster, and the decrease in the interatomic distance within the B atoms is reflected in the increase in the B.E. of the system. Although B is more electronegative than Al, it is surprising to see from the ELF graphs, electron localization region is also seen on the Al atoms. A charge density plot of Al_4B_4 clearly shows that most of the charge is on the B atoms.

An interesting bonding region is found in the structure of Al_4Si_4. The charge density isosurface of Al_4Si_4 (Fig. 3.12(f)) shows that the charge density is shared between Si atoms and the Al atom. However, ELF also shows the same trend. At the ELF value of 0.8, (Fig. 3.12 (b)) , we see that there is covalence in the system arising due to the covalent bonding between Al–Al, Al–Si, and Si–Si which is along the distorted hexagon ring (D_{3d}) symmetry in the system. A more careful look at the plot of ELF isosurface of 0.72 (Fig. 3.12(h)) shows that the two Si atoms capped on the hexagon ring prefer to bond with the Si atoms rather than with the Al atoms. But, at a lower ELF value 0.65 (Fig. 3.12(i)), we see a weak bond formed between the capped Si atoms and the Al atoms in the ring. At a low ELF value 0.62, (Fig. 3.12(j)), no multicenter bonding is seen in the cluster. The HOMO (Fig. 3.13(c)) of Al_4Si_4 cluster clearly shows that the two Al atoms and two Si atoms show a sidewise p_y -type overlap. It is also seen that the electrons on the capped Si atoms interact with the bond- ing electrons in the ring. This is exactly what is inferred from the ELF picture (Fig. 12 (h)). This clearly implies that a strong covalency exists in the Al_4Si_4 cluster. This strong co- valency in the system is due to the fact that the Si atoms induces covalency in the Al–Al bonds and Al atoms mimic the behavior of Si atoms. Since the Si atom is more electronegative than the Al atom, one expects that the Si atoms in Al_4Si_4 cluster should occupy the central position, as it was seen for a single Si atom impurity in Aln clusters studied earlier. However, in Al_4Si_4 cluster we see that the cluster opens in a more symmetric ring with a D_3d symmetry and two Si atoms capped on it. This is due to the higher

atomic radius of Si.

3.4 Conclusion and Scope

Our study throws light on the intuitive concept of bonding in two different classes of heteroatomic metal clusters using quantitative approach to ELF, charge density, and valence molecular orbital isosurfaces. In the present work we show with the help of ELF predominantly an ionic bond in Li_nSn ($n \leq 4$) clusters, an unstable ionic metallic bond in the Li_nSn (n=5, 6, 7) clusters, and metallic bonding in Li_8Sn and Li_9Sn clusters. The other class of compounds Al_4X_4 (X = Be, Mg, B, Si) shows a different kind of bonding nature. Although Al_4Be_4 and Al_4Mg_4 clusters show the same structural properties, bonding in Al_4Be_4 cluster exhibits a lone pair of electrons, while a multicenter bonding is seen in the Al_4Mg_4 cluster. In Al_4B_4 cluster a polar covalent bond exists between the Al and B. However, Al_4Si_4 cluster is seen to behave as a covalently bonded system. Our study throws light on the intuitive concept of bonding in two different classes of heteroatomic metal clusters using quantitative approach to ELF, charge density, and valence molecular orbital isosurfaces.

Chapter 4

Structure, Bonding and Magnetic Properties of Metallo–anti–aromatic Compounds

Abstract:

In the present work, we discuss the concept of anti-aromaticity on the basis of structural, bonding, electronic and magnetic properties in all-atom-metal clusters *viz.* Al_4Li_4, Al_4Na_4 and anionic $Al_4Na_3^-$. The structural, electronic and bonding properties of the metal clusters reveal that the Al_4 unit in Al_4Li_4, Al_4Na_4 and $Al_4Na_3^-$ clusters has 4 π–electrons and has a rectangular structure with alternate π bonds. Hence, saitisfying the criteria of anti-aromaticity. However, the magnetic ring current analysis shows that the Al_4 system has a paratropic π ring current, satisfying the anti–aromaticity and addition to this a σ diatropic ring current showing σ aromaticity.

4.1 Introduction

Aromaticity and anti-aromaticity are well-established concepts in the field of organic chemistry. [54] Aromaticity of a molecule is discussed in terms of Hückel's rule, [55] which suggests that a planar monocyclic hydrocarbon with complete cyclic delocalization of (4n+2) π–electron, where n is an integer, will be aromatic. Additional stabilization caused by the cyclic electron delocalization represents the most important feature of the aromatic character of a compound. Various properties resulting from these cyclic

electron delocalization have been used to establish indices of aromaticity. There is no unique and generally accepted definition of aromaticity. However, in the last few decades, it has been generally accepted that aromaticity is associated with the ground state properties of cyclic π electron compounds which (i) are more stable than their chain analogues (resonance energy) (ii) have intermediate bond lengths between single and double bonds (bond equalization) and (iii)ability to sustain diamagnetic ring current that is induced when the system is exposed to the external magnetic field. Benzene is considered to be the prototypical aromatic molecule and based on it [54], the above attributes of aromaticity have been proposed. However, there have been contrary opinions regarding the definition of aromaticity. Some have proposed that it is the σ–electron delocalization that makes benzene a regular hexagon and that the π–electrons would prefer a D_{3h} distorted structure. [124] The best choice of indicators of aromaticity and the relationship between these different quantities (i.e., their orthogonality or nonorthogonality) is still a matter of debate. [125, 126] Schleyer *et al* . [125] claimed that, linear relationships do exist among the energetic, geometric, and magnetic properties of aromaticity. Such effects manifest in broad varieties of π conjugated organic and organometallic ring systems, for which reason aromaticity as a theoretical concept appears to be among the most widely used in organic chemistry.

Apart from the aromaticity, there are two more classes, in which π conjugated systems can be further divided, *viz.* non-aromaticity and anti–aromaticity. Both the later classes do not follow the Huckel's (4n+2) rule, and have 4n π–electrons. The origin of anti–aromaticity and non–aromaticity is somewhat elusive. If we restrict ourselves to the conventional definition of anti–aromaticity, then it is known that if the system is planar with 4n π–electrons and is destabilized due to the electron delocalization, it will be antiaromatic, e.g., cyclobutadiene. [127]–[130] As a consequence, anti-aromatic compounds favors bond alternation in their ground state. On the other hand, if the system with 4n π–electrons buckle to become nonplanar, it is known to lose the anti–aromaticity and the system would be non–aromatic. As an example cyclooctatetraene

can be cited. [131] Nevertheless, the property of anti–aromaticity has attracted continued attention for its unusual behavior, such as instability, magnetic properties and high reactivity compared to aromatic systems. Cyclobutadiene is a well-known example of anti–aromatic compounds. In the last few decades, various attempts have been made to understand these properties using quantum chemical calculations. [130] Despite of wide applications of aromaticity and anti–aromaticity, a key question has always been raised, whether these properties are applicable outside the regime of organic chemistry?

However, in recent years, researchers have made an attempt to answer the above question by investigating the existence of aromaticity in organometallic compounds and metal clusters. [56] In a combined experimental and theoretical work, Li *et al.*, have shown aromaticity for the first time in all-metal atom clusters, e.g., MAl_4^- and M_2Al_4 (M = Li, Na, and Cu), [35] thus, opening a new branch of metallo-aromatic compounds. They extended their investigation to find more metallo–aromatic compounds such as, MAl_3^- (M = Si, Ge, Sn, Pb). [132]

Moreover, the Al-Li compounds have been extremely useful in the industrial applications. The Al-Li alloys form very strong and light alloy. Hence, are used for aerospace engineering. [133] Recently, it has been shown that, when the Li is alloyed with Al, they form very efficient electron injecting devices and can be used as cathodes in OLED's. [134, 135]

In the present chapter, we discuss the structural, electronic, bonding and magnetic properties of some metallo–anti–aromatic compounds *viz.* Al_4Li_4, Al_4Na_4, $Al_4Na_3^-$ clusters. The chapter has been organized as follows, in Section 4.1, we discuss the computational details, Section 4.2 is results and discussion, where we present subsections on structural, electronic, bonding and magnetic properties.

4.2 Computational Details

Search for the ground state geometries of Al_4Li_4, Al_4Na_4, clusters have been carried out in two steps. Initially, we have used BOMD based on Kohn–Sham formulation of DFT using damped equations of motion to obtain the equilibrium geometries. [121] Structure of the Al_4 metal cluster was already known from the earlier studies. Starting with the random distribution of alkali atoms around the Al_4 system, they were heated upto 600–900 K followed by slow cooling. We have chosen box length of 20 Å. In this case also we have used the norm–conserving pseudopotential of Bachelet *et al.*, [122] in Kleinman and Bylander form [123]. The equilibrium geometries were again optimized by conjugate gradient method.[1] The structures were considered to be converged when the forces on all the atoms were less than 10^{-5} eV/Å. In the second step these systems were reoptimized using MP2 method using 6–31G(d,p) basis sets. Further, the clusters were refined using CCD/6–31G(d,p) level. Surprisingly it was seen that, in the case of Al_4Na_4 the ground state and the excited state structures obtained through BOMD were reversed in the second step of optimization.

For the magnetic properties calculations, only the Al–Li systems belonging to the metallo-aromatic and anti-aromatic systems were optimized at the RHF level of theory using 6-31++G(3df) with GAMESS–UK. [136] The resulting geometries were in excellent agreement with those previously reported.

Induced current density was calculated for all six structures using the ipsocentric CTOCD-DZ method, using SYSMO package, [137] in these calculations the magnetic field was directed perpendicular to the Al_4 plane, and current density maps were plotted in a plane and a0 above that plane, except where stated otherwise. Diatropic (diamagnetic) current is shown as anti–clockwise circulation in the maps, and paramagnetic current as clockwise.

[1]The optimization techniques have been explained in Chapter 2

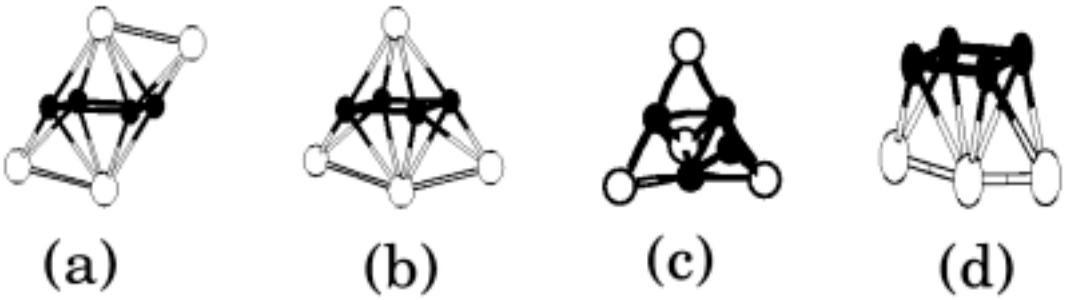

Fig. 4.1: Ground state structure of (a)Al_4Li_4, (b)Al_4Na_4 and excited state structure of (c) Al_4Na_4. Ground state structure of (d)$Al_4Na_3^-$: Black spheres indicate the Al atoms and the white spheres indicate the X (Li and Na) atoms

4.3 Results and Discussion

4.3.1 Structure and Energetics

Table 4.1 present the geometrical parameters of Al_4Li_4, Al_4Na_4, $Al_4Na_3^-$ clusters. Fig. 4.1 shows the optimized ground and the excited state geometries of the clusters obtained from the *ab initio* calculations. Table 4.2 presents the ground state energy and the HOMO–LUMO gap of the clusters. The ground state structure of Al_4Li_4 cluster is a capped octahedron (Fig. 4.1(a)) with four Al atoms forming a rectangular planar structure with two of its bond length being 2.835 Åand the other two are 2.690 Å. This is in contrast to the Al_4 structure found in the metallo–aromatic Al_4Li_2 cluster, where the Al_4 possesed a square planar structure. Hence, follows the bond equalization criteria for aromaticity. On the other hand, the Al_4 structure, found in the Al_4Li_4 cluster, has bond alternation and satisfies one of the criteria of anti-aromaticity. [129] The Al_4Na_4 and the $Al_4Na_3^-$ clusters are also a capped octahedron with two of their Na atoms capping differently than the Li atoms in the Al_4Li_4 cluster. Similar to the Al_4 structure in Al_4Li_4 system, the Al_4 in Al_4Na_4 and $Al_4Na_3^-$ clusters has a rectangular geomtery. The bond lengths of the Al_4 are given in Table 4.1.

Table 4.1: The Al-Al bond lengths of the Al_4 unit of the optimized ground state of Al_4Li_4, Al_4Na_4, $Al_4Na_3^-$ clusters

Al_4X_4	Al-Al (long)	Al-Al (short)
Al_4Li_4	2.835	2.690
Al_4Na_4	2.852	2.680
$Al_4Na_3^-$	2.443	2.288

Table 4.2: The Energies and the Difference between the HOMO and the LUMO for Ground and Excited States of the Al_4Li_4 and Al_4Na_4 Cluster and the Ground State of the $Al_4Na_3^-$ Cluster obtained through Coupled-Cluster Calculations

Al_4X_4	Total Energies (Hartrees)	HOMO-LUMO gap (eV)
Al_4Li_4	-997.5914	4.520
Al_4Na_4	-1615.2049	4.042
$Al_4Na_3^-$	-1435.0128	1.240

This excited state geometry of Al_4Na_4 (Fig. 4.1(c)) is seen to form a quinted roof with buckled Al_4 unit and is 4–5 kcal/mol higher in energy than the ground state. The Al_4 structure in the anion $Al_4Na_3^-$ was found to have a rectangular structure, unlike the distorted Al_4 unit found in the $Al_4Li_3^-$ system. This is due to the symmetric capping of Na atoms around the Al_4 unit of the anion. Surprisingly, the Al_4 unit in the $Al_4Na_3^-$ contracts, compared to Al_4Na_4 system. It is very interesting to see that, in these systems the Al_4 unit occupies the interstitial position in the whole cluster and attains a rectangular geometry.

It can be seen from Table 4.2, the HOMO-LUMO gap of Al_4Li_4 cluster is higher than the Al_4Na_4 and $Al_4Na_3^-$ clusters. Hence, Al_4Li_4 can be supposed to be more stable than the other two clusters.

4.3.2 Bonding

The electronic configuration of Al atom is $3s^23p^1$ and hence, its a trivalent atom with 3.6 eV gap between the filled 3s level and the partially filled 3p levels in the atom. In addition the core is less shielded in Al, so the interaction of the electrons with the core

will be stronger. It is very well known that, Al bulk is a free electron metal. Thus, the electronic structure of the Al clusters were expected to be described by the jellium model. For the delocalization of the electron density in the Al metal, one of the 3s electron should be promoted to a 3p orbital. Hence, leading to hybridization of 3s and 3p orbitals. However, in small clusters the hybridization of 3s and 3p orbitals is not expected, which is due to the large 3s-3p energy separation. [138] Thus, one should expect a transition from localized to a delcoalized state at a particular cluster size, as the 3s and the 3p orbitals hybridize due to change in the cluster size. Li *et al.*, proved by electron spectroscopy that the 3s and 3p orbitals hybridize around the Al_8 to Al_{10} and marks the transition from localized to delocalized state. [138] As a consequence of the s-p mixing, 2D to 3D transition occurs in the Al_n ($n \geq 6$) clusters.

In the present work, the Al_4 system is mixed with alkali atoms (Li, Na) to give Al_4Li_4, Al_4Na_4, $Al_4Na_3^-$ clusters. The hybridization of the s and p orbitals in the Al atoms of these systems may be considered as sp^2, leaving one empty unhybridized p orbital on each Al atom in the Al_4 species. Despite, small differences in the ionization potentials of Al and alkali atoms, earlier studies have shown that in these classes of heteroclusters, the more electronegative atom occupies the interstitial position and behaves as a single entity or a sub-cluster and can be described as a superatom. [51, 139] It is very well-known that as the atomic size decreases, its electronegativity increases. Formation of superatom allows the atoms to come closer and hence increases its electron affinity. In the present study Al_4 behaves as superatom. This arrangement of the Al_4 superatom in the Al_4Li_4, Al_4Na_4 and $Al_4Na_3^-$ clusters allow the less electronegative alkali atoms to donate their one valence electron ($2s^1$) to the unoccupied p_z orbital of the four Al atoms in the Al_4 superatom. This charge transfer from the alkali atoms to the Al_4 unit, provide the necessary 4 π–electrons for satisfying the criteria of anti-aromaticity. It should be noted that, if there is no formation of Al_4 superatom than there is no charge transfer from the alkali atoms and no aromaticity or anti-aromaticity would exist in the above mentioned Al based alkali metal clusters.

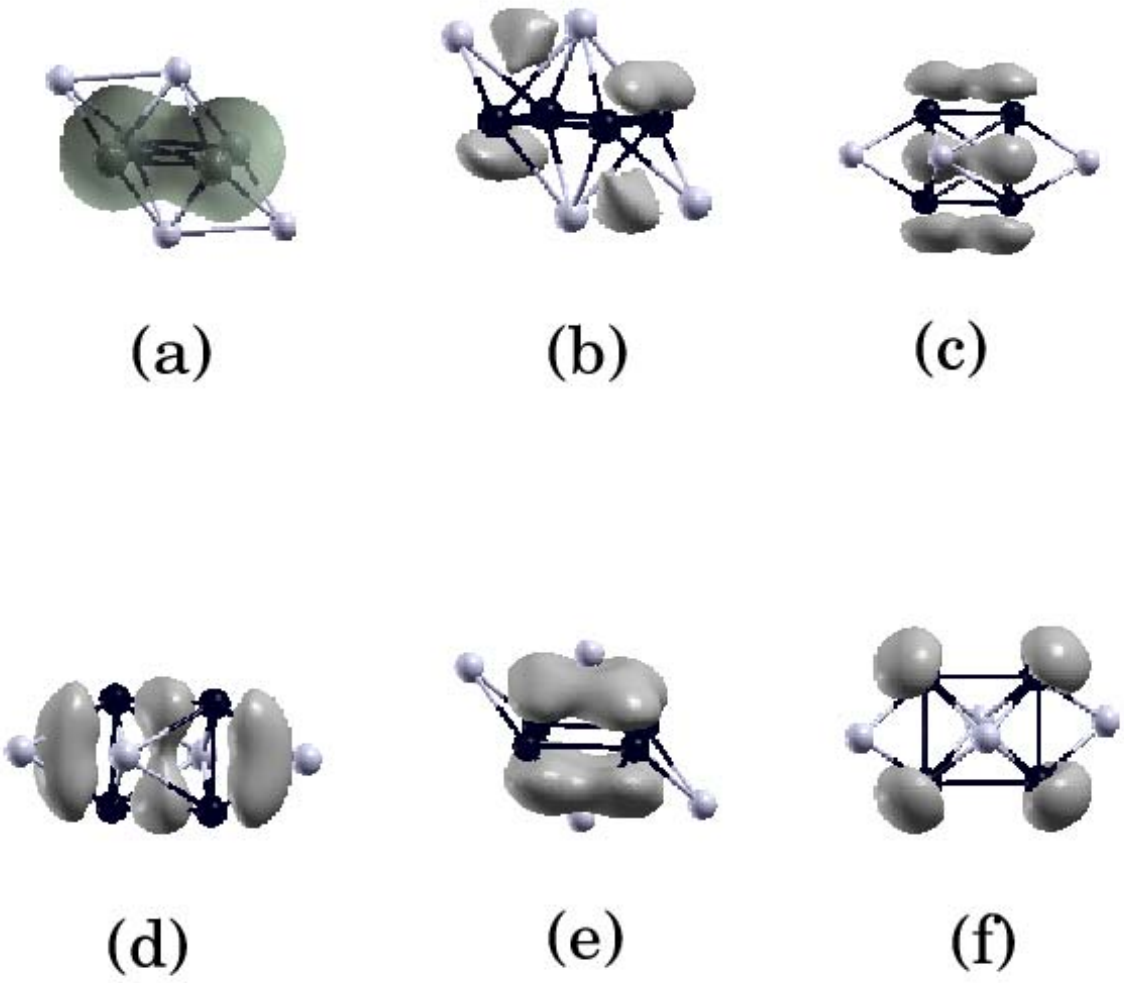

Fig. 4.2: Charge density, HOMO isodensities of Al_4Li_4. (a) Charge density, (b) HOMO, (c) HOMO–1, (d) HOMO–2, (e) HOMO–3 and (f) HOMO–4 : Black spheres indicate the Al atoms and the white spheres indicate the Li atoms.

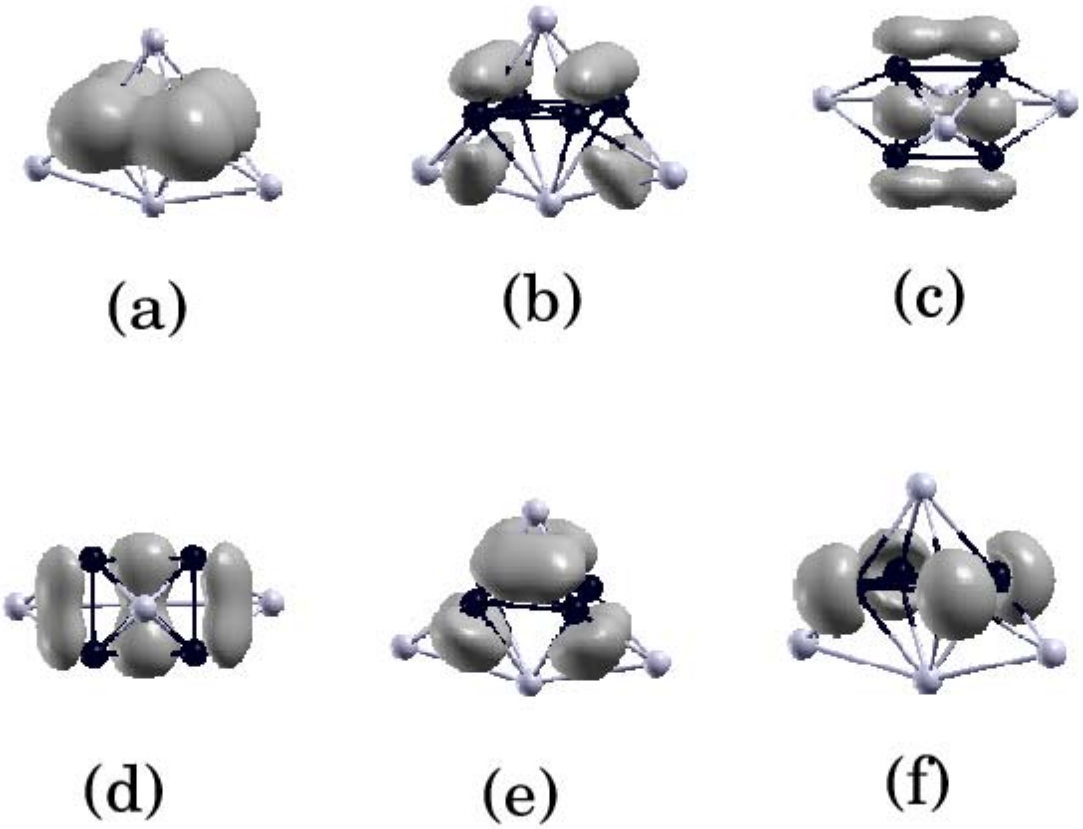

Fig. 4.3: Charge density, HOMO isodensities of Al_4Na_4. (a) Charge density, (b) HOMO, (c) HOMO–1, (d) HOMO–2, (e) HOMO–3 and (f) HOMO–4 : Black spheres indicate the Al atoms and the white spheres indicate the Na atoms.

Fig. 4.2 shows the isodensities of electron density and various HOMOs of Al_4Li_4 cluster. The charge density of Al_4Li_4 cluster shows that the electron density is completely localized on the Al_4 unit. This justifies the charge trasnfer from the Li atoms to the more electronegative Al_4 unit. The HOMO isodensity of Al_4Li_4 system shows localized π bonds along the short Al-Al bonds (Fig. 4.2(b)). These localized bonds are formed due to the 4 electrons donated by the alkali atoms to the p_z orbital of the four Al atoms. Thus, satisfying the criteria of anti–aromaticity of 4 π–electrons with localized π bonds. The HOMO–1 (Fig. 4.2(c)) shows a trans-annular or intra-bridgehead bonding between the pair of Al–Al bonds having shorter bond lengths. This kind of trans-annular bonding has been shown in the $Ga_4H_2^{2-}$ compound. [140] It also shows a lone pair of electrons of π character. HOMO–2 shows a similar bonding picture as the HOMO–1. The only difference is that the trans-annular bonding is between the other two pair of Al-Al bonds. Interestingly, HOMO–3 shows a delocalized bonding between four Al atoms. HOMO–4 shows lone pair of electrons on the Al atoms.

The bonding analysis of Al_4Na_4 cluster shows a similar trend to Al_4Li_4 system. The charge density shows that the density is completely localized on the Al_4 unit (Fig. 4.3(a)), similar to the Al_4 unit of Al_4Li_4 cluster. The HOMO isodensity of Al_4Na_4 are shown in Fig. 4.3 clearly shows two localized bonds along the two Al atoms having shorter bond lengths (2.68) of the Al_4 unit in the Al_4Na_4 cluster. HOMO-1 (Fig. 4.3), is mainly a trans-annular bonding between the pair of bonds of Al–Al HOMO–2 (Fig. 4.3(d)) also shows a similar kind of trans-annular bonding between the pair of Al-Al bonds having higher bond lengths. HOMO-3 (Fig. 4.3(e)) also shows a trans- annular bonding, but it is seen between the orbitals of the pair of Al-Al bonds. HOMO-4 (Fig. 4.3(f)) shows a lone pair of electrons on the four Al atoms. The two localized bonds in the HOMO of the Al_4Na_4 cluster. We also see from Table 4.2 that the difference in the energy of the HOMO and the LUMO of the Al_4Na_4 ground state and the excited state is almost the same. Interestingly, the bonding nature in the $Al_4Na_3^-$ cluster (not shown) is similar to that in the Al_4Na_4 and Al_4Li_4 cluster.

Furthermore, for understanding the stability of Al_4^{4-} superatom, we have performed the geometry optimization of the Al_4^{4-} system (without the alkali atoms). The calculations show that the Al_4^{4-} system was highly unstable. We do agree with the fact that, like the instability of the Al_4^{2-} system discussed earlier, the instability in the Al_4^{4-} system is due to the Coulombic repulsion from the four negative charges on Al_4^{4-}. This indicates that the presence of the alkali (Li^+ and Na^+) cations in the Al_4Li_4, Al_4Na_4 and $Al_4Na_3^-$ clusters, are required to suppress the electron–electron interaction on the Al_4^{4-} unit and to stabilise the Al_4^{4-} species.

The preference of the rectangular geometry of Al_4 species in Al_4Li_4, Al_4Na_4 and $Al_4Na_3^-$ clusters, which is a singlet state, as discussed earlier, is due to the mixing of energetically close states (pseudo- Jahn-Teller or second-order Jahn-Teller effect). [141] This can also be explained by the fact that the distortion of the π electrons drives the molecule to a bond-alternated geometry where short and localized bonds are achieved.

4.3.3 Magnetic Properties: Ring Current

In the present section we discuss the magnetic properties of the metallo-anti-aromatic systems using the ring current maps.

As a result of conjugation in an aromatic and anti-aromatic systems, an external magnetic field induces a ring current in the aromatic/anti–aromatic molecules. This ring current leads to magnetic properties such as magnetic anisotropies and magnetic susceptibility exaltation. The induced dimagnetic ring current also defined as diatropicity and paramagnetic ring current (paratropicity) are associated to the aromaticity and anti-aromaticity of the organic molecule. Diatropicity and paratropicity of a molecule can be easily detected by proton NMR chemical shifts. Schleyer proposed that diamagnetic susceptibility exaltation is the only measurable property uniquely associated with aromaticity. [125] The concept of ring current has been and remains one of the useful test for characterizing the aromaticity and anti-aromaticity on the basis of magnetic properties. Fowler *et al.* have used the ipsocentric CTOCD-DZ approach to diagnose

the ring current effects in some chemical systems. [57] This method yields the first-order response of the current density to an external field, by taking a distributed origin such that the induced current density at any point is calculated with that point as origin. It has been used to give qualitative pictorial interpretations of currents in a wide variety of ring systems and it has the advantage that even with modest basis sets it leads to an essentially accurate map of the Hartree-Fock current density. More importantly this method allows the total current density to partition into molecular orbital contributions.

Very recently, Fowler *et al.*, calculated the ring current in the metallo–aromatic Al_4^{-2} and MAl_4^{-1} systems using CTOCD-DZ approach. [57] They showed that the delocalized magnetic current induced by a perpendicuar magnetic field is carried by σ electrons and not by π electrons. This was in contrast to the aromatic organic molecules, in which the current is carried by the π electrons. Moreover, Chen *et al.*, have have debated on the existence of metallo–anti–aromatci compounds on the basis of ring currents. [142] We have extended this work to study the ring current effect in the metallo–anti–aromatic Al_4Li_4 and $Al_4Li_3^-$ compound. We have also compared them with the metallo-aromatic compounds.

The maps of total induced current density (Figs. 4.4 and 4.5) for these two species have appearances that vary strongly with distance between the plotting and Al_4 planes. In the Al_4 plane, both systems exhibit a strong diatropic σ current similar to that found for their 2π homologues; at 1 *a0* above the Al_4 plane, the total current is of mixed character, with competing diatropic and paratropic subpatterns; at 2 *a0* above the Al_4 plane, the current in $Li_3Al_4^-$ is purely paratropic. The source of the mixed nature of the current is not far to seek: the diatro- pic component arises as usual from the two high lying σ orbitals that approximate b1g + b2g orbitals of Al_4^{2-}, and the paratropic component is a two-electron contribution from the π or π-like HOMO in each (Fig. 4.5). The explanation of the opposed senses of σ and π currents is also clear on the orbital model. Diatropicity of the σ orbitals arises from translationally allowed σ–σ^* excitations. Paratropicity of the π HOMO arises from the rotationally allowed

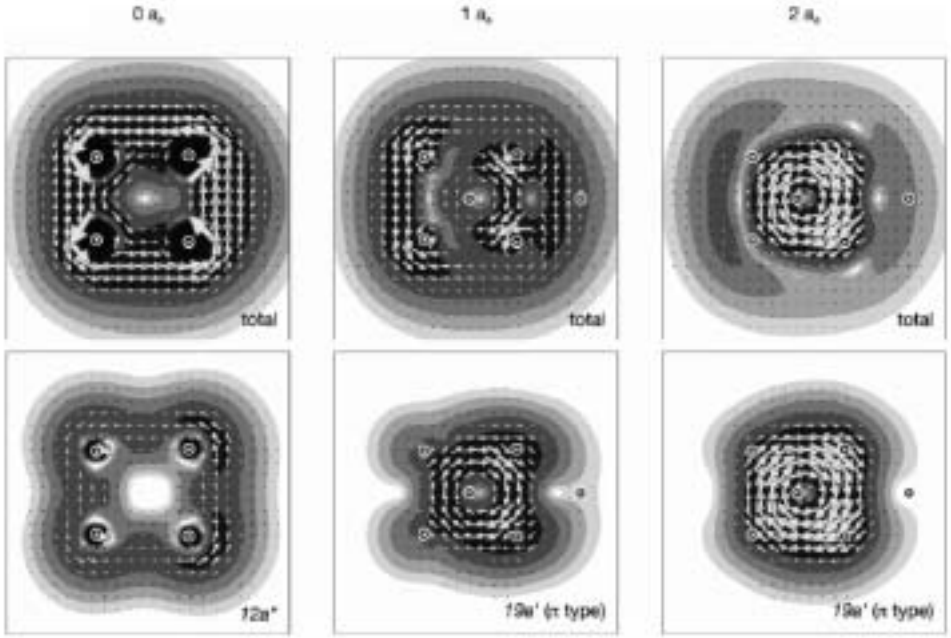

Fig. 4.4: The total induced current density, and the orbital contributions to the current density for Li_3Al_4 C_s , plotted at different heights above the Al_4 square.

π–π^* transition across the Jahn–Teller split pair of orbitals of unit angular momentum that are found for all unsaturated four-atom cycles. In the cases of $Al_4Li_3^-$ and Al_4Li_4 , the active π orbital is the HOMO. The orbital model predicts that such paratropic currents should be strong, as in a first-order picture they arise from exactly matched orbitals that are interconverted by a rotation and separated by a small energy gap.

The question of aromaticity/anti–aromaticity is complicated for these species by the cancellation of currents. The current in $Al_4Li_3^-$ is diatropic in the plane but paratropic out of the plane. A description of four-electron σ-diatropic/two-electron π-paratropic seems appropriate. Note that only two of the four π electrons (those in the π-like $19a0$) are active in the anti-aromatic paratropic current.

Al_4Li_4 is a doubtful case, in that the current is initially diatropic in–plane and remains mixed out-of-plane. Although it has the same 4π electron count as the anionic $Al_4Li_3^-$, the neutral species exhibits a more localised paratropic current. The net di-

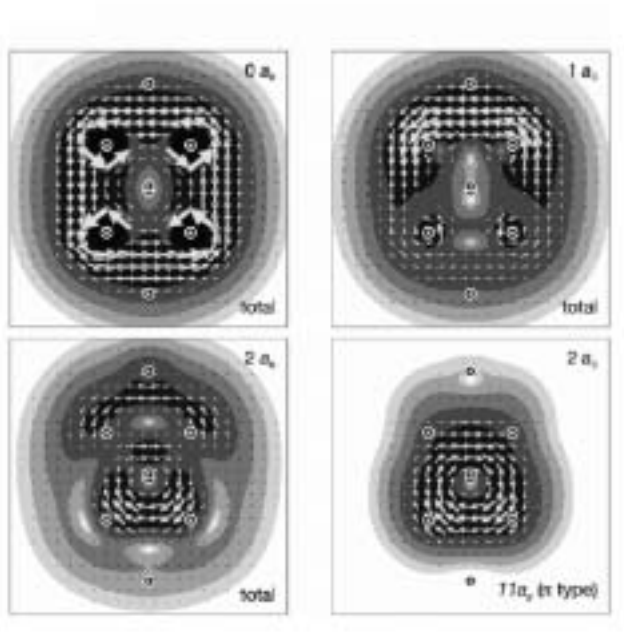

Fig. 4.5: The total induced current density, and the orbital contributions to the current density for Li_4Al_4 C_{2h}, plotted at different heights above the Al_4 square.

atropicity or paratropicity of the induced current depends on the position of the test probe used to measure it.

4.4 Conclusion and Scope

The present investigation reveals that the Al_4 unit in the Al_4Li_4 Al_4Na_4 $Al_4Na_3^-$ satisfies the basic criteria of anti-aromaticity such as the planarity, 4n π electron rule and bond alternation and were considered to be metallo-anti-aromatic compounds. Interestingly, Kuznetsov *et al* used the photoelectron spectroscopy to synthesize the $Al_4Li_3^-$ metal cluster and theoretically proved that it also has similar characteristics of the Al_4Li_4 cluster. [143]. This confirmed the theoretical results discussed about the Al_4Li_4 cluster.

However, the magnetic properties are not in the favor of anti–aromaticity in the Al_4Li_4 cluster. Moreover, the magnetic properties show a σ diamagnetic ring current dominating over the π paramagnetic ring current, resulting into a sigma aromaticity

rather than pi anti-aromaticity. Hence, it is clear that simple electron counting can be misleading as a method of assignment of aromaticity and antiaromaticity. However, more work is needed to claim the aromaticity and anti-aromaticity in metal clusters. This would motivate the experimentalists to understand the chemical properties such as stability, reactivity, and magnetic properties and to compare them with the aromatic and anti-aromatic organic compounds.

Nevertheless, the concept of aromaticity and anti-aromaticity in metal clusters will lead to the exploration of new materials and understanding of their electronic and bonding properties.

Chapter 5

A Periodic Density Functional Study of Sn Substituted Beta Zeolite

Abstract:

The structural, electronic and the bonding properties of the Sn–BEA are investigated using the periodic density functional approach. Each of the 9 different T–sites in the BEA were substituted by the Sn atom and all the 9 geometries were completely optimized using the plane wave basis set in conjunction with the ultra-soft pseudopotential. On the basis of the structural and the electronic properties, it has been demonstrated that the substitution of the Sn atom in the BEA framework is an endothermic process and hence the incorporation of the Sn in the BEA is limited. The LUMO energies have been used to characterize the Lewis acidity of each T-site. On the basis of the relative cohesive energy and the LUMO energy, T2 site is shown to be the most favorable site for the substitution and for the oxidation reaction respectively, in the Sn–BEA framework.

5.1 Introduction

BEA was initially synthesized in 1967. [144] However, due to severe faulting and hence, being highly disordered structure, it showed strong diffuse scattering in diffraction pattern. This made it difficult to obtain its structure experimentally. In 1988 Newsam *et al.*, succeeded in solving the structure mainly with the help of electron microscopy. [145] This solved a longstanding problem in zeolite crystallography and made it possible for understanding the complicate structure of BEA. They showed that the structure of

BEA consisits of random inter–grown hybrid of two distinct polytypic series of layers *viz.* polymorph A and B, a third polytype was also predicted without any experimental evidence. Very recently, the third polytype C, was also proposed by Corma *et al.* [146] BEA has two mutually perpendicular straight channels each with a cross section of 0.76 x 0.64 nm along the a and b direction and a helical channel of 0.55 x 0.55 nm along the c-axis.

Due to high Si/Al ratio and large pore size (12-membered ring channel), BEA has attracted a great industrial interest in organic chemical conversions. [147]–[150] It has been successfully used for acid catalyzed reactions, [147] catalytic cracking,[149] aromatic and aliphatic alkylation[150]. The reason of BEA being highly catalytically active is due to presence of dual acidity, that is, along with Bronsted acidity it also displays Lewis acidity. [151] It has been shown that the acidity of BEA can be tuned by the incorporation of trivalent and tetravalent atoms (B, Al, V, Ti, Sn, Cr, Fe) into framework positions. [152] The isomorphous substitution creates various Bronsted and Lewis acid sites in BEA. It has been shown in the earlier studies that the Bronsted acid sites are present, both in the internal as well as on the external surface. [153] However, this is not true for the Lewis acid sites. They are predominantly present within the framework. Several experimental techniques such as IR, UV, NMR, etc., have been employed to characterize various active sites in BEA. [155] Interestingly, Valerio et al have correlated the ^{29}Si NMR with the Si–O–Si bond angles in the BEA. [156] They further showed that the 9 T sites in BEA belong to three categories, as follows; sites T7, T8 and T9 are not associated with any four-membered rings, T1 and T2 are associated with one four-membered ring and T3, T4, T5 and T6 are associated with two four-membered rings. In the last decade, it has been proved that the isomorphous substitution of Ti into the zeolite framework provides useful catalyst for the oxidation of organic compounds which is attributed to the strong Lewis acidity of Ti.[157] From the experiments it is well known that that the Ti T–atoms which act as Lewis acid are also the active sites and are located inside the BEA framework in a tetrahedral

coordinated position. [155] One of the major advantage of the Ti-BEA over TS-1 is its pore size which allows an easy access to larger reactant molecules. Sastre and Corma in a quantum chemical study showed that the Ti-BEA has higher lewis acidity than TS-1. van Bekkum *et al.*, have shown that the Ti-BEA acts as an active catalyst for MPV reduction of aldehydes and ketones and Oppenauer's oxidation of alchols. [153]

Recently, in some of the works, Sn-BEA was shown to have better catalytic activity than Ti-BEA. [158, 159] Sn was predicted, to be a stronger Lewis acidic site than the Ti, due to higher elctronegativity of Sn than Ti. Mal and Ramaswamy, for the first time, synthesized and characterized the Al–free–Sn BEA. [160] In their study, they proposed that the Sn in the Al–free–Sn BEA was in a tetrahedral coordination. Later, in a very inetersting work Corma et al, for the first time showed that the Sn-BEA acts as an efficient catalyst for the Baeyer-Villiger oxidation reaction in the presence of H_2O_2. [158] They further showed the probable reaction mechanism of the Baeyer–Villiger oxidation reaction, in which the carbonyl group of the ketone is initially activated followed by a reaction with the non-activated H_2O_2, unlike the Ti-BEA zeolite, where the H_2O_2 gets activated. This shows that the combined property of large pore dimension and high Lewis acidity of Sn–BEA makes it a highly active stereo-selective catalyst for many oxidation and reduction reactions. There has been a debate on the tetrahedral or octahedral coordination of Sn in Sn–BEA. [154, 155] However, it has been confirmed from the Sn^{119} MAS NMR that the coordination of Sn in Sn–BEA is tetrahedral rather than octahedral. [154, 159] The tetrahedral coordination of Sn was attributed to its location within the framework and not on the external surface in the form of SnO_2. It is known that the crystallographically inequivalent T–sites will have different activity and shape selectivity due to the differences in the topological environment around the T–sites. The nature and the formation of the active sites has not yet been resolved in the Sn–BEA. However, in isomorphically substituted zeolites such as Sn-BEA or Ti-BEA, where the concentration of the substituted atom is low in the framework, it becomes difficult to obtain the structural features of the local active sites using experimental

techniques. Hence, in the isomorphically substituted zeolites such as Sn–BEA and Ti–BEA, it is important to understand the nature of the active sites and to investigate their structures using theoretical models.

To acheive this task, various quantum mechanical methods have been implemented to study the structural and electronic properties of the active sites in zeolites. To make the calculations computationally cheaper, finite cluster models of an active site, cut out of the zeolite crystal have been modeled for theoretical investigation, where the dangling bonds of the cluster are saturated by hydrogen atoms. Sauer and coworkers have done extensive study on the cluster models of zeolites. [36, 90] The other advantage of using the cluster model is that it avoids artificial periodicity for systems with large Al and cation content. It is also a better model for representing the active sites on the surface. However, cluster models neglect the effect of long range interactions and some artificial states are introduced due to the atoms lying at the boundary of the truncated fragment. Periodic methods are the only way to overcome all these problems, which include the long range electrostatic interactions. Studies on the comparison of clusters versus the periodic calculations have been carried out in past. A comparative study of the structural and electronic properties of Ti-BEA and TS-1 has been carried out by Sastre and Corma. [161] On the basis of LUMO energies they characterized the acidity of these two zeolites and proved that Ti-BEA is more Lewis acidic than TS-1. Interestingly, Zicovich-Wilson and Dovesi showed that the substitution of Si atom by Ti atom in a zeolite such as SOD, CHA and alpha-quartz, is an endothermic process when evaluated with respect to pure silico–zeolite. [91] They also proved that the incorporation of Ti within the zeolite framework is thermodynamically less favored than the formation of extra–framework TiO_2 clusters. This explained the difficulty of synthesizing high Ti content zeolites. Moreover, there has been several studies on other zeolites using a periodic description. Recently, Rozanska *et al* have used a periodic approach to study the chemisorption of several organic molecules in zeolites. [162]

Since it has been shown by the experimentalist, the importance of Sn–BEA in

various oxidation and reduction reaction. It is necessary to have a deeper insight into the structural and electronic properties of the active sites in Sn–BEA. In the present work we carry out a periodic density functional calculation to investigate each of the active site, out of the 9 crystallographically defined T sites in Sn–BEA. We wish to discuss the structural change due to the substitution of Sn in BEA and its effect on the energetics. On the basis of the LUMO energies, we analyse the Lewis acidity of each site.

5.2 Computational Details

All the calculations presented in this paper have been performed using the VASP code. [101] The instantaneous electronic ground state is calculated by solving the Kohn–Sham equation based on DFT. PBC has been used to take care of the periodicity of the solid. The present method uses the plane wave basis set in conjunction with the ultra-soft Vanderbilt pseudopotentials. [97] Advantage of using this computationally efficient scheme is that it permits the use of Fast Fourier transform technique. The exchange correlation functional is expressed within the GGA with the PW91 functional. [103] The Brillouin zone sampling was restricted to the gamma point. Structural relaxation of the coordinates of the BEA and the Sn–BEA has been performed in two steps. Initially, the conjugate gradient method has been employed to optimize the structures during which the cell shape of the unit cell has been fully relaxed by keeping the volume fixed. This was done until the forces on the atoms were less than 0.1 eV/Å. In the next step the optimized structure obtained from the conjugate gradient was used as the starting geometry and was re-optimized using the quasi–Newton method (volume fixed), unless the forces on the atoms were less than 0.06 eV/Å. BEA has 9 inequivalent x-ray crystallographically defined T-sites. During the Sn–BEA unit cell optimization, all these 9 T-sites were substituted one by one by Sn atom such that only one Sn atom is present per unit cell i.e. Si/Sn=63/1. The unit cell was also optimized with two Sn atoms per unit cell as described above i.e. Si/Sn=62/2. In this optimization, the two Sn atoms

were substituted at the two T9 sites.

5.3 Structural Properties

The optimized structural parameters of Sn-BEA for all the 9 T-sites (T1 to T9) are given in Table. 5.1. As discussed in the introduction, BEA has 9 inequivalent X-ray crystallographically defined T-sites (Fig. 1). There are 192 atoms in the unit cell with 64 Si atoms and 128 O atoms. [81] The distribution of these 64 Si atoms are as follows; There are 8 Si atoms placed at the T1 to T6 and T8 positions, while 4 Si atoms are placed at the T7 and T9 positions. Only the average Sn–O, Sn–Si bond lengths and Sn–O–Si bond angles are presented. The optimized average, Si–O bond distance and the Si–O–Si bond angles of BEA are 1.612±0.002 Åand 149.2±1.5 deg respectively, which are in good agreement with the earlier studies. As expected, after the substitution of the Sn atom in the BEA the average Sn–O bond distance amounts to 1.91±0.002 Åand the bond angles range from 137 to 147 deg. As expected, this shows that, after replacing Si by Sn at the active sites in the BEA framework, the Sn–O bond distance increases by about 0.3 Åcompared to the Si–O bond distance and the Sn–O–Si bond angles decreases by about 2 to 10 deg compared to the Si–O–Si bond angles. Although there is a decrease in the bond angle of the Sn–O–Si, the Sn–Si distance is more than the Si–Si distance in BEA, which is due to the increase in the Sn–O distance.

It has been already confirmed by the experimental studies such as the ^{1}19Sn MAS NMR, that the Sn in the Sn–BEA is situated in the framework and in a tetrahedral co-ordination. [154] The O–Sn–O angles have also been calculated and it was seen that each of the angles significantly deviates from the tetrahedral value. These kind of O–T–O angle deviations from the tetrahedral values are also reported for the titanosilica zeolite models. However, the average of all the O–Sn–O bond angles is close to 109.5 deg. Unfortunately, there are no earlier theoretical studies on Sn-BEA to compare with the results presented in this work. The change in the bonding due to the distortion

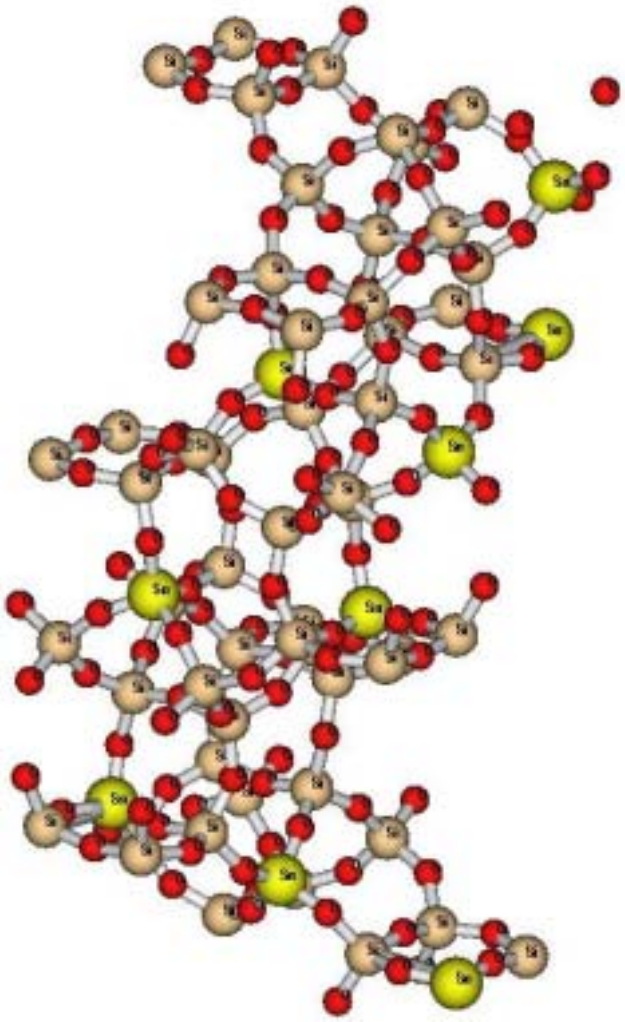

Fig. 5.1: Unit cell of BEA consisting of 192 atoms. The 9 active sites are shown by the Sn atoms (orange spheres). The other are the Si (brown spheres) and the O (red spheres) atoms.

Table 5.1: Average Bond lengths (Å) and bond angles of Sn-O and Sn-O-Si and the next nearest neighbor Sn-Si distance (Å) of the optimized structures for the 9 different T-sites in Sn-BEA.

Sn-Sites	Sn–O	Sn–O–Si	Sn–Si
T1	1.911	143.5	3.336
T2	1.909	144.2	3.341
T3	1.910	140.6	3.241
T4	1.917	136.0	3.281
T5	1.913	142.2	3.297
T6	1.910	141.2	3.297
T7	1.911	140.6	3.282
T8	1.908	140.0	3.282
T9	1.912	137.8	3.270

in the the local Sn–site of Sn–BEA is discussed in the next section. We observe from Table. 5.1, that the T2 and the T8 positions have the shortest Sn–O bond lengths of 1.909 and 1.908 Årespectively. However, the bond angle of the Sn–O–Si at the T2 position is the largest with 144.2 deg. The Sn–Si distance is the largest for T2 position, which can be attributed to the larger Sn–O–Si bond angle. The T4 position has the largest Sn-O bond distance of about 1.917 Åand a shortest Sn–O–Si bond angle of 136.0 deg. The change in the structural parameters of each T site can drastically affect the energetics of the zeolite. Hence, the stability and the reactivity of each site would be different.

5.4 Energetics

In this subsection we discuss the relative cohesive energies and hence the stabilities of all the 9 substituted Sn–sites. The cohesive energies for all the 9 T sites are given in Table. 5.2. The cohesive energy is the difference between the energy of the bulk (solid) at equilibrium and the energy of the constituent atoms in their ground state [Eqn. 5.1]. Hence, in the present study the cohesive energy can be taken as a measure

of the stability with respect to the decomposition. The cohesive energy is defined as

$$E_{coh} = E_{solid} - \sum_{i} E_i \tag{5.1}$$

where, i represents the individual atoms that constitute the solid. Higher the cohesive energy of the solid more stable it is i.e. more energy is required to decompose the solid. The cohesive energy of a fully siliceous BEA is -1527.9026 eV. From Table. 5.2, we see that the cohesive energy of Sn-BEA ranges between -1521.32 to -1521.68, which is about 6 eV lower than the BEA. This explains the fact that the substitution of Sn in the BEA framework decreases the cohesive energy. To confirm this, we performed an optimization of Sn-BEA with 2 Sn atoms in the unit cell and it was seen that the cohesive energy is decreased by about 6 eV (138 kcal/mol) compared to 1 Sn atom in the unit cell. It has been shown by the experiments that the turn-over number and selectivity of cyclohexanone in the Baeyer–Villiger reaction decreases with increase in the Sn content in the framework. Very interestingly, we can say that the decrease in the cohesive energy of Sn–BEA with increase in the Sn content, affects the turn-over number and selectivity of cyclohexanone in the Baeyer–Villiger oxidation reaction. [155] This kind of experimental evidence was provided for Ti content in TS–1. However, more discussion is needed to understand this issue. Among the 9 T–sites, the T2 site has the highest cohesive energy (Table. 5.2), and hence shows the most stable site for the substitution of Sn atom in Sn-BEA. This can also be attributed to the shorter Sn–O distance and longer Sn-O-Si bond angle. The next most stable site is the T8 site which has 1.5 kcal/mol less cohesive energy than the T2 site. One should note that, the difference in the cohesive energy of the T2 and the T8 site is very less. Hence, in a kinetic controlled synthesis one cannot predict the most probable site between the T2 and T8 sites. The most unstable site is the T9 site which has 8.23 kcal/mol less energy than the T2 site (Table. 5.2).

Table 5.2: Cohesive energies, HOMO, energies the LUMO energies and the HOMO-LUMO gap of the 9 different T-sites

Sn-Sites	Cohesive Energy (eV)	HOMO Energies (eV)	LUMO Energies (eV)	HOMO-LUMO Gap (eV)
T1	-1521.3871	-3.124	1.333	4.457
T2	-1521.6818	-3.125	1.366	4.491
T3	-1521.4687	-3.131	1.557	4.688
T4	-1521.5232	-3.117	1.421	4.538
T5	-1521.4052	-3.131	1.450	4.581
T6	-1521.4316	-3.120	1.426	4.546
T7	-1521.4571	-3.121	1.419	4.540
T8	-1521.6215	-3.117	1.497	4.614
T9	-1521.3239	-3.114	1.506	4.620

5.5 Electronic and Bonding Properties

It has been known that, lower the LUMO energy of a system, higher is its ability to gain electron density and hence has a higher Lewis acidity. Sastre and Corma, used the LUMO energies to characterize the Lewis acidity of the Ti sites in Ti–BEA and TS–1. [161] They showed that the average LUMO energy of the Ti sites in Ti-beta is lower than the TS–1 and hence Ti–beta was shown to have a higher Lewis acidity than TS-1. On this basis, in the present work we use the LUMO energies to discuss the Lewis acidity of all the 9 T sites in Sn-BEA. The HOMO energies, LUMO energies and the HOMO-LUMO gap of all the 9 T-sites are given in Table. 5.2. The results show that the T1 and the T2 sites in Sn-BEA have the lowest LUMO energies and should be the most probable Lewis acid sites. It is worth mentioning, that the reason for this would be their association to one four-membered ring as discussed by Valerio *et al.* [156] One should note that LUMO energies only decide the strength of the Lewis acidity of a particular T site and hence, favorable site for a oxidation reaction. It can also be said that the cohesive energy and the LUMO energy together decide the most favorable site for the substitution and reaction, respectively. Hence, on the account of high cohesive energy and low LUMO energy, the T2 site would be the most probable site for the substitution

for the Sn atom and for the oxidation reactioin in Sn-BEA, if the most stable site of the dehydrated zeolite is also the most favorable for Sn incorporation at the synthesis conditions. We can also see that the HOMO–LUMO gap of the T1 and T2 sites are the least. Hence, would be the most reactive sites

The LUMO energy calculated for BEA is 2.643 eV, which is about 1.2 to 1.3 eV higher than the Sn–BEA (Table. 5.2). This, shows that the substitution of Sn in BEA drastically increases the Lewis acidity. In this subsection we focus on the nature of bonding in the Sn–BEA and compare this to the same in BEA. In Fig. 5.2 and 5.2 we plot the LUMO isodensities of the Si–BEA and Sn–BEA respectivel at one third of the maximum isosurface value. We can clearly see that the The electron localization on the O atom attached to the central Si atom of the Si–BEA (shown in Fig. 5.2) is completely spherical. Interestingly, the LUMO isodensity (Fig. 5.3) of the Sn–BEA shows that the localization on the O atoms attached to the Sn atom is deformed towards the Sn atom. This is due to the polarization of the density of the O atoms by the Sn atom. This polarization of the electron density along the Sn–O bond can be attributed to the high Lewis acidity of the Sn atom.

5.6 Conclusion and Scope

In the present work we have discussed the structure, bonding and acidity of the Sn substituted BEA using a periodic approach, based on density functional theory. The results demonstrate that the incorporation of Sn in the BEA framework decreases the cohesive energy and is an endothermic process. Hence, it is clear that the incorporation of Sn in the BEA is limited. This would be the reason for the decrease in the turn-over number as the Sn content is increased in BEA during the Baeyer-Villiger oxidation reaction. The structural parameters, as expected, show longer Sn-O bond lengths compared to the Si-O bond lengths in BEA. Among the 9 T-sites, T2 site proves to be the most stable site for the substitution of Sn in the BEA framework, which is due to the

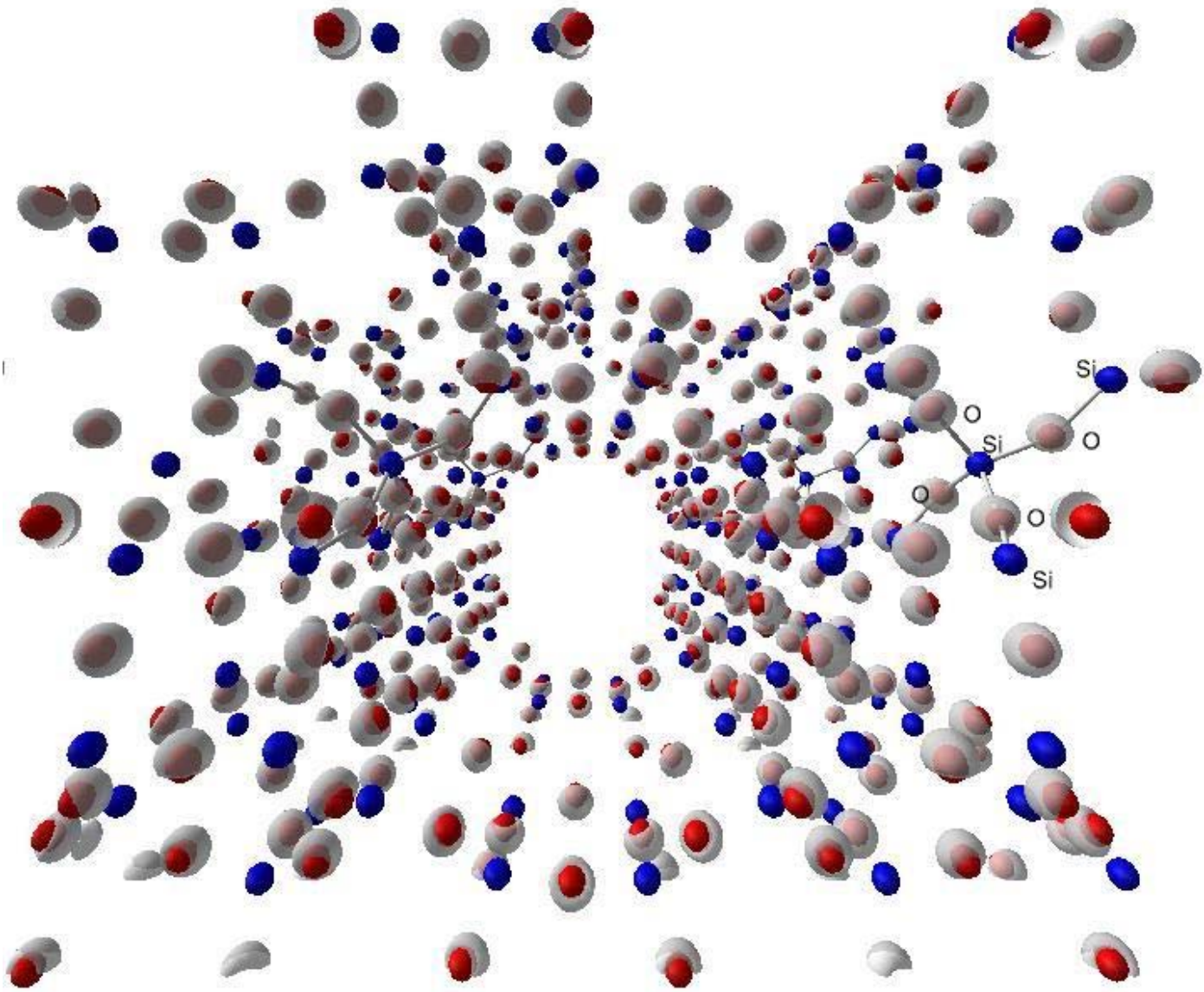

Fig. 5.2: LUMO isodensity of Si–BEA. Blue and red spheres indicate the Si and O atoms, respectively.

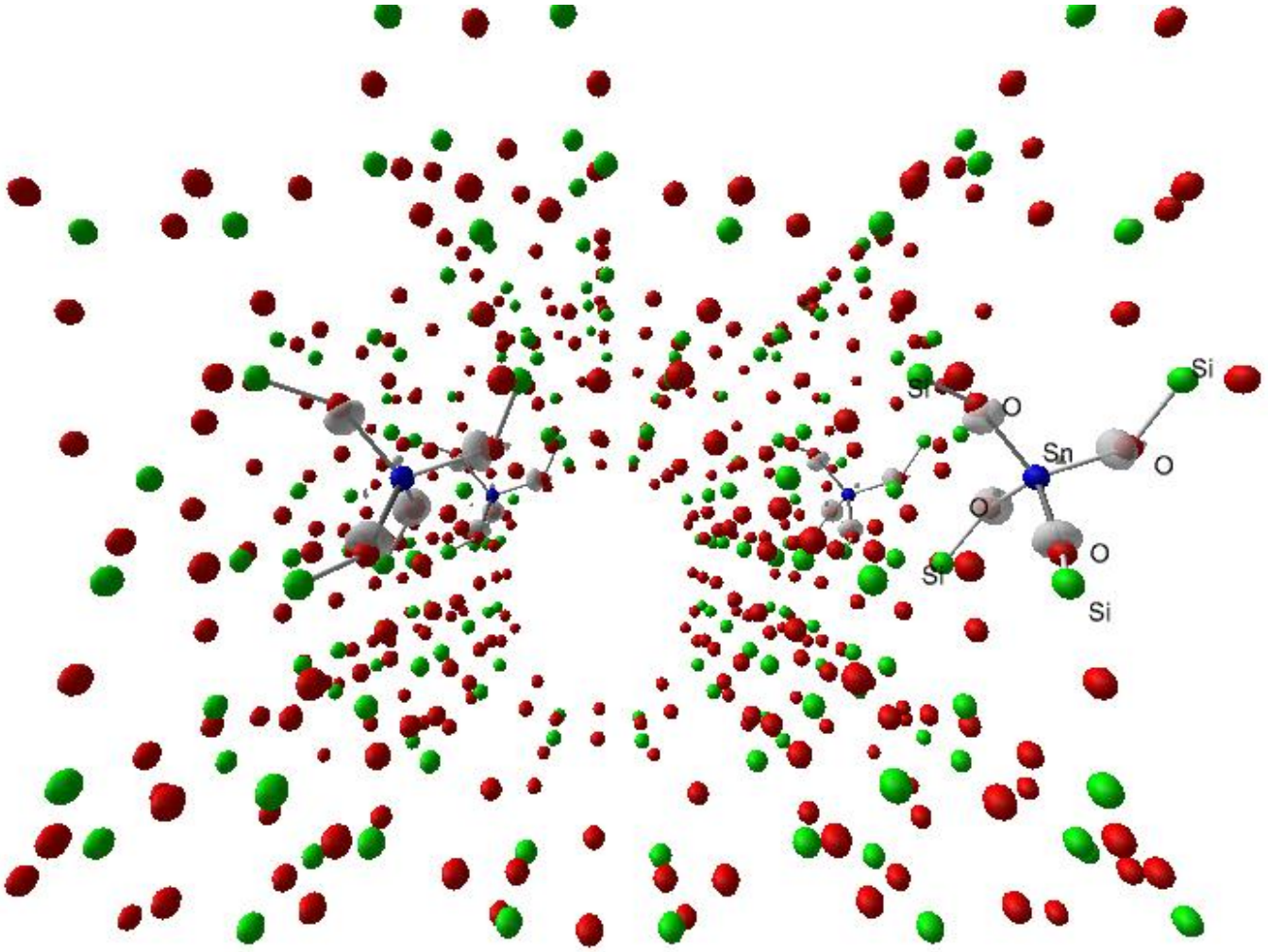

Fig. 5.3: LUMO isodensity of Sn–BEA. Blue sphere indicate the Sn atom, while red and green spheres indicate the Si and O atoms.

higher cohesive energy compared to the other T sites. Moreover, the T2 site is a higher Lewis acidic site compared to the other T-sites. The bonding analysis is necessary for a qualitative description of the electronegativity of Sn in Sn-BEA compared to Si-BEA. The analysis shows that the Sn atom in the Sn-BEA polarizes the orbital of O atoms, which can be attributed to its higher electronegativity and hence higher Lewis acidity, confirming the quantitative results.

The present theoretical study gives an insight into the structural and the electronic properties of the T sites in Sn-BEA which is otherwise difficult by using the experimental techniques. Further work on the effect of solvent molecules on the Sn-sites is still in progress.

Epilogue

A theory is something nobody believes,
except the person who made it.
An experiment is something everybody believes,
except the person who made it.
....Albert Einstein

In one of the classic articles titled, *There's plenty of room at the bottom*, Richard P. Feynman,[1] said that "But I am not afraid to consider the final question as to whether, ultimately—in the great future—we can arrange the atoms the way we want; the very atoms, all the way down ! What would happen if we could arrange the atoms one by one the way we want them." He further went on to say that "When we get to the very, very small world—say circuits of seven atoms—we have a lot of new things that would happen that represent completely new opportunities for design. Atoms on a small scale behave like nothing on a large scale, for they satisfy the laws of quantum mechanics. So, as we go down and fiddle around with the atoms down there, we are working with different laws, and we can expect to do different things. We can manufacture in different ways. We can use, not just circuits, but some system involving the quantized energy levels, or the interactions of quantized spins, etc."

The present work discusses some interesting behavior of metal clusters. The focus of the study is on the structural evolution of Li clusters when it is doped with Sn atom and how this change affects the electronic and the bonding properties of these systems. Unfortunately there is no experimental evidence to check this. However, experimental techniques would be useful to synthesize these kind of impurity doped systems and justify the theoretical results.

Further theoretical work on the formation and dissociation of the metal clusters would be interesting to give an insight into the reaction dynamics of the clusters. Hence,

[1]First published in February 1960 issue of Caltech's Engineering and Science, which owns the copyright.

it is interesting to look at the transition state and different paths of formation of clusters. Moreover, it is intriguing to understand whether the paths of the formation and dissociation of a particular cluster are same or different. This would be rather difficult to study through experimental techniques.

The work on the metallo–anti–aromaticity is quite interesting. In this work, for the first time we propose anti–aromaticity in Al–Li metal clusters and then extend the same, to prove the anti–aromaticty in Al–Na clusters. The proposition was completely based on the basic theoretical criterias. Surprisingly, the magnetic calculations did not support the anti–aromatic property in these systems. It is very appealing to compare other electronic properties such as reactivity, polarizability, optical properties etc., of organic aromatic or anti–aromatic systems with the metallo–aromatic and anti–aromatic systems. This work would inspire the experimentalist and the theoreticians to look at these new compounds which behave like organic systems. One of the technologically important applications of the Al—Li systems is that, their alloys are used as electron injecting devices (cathodes) in OLED's. So the next question would be, is it possible to use the Al–Li metal clusters as molecular cathodes in molecular electronics??

The last part of the thesis was to discuss the active sites for the Sn substitution in the Sn substituted BEA zeolite. This work followed the experimental work done on the Baeyer–Villiger oxidation reaction on the Sn–BEA zeolite. As it has been discussed in the thesis that, it is difficult to employ the experimental technique to understand the active sites in zeolite. The present work uses the DFT with PBC to discuss the active sites in a crystalline phase. This would help the experimentalists to understand the properties of the active sites of a zeolite at the atomic level. This work can be extended to study the role of the active sites in presence of the solvent such as water. There is also a need for a cluster calculation of the active site with the crystal phase. Moreover, the important step would be to search the transition state during the Baeyer–Villiger oxidation reaction at that site. It would also be important to compare the properties of active site of Sn–BEA with other substituted T atoms in BEA such as Ti–BEA.

At the end one would agree that

"there is* still *plenty of room at the bottom"...

References

[1] G. N. Lewis. *J. Am. Chem. Soc.* **38**, 762, (1916).

[2] W. Heitler, F. London. *Z. Physik.* **44**, 455, (1927).

[3] L. Pauling. *J. Am. Chem. Soc.* **53**, 1367, (1931).

[4] L. Pauling. *The Nature of the Chemical Bond*, (3rd edn) Oxford and publishing co. (1960).

[5] J. C. Slater. *Phys. Rev.* **36**, 57, (1930).

[6] C. A. Coulson. *Proc. R. Soc.* A **169**, 413, (1939)

[7] R. Mcweeny. *Coulson's Valence*, (3rd edn) Oxford University Press. (1979).

[8] I. N. Levine. *Quantum Chemistry*, (4th edn) Prentice–Hall of India, (1995).

[9] R. G. Parr, W. Yang. *Density Functional Theory of Atoms and Molecules*, Oxford University Press, (1989).

[10] M. Levy. *Phys. Rev.* A **26**, 1200, (1982).

[11] *Physics and Chemistry of Finite Systems: From Clusters to Crystals*. edited by P. Jena. S. N. Khanna, B. K. Rao. Kluwer Academic, Dorderecht, Netherlands, Vol. 1 and Vol. 2 (1992).

[12] *Clusters and Nanostructuredl Materials* edited by P. Jena, S. n. Behera. Nova Science Publishers. Inc. (1996).

[13] X. Li, H. Wu, X-B. Wang, L-S. Wang. *Phys. Rev. Lett.* **81**, 1909, (1998).

[14] *Clusters of Atoms and Molecules: Theory, Experiment, and Clusters of Atoms*. edited by H. Haberland, Springer–Verlag, Heidelberg, (1994).

[15] *Methods of Electronic Structure Calculations*. Edited by V. Kumar, O. K. Andersen, A. Mookerjee. World Scientific, Singapore. pg. 317, (1994).

[16] H. W. Kroto. *Science.* **242**, 1139, (1988); R. F. Curl, R. E. Smalley. *Science.* **242**, 1017, (1988).

[17] *Clusters and Fullerenes*. Edited by V. Kumar, T. P. martin, E. Tosatti, World Scientific (1993).

[18] S. Ijima. *Nature.* **359**, 707, (1992).

[19] A. F. Hebard, M. J. Rosseinsky, R. C. Haddon, D. W. Murphy, S. H. Glarum, T. T. M. Palstra, A. R. Kortan, S. M. Zahurak, A. V. Makhija. *Phys. Rev. Lett.* **66**, 2830, (1991).

[20] Y. Chai, T. Guo, C. Jin, R. E. Haufler, L. P. Chibante, J. Fure, L. Wang, J. M. Alford, R. E. Smalley. *J. Phys. Chem.* **95**, 7654, (1991).; K. Holczer, O. Klein, S. M. Huang, R. B. Kaner, K. J. Fu, R. L. Whetten, F. Diederich. *Science.* **252**, 1154, (1991).

[21] V. Bonačić-Koutecký, P. Fantucci, J. Koutecký. *Chem. Rev.* **91**, 1035, (1991).

[22] W. A. de Heer. *Rev. Mod. Phys.* **65**, 611, (1993).

[23] J. A. Alonso. *Chem. Rev.* **100**, 637, (2000).

[24] W. D. Knight, K. Clemenger, W. A. de Heer, W. A. Saunders. *Phys. Rev.* B **31**, 1539, (1985).

[25] V. Bonačić-Koutecký, I. Boustani, M. F. Guest, J. Koutecký. *J. Chem. Phys.* **89**, 4861, (1988).

[26] *Lithium–ion Batteries* Edited by Balbuena, Y. Wang, Imperial College Press. (2004)

[27] L. Hanley, J. Witten, S.L. Anderson. *J. Phys. Chem.* **92**, 5803, (1988) .

[28] H.-J. Zhai, L. -S. Wang, A. N. Alexandrova, A. I. Boldyrev. *J. Chem. Phys.* **208**, 233, (2002).; H.-J. Zhai, A. N. Alexandrova, K.A. Birch, A. I. Boldyrev, L. -S. Wang. *Angew. Chem. Int. Ed.* **42**, 6004, (2003).

[29] L. Hanley, S. L. Anderson. *J. Phys. Chem.* **91**, 5161, (1987).; L. Hanley, S. L. Anderson. *J. Chem. Phys.* **89**, 2848, (1988).

[30] W. Begemann, K. H. Meiwes-Broer, H. O. Lutz. *Phys. Rev. Lett.* **56**, 2248, (1986).

[31] M. Y. Chou, M. L. Cohen. *Phys. Lett.*A **113**, 420, (1986).

[32] D. M. Cox, D. J. Trevor, R. L. Wheten, A. Kaldor. *J. Phys. Chem.* **92**, 421, (1988).

[33] M. F. Jarrold, J. E. Bower. *J. Am. Chem. Soc.* **110**, 70, (1988).; M. F. Jarrold, J. E. Bower. *Chem. Phys. Lett.* **144**, 311, (1988).

[34] S. B. Zhang, M. L. Cohen, M. Y. Chou *Phys. Rev.*B **36**, 3455, (1987).; U. Röthlisberger, W. Andreoni. *Chem. Phys. Lett.* **198**, 478, (1992).; C. Yannouleas, P. Jena. S. N. Khanna. *Phys. Rev.* B **46**, 9751, (1992).; M. J. López, P. A. Marcos, J. A. Alonso. *J. Chem. Phys.* **104**, 1056, (1996).

[35] X. Li, A. E. Kuznetsov, H–F. Zhang, A. I. Boldyrev, L–S. Wang. *Science.* **291**, 859, (2001).

[36] J. Sauer. *Chem. Rev.* **89**, 199, (1989).

[37] R. M. Barrer. *Zeolites and Clav Minerals as Sorbents and Molecular Sieves*, Academic, London. (1978).

[38] D. W. Breck. *Zeolite Molecular Sieves. Structure, Chemistry, and Use*, wiley–Interscience, new. York (1974).

[39] J. R. Hill, C. M. Freeman, B. Delley. *J. Phys. Chem.* A **103**, 3772, (1999).

[40] C. Pisani, R. Dovesi, and C. Roetti. *Hartree-Fock Ab Initio Treatment of Crystalline Systems* Springer-Verlag, Berlin, (1988).; E. H. Teunissen, C. Roetti, C. Pisani, A. J. M. de Man, A. P. J. Jansen, R. Orlanso, R. A. van Santen. R. Dovesi. *Simul. Mater. Sci. Eng.* **2**, 921, (1994).

[41] L. Campana, A. Selloni, J. Weber, A. Pasquarello, I. Pápai, A. Goursot. *Chem. Phys. Lett.* **226**, 245, (1994). R. Shah, J. D. Gale, M. C. Payne. *J. Phys. Chem.* **100**, 11688, (1996).

[42] B. K. Rao, P. Jena. *Phys. Rev.* B **32**, 2058, (1985). P. Jena, B. K. Rao, R. M. Nieminen. *Solid State Commun.* **59**, 509, (1986).; P. Fantucci, J. Koutecký, G. Pacchioni. *J. Chem. Phys.* **88**, 325, (1988).; P. Blaise, F. Spiegelmann, D. Maynau, J. P. Malrieu. *Phys. Rev.* B **41**, 5566, (1990).

[43] C. Majumder, V. Kumar, H. Mizuseki, Y. Kawazoe. *Phys. Rev.* B **64**, 233405, (2001).; C. Majumder, V. Kumar, H. Mizuseki, and Y. Kawazoe *Chem. Phys. Lett.* **356**, 36, (2002).; K. Rademann, B. Kaiser, U. Even, F. Hensel. *Phys. rev. Lett.* **59**, 2319, (1987).

[44] F. L. King, M. M. Ross. *Chem. Phys. Lett.* **164**, 131, (1989).

[45] V. Kumar, Y. Kawazoe *Appl. Phys. Lett.* **83**, 2677, (2003).

[46] . C. Thomas, W.-J. Zheng, T. P. Lippa, S.-J. Xu, S. A. Lyapustina, and K. H. Bowen, Jr. *J. Chem. Phys.* **114**, 9895, (2001).

[47] J. Zhao, B. Liu, H. Zhai, R. Zhou, G. Ni, Z. Xu *Solid. State. Commun.* **122**, 543, (2002).

[48] V. Kumar, V. Sundarajan. *Phys. Rev.* B **57**, 4939, (1998).

[49] K. Joshi, D. G. Kanhere. *Phys. Rev.* A **65**, 043203, (2002).

[50] S. Hunsicker, R. O. Jones. *J. Chem. Phys.* **105**, 5048, (1996).; J.A. Alonso, L.M. Molina, M.J. Lopez, A. Rubio, M.J. Stott. *Chem. Phys. Lett.* **289**, 451, (1998).; B. Wang, M. J. Stott, J. A. Alonso. *Phys. Rev.* B **65**, 045410, (2002).

[51] S. Chacko, M. Deshpande, D. G. Kanhere. *Phys. Rev.* B **64**, 155409, (2003).

[52] W. Andreoni. *Phys. Rev.* B **45**, 4203, (1992).

[53] M. Heinebrodt, N. Malinowski, F. Tast, W. Branz, I. M. L. Billas, and T. P. Martin. *J. Chem. Phys.* **110**, 9915, (1999).

[54] R. T. Morrison, R. N. Boyd. *Organic Chemistry* Prentice-Hall of India, New Delhi, (1991).; P. J. Garrat *Aromaticity.* Wiley, new York (1986).

[55] E. Hückel. *Z. Phys.* **70**, 20, (1931).

[56] X-W. Li, W. T. Pennington, G. H. Robinson, *J. Am. Chem. Soc.* **117**, 7578, (1995).; Y. Xie, P. R. Schreiner, H. F. Schaefer, X-W. Li, G. H. Robinson, *J. Am. Chem. Soc.* **116**, 10635, (1996).

[57] P. W. Fowler, R. W. A. Havenith and E. Steiner. *Chem. Phys. Lett.* **342**, 85, (2001).; P. W. Fowler, R. W. A. Havenith and E. Steiner. *Chem. Phys. Lett.* **359**, 530, (2002).

[58] H. Haberland. pg. 205 from ref *Clusters of Atoms and Molecules: Theory, Experiment, and Clusters of Atoms.* edited by H. Haberland, Springer–Verlag, Heidelberg, (1994).

[59] P. Weis, T. Bierweiler, S. Glib, M. M. Kappes. *Chem. Phys. Lett.* **355**, 355, (2002).

[60] D. M. Mann, H. P. Broida. *J. Appl. phys.* **44**, 4950, (1973).

[61] L. Hanley, S. A. Ruatta, S. L. Anderson. *J. Chem. Phys.* **87**, 260, (1987). K. E. Schriver, J. L. Persson, E. C. Honea, R. L. Whetten. *Phys. Rev. Lett.* **64**, 2539, (1990).

[62] U. Ray, M. F. Jarrold, J. E. Bower. J. S. Kraus. *Chem. Phys. Lett.* **159**, 221, (1989).

[63] A. Fielicke, A. Kirilyuk, C. Ratsch, J. Behler, M. Scheffler, G. von Helden, G. Meijer. *Phys. Rev. Lett.* **93**, 023401, (2004).

[64] J. A. Harris, R. S. Kidwell, J. A. Northby. *Phys. rev. Lett.* **53**, 2390, (1984). O. Echt, K. Sattler, E. Recknagel. *Phys. Rev. Lett.* **47**, 1121, (1981).

[65] S. Kirkpatrick, C. D. Gelatt, M. P. Vecchi. *Science* **220**, 671, (1983).

[66] G. Galli, R. Martin, R. M. Car, M. Parrinello. *Science* **250**, 1547, (1990).

[67] P. Ballone, W. Andreoni, R. Car, M. Parrinello. *Phys. Rev. Lett.* **60**, 271, (1988). D. Hohl, R. O. Jones, R. Car, M. Parrinello. *Phys. rev. Lett.* **139**, 540, (1987).

[68] M. P. Allen, D. J. Tildesley. *Computer Simulation of Liquids.* Claredon Press, Oxford (1987).

[69] W. D. Knight, W. A. De Heer, W. A. Saunders, K. Clemenger, M. Y. Chou, M. L. Cohen. *Chem. Phys. Lett.* **134**, 1, (1987).

[70] W. Ekardt. *Phys. Rev.* B **29**, 1558, (1984).

[71] M. Brack. *Rev. Mod. Phys.* **65**, 677, (1993).

[72] I. Boustani, W. Pewestorf, P. Fantucci, V. Bonačić-Koutecký, J. Koutecký. *Phys. Rev.* B **B35**, 9437, (1987).

[73] P. Jena, S. N. Khanna, B. K. Rao, *Microclusters.* Edited by S. Sugano, Y. Nishina, S. Ohnishi. Springer–Verlag, Heidelberg, (1987).

[74] Ph. D. Thesis, Mrinalini Deshpande, Pune University, (2003).

[75] Ph. D. Thesis, Mrinalini Deshpande, Pune University, (2004).

[76] Ph. D. Thesis, Mrinalini Deshpande, Pune University, (2005).

[77] R. Car, M. Parrinello. *Phys. Rev. Lett.* **55**, 2471, (1985).

[78] W. M. Meier, D. H. Olson *Atlas of Zeolites Structure Types* Juris Druck: Zurich and Polycrystal Book Service: Pittsburgh, (1978).

[79] *Studies in Surface Science and Catalysis.* Edited by P. J. Grobet, W. J. Mortier, E. F. Vansant, G. Schulz–Ekloff. Amsterdam, **37**, (1988).

[80] *Introduction to Zeolite Science and Practice.* Edited by H. van Bekkum, E. M. Flanigen, P. A. Jacobs and J. C. Jansen. Elsevier, Amsterdam, **58**, (2001)

[81] R. Szostak. *Molecular Sieves.* Blackie Academic, (1998).

[82] *Modelling of Structure and Reactivity in Zeolites.* Edited by, C. R. A. Catlow, Academic Press. (1992).

[83] A. Carati, C. Flego, E. Previde Massara, R. Millini, L. Carluccio, W.O. Parker Jr, G. Bellussi. *Microporous and Mesoporous Materials.* **30**, 137, (1999).

[84] A. Corma, P. Esteve, A. Martinez. *J. Catal.* **161**, 11, (1996).

[85] X. Yang. *J. Phys. Chem.* **99**, 1276, (1995).

[86] M. Hunger, T. Horvath, G. Engelhardt, H. G. Karge. *Stud. Surf. Sci. Catal.* **756**, (1995).

[87] *Molecular Sieves; Structures and Structure Determination.* Edited by H. G. Karge, J. Weitkamp, Springer–Verlag, **2**, (1999).

[88] *Theoretical aspects of Heterogeneous Catalysis.* Edited by J. B. Moffat, Van Nostrand Reinhold, New York, (1990).

[89] Ph. D. Thesis, Sailaja Krishnamurty, Pune University, (1999).

[90] J. Sauer, P. Ugliengo, E. Garrone, V. R. Saunders. *Chem. Rev.*, **94**, 2095, (1994).

[91] C. M. Zicovich-Wilson, R. Dovesi. *J. Phys. Chem.* **102**, 1411, (1998).

[92] M. C. Payne, M. P. Teter, D. C. Allan, T. A. Arias, J. D. Joannopoulos. *Rev. Mod. Phys.* **64**, 1045, (1992).

[93] C. Kittel. *Solid State Physics.* John Wiley and Sons Inc. New. York. (1971).

[94] G. Galli, A. Pasquarello. pgs. 261 in *Computer Simulation in chemical Physics.* Edited by M. P. Allen, D. J. Tildesley, Kluwer Academic Publishers. (1993).

[95] D. R. Hamann, M. Schlueter, C. Chiang. *Phys. Rev.* B **43**, 1494, (1979).

[96] D. Vanderbilt. *Phys. Rev.* B **32**, 8412, (1985).

[97] D. Vanderbilt. *Phys. Rev.* B **41**, 7892, (1990).

[98] M. E. Tuckerman, P. J. Ungar, T. von Rosenvinge, M. L. Klein. *J. Phys. Chem.* **100**, 12878, (1996).

[99] D. Marx, J. Hütter. *Ab Initio Molecular Dynamics: Theory and Implementation* published in Modern Methods and Algorithms of Quantum Chemistry, Edited by J. Grotendorst, NIC series **3** (2000).

[100] D. Gibson, I. V. Ionova, E. A. Carter. *Chem. Phys. Lett.* **240**, 261, (1995).

[101] Vienna Ab initio Simulation Package (VASP). J. Hafner, G. Kresse. University of Vienna. (1999).

[102] A. D. Becke. *Phys. Rev.* A **38**, 3098, (1988). C. Lee, W. Yang, R. G. Parr. *Phys. Rev.* B **37**, 785, (1988).

[103] J. Perdew, K. Burke, Y. Wang. *Phys. Rev.* B **54**, 16533, (1996).

[104] A. D. Becke and K. E. Egecombe. *J. Chem. Phys.* **92**, 5397, (1990).

[105] A. Savin, R. Nesper, S. Wengert, and T. F. Fasssler. *Angew. Chem. Int. Ed. Engl.* **36**, 1809, (1997).

[106] A. Savin, O. Jaspen, J. Fald, K. O. Anderson, H. Preuss, and H. G. von Schnering. *Angew. Chem. Int. Ed. Engl.* **31**, 187, (1992).

[107] U. Haussermann, S. Wengert, P. Hofmann, A. Savin, O. Jespen, and R Nesper. *Angew. Chem. Int. Ed. Engl.* **33**, 2069, (1994).

[108] F. Fuster, A. Sevin, B. Silvi. *J. Phys. Chem.* A **104**, 852, (2000).

[109] T. A. Keith, R. F. W. Bader. *Chem. Phys. Lett.* **210**, 223, (1993).

[110] S. Yang, M. B. Knickelbein. *J. Chem. Phys.* **93**, 1533, (1990).

[111] I. Boustani, J. Koutecky. *J. Chem. Phys.* **88**, 5657, (1988).

[112] R. O. Jones, A. I. Lichtenstein, J. Hutter. *J. Chem. Phys.* **106**, 4566, (1997).

[113] C. Gatti, P. Fantucci, G. Pacchioni. *Theor. Chim. Acta* **72**, 433, (1987).

[114] R. Rousseau, D. Marx. *Chem. Eur. J.* **6**, 2982, (2000).

[115] J. Alper. *Science.* **296**, 1225, (2002).

[116] M. Hansen. *Constitution of Binary Alloys.* McGraw–Hill, New York, (1958).

[117] T. B. Massalski, H. Okamoto, P. R. Subramanian, L. Kacprzak, Binary Alloy Phase Diagrams ASM International, Materials Park, OH, (1990).

[118] B. Wang, M. J. Stott, J. A. Alonso. *Phys. Rev.* B **65**, 045410, (2002).

[119] B. K. Rao and P. Jena, *J. Chem. Phys.* **111**, 1890, (1999).

[120] B. K. Rao, P. Jena. *J. Chem. Phys.* **113**, 1508, (2000).

[121] Born–Oppenheimer Molecular Dynamics package, D. G. Kanhere, University of Pune. (1999)

[122] B. Bachelet, D. R. Hamann, M. Schluter. *Phys. Rev.* B **26**, 4199 (1982).

[123] L. Kleinmann, D. M. Bylander. *Phys. Rev. Lett.* **48**, 1425, (1982).

[124] S. Shaik, P. C. Hiberty, J. M. Lefour, G. Ohanessian. *J. Am. Chem. Soc.* **109**, 363, (1987).

[125] P. v. R. Schleyer, P. K. Freeman, H. Jiao, B. Goldfuss. *Angew. Chem., Int. Ed. Engl.* **34**, 337, (1995)

[126] A. R. Katritzky, P. Barczynski, G.Musumarra, D.Pisano, M. Szafran. *J. Am. Chem. Soc.* **111**, 7, (1989)

[127] R. Breslow. *Chem. Eng. News.* 90, (1965).

[128] R. Breslow. *Acc. Chem. Res.* **6**, 393, (1973).

[129] V. I. Minkin, M. N. Glukhovtsev, Y. B. Simkin *Aromaticity and Antiaromaticity.*; Wiley: New York, (1994).

[130] K. B. Wiberg. *Chem. Rev.* **101**, 1317, (2001).

[131] R. Willstätter, E. Waser. *Chem. Ber.* **44**, 3423, (1911).

[132] X. Li, H. F. Zhang, L. S. Wang, A. E. Kuznetsov, N. A. Cannon, A. I. Boldyrev. *Angew. Chem. Int. Ed.* **40**, 1867, (2001).; A. E. Kuznetsov, J. D. Corbett, L. S. Wang, A. I. Boldyrev. *Angew. Chem. Int. Ed.* **40**, 3369, (2001). A. E. Kuznetsov, A. I. Boldyrev, X. Li, L. S. Wang. *J. Am. Chem. Soc.* **123**, 8825, (2001).

[133] E. Nembach. *Prog. Mater. Sci.* **275**, 45, (2000).

[134] E. I. Haskal, A. Curioni, P. F. Seidler, W. Andreoni. *Appl. Phys. Lett.* **71**, 1151, (1997).

[135] A. Curioni, W. Andreoni. *J. Am. Chem. Soc.* **121**, 8216, (1999).

[136] M.F. Guest et al., GAM ESS -UK , a package of *ab initio* programs, (2000). With contributions from R.D. Amos *et al.*, and derived from the original Gamess code due to M. Dupuis, D. Spangler and J. Wendolowski, NRCC Software Catalog, vol. 1, Program no. QG01 (Gamess) 1980.

[137] P. Lazzeretti, R. Zanasi, SYSMO package, University of Modena, (1980).

[138] X. Li, H. Wu, X–B. Wang, L–S. Wang. *Phys. Rev. Lett* **81**, 1909, (1998).

[139] V. Kumar. *Phys. Rev.* B **60**, 2916, (1999).

[140] P. P. Power. *Struct. Bonding.* **103**, 57, (2002).

[141] H. W. de Boer, H. C. Longuet–Higgins. *Mol. Phys.* **5**, 387, (1962).

[142] Z. Chen, C. Corminboeuf, T. Heine, J. Bohmann, P. v. r. Schleyer. *J. Am. Chem. Soc.* **125**, 13930, (2003).

[143] A. E. Kuznetsov, A. K. Birch, A. I. Boldyrev, X. Li, H-J. Zhai, L-S. Wang *Science* **300**, 622, (2003).

[144] R. L Wadlinger, G. T. Kerr, E. J. Rosinski. U.S. Pat. 3 308 069, (1967).

[145] J. M. Newsam, M. M. J. Treacy, W. T. Koestsier, C. B. de Gruyter. *Proc. R. Soc. London.* **A420**, 375, (1988).

[146] A. Corma, M. T. Navarro, F. Rey, J. Rius, S. Valencia, *Angew. Chem. Int. Ed.* **40**, 2277, (2001).; A. Corma, M. T. Navarro, F. Rey, S. Valencia, *Chem. Commun.* 1486, (2001).

[147] G. Bellusi, G. Pazzuconi, C. Perego, G. Girotti, G. Terzoni. *J. Catal.* **157**, 227, (1995).

[148] J. A. Martens, J. Perez-Pariente, E. Sastre, A. Corma, P. A. Jacobs, *Appl. Catal.* **45**, 85, (1988).; P. Ratnasamy, R. N. Bhat, S.K. Pokhriyal, S. G. Hagde, R. Kumar, *J. Catal.* **119**, 65, (1989).

[149] L. Boretto, M. A. Camblor, A. Corma, J. Perez-Pariente, *J. Appl. Catal.* **82**, 37, (1992).

[150] A.J. Hoefnagel, H. van Bekkum, *Appl. Catal. A.* **97**, 87, (1993).

[151] I. Kiricsi, C. Flego, G. Pazzuconi, W. 0. Parker, Jr., R. Millini, C. Perego, G. Bellussi *J. Phys. Chem.* **98**, 4627, (1994).

[152] M. A. Camblor, A. Corma, J. Perez–Pariente. *Zeolites.* **13**, 82, (1993).

[153] J. C. Jansen, E. J. Creyghton, S. L. Njo, H. van Koningsveld, H. van Bekkum. *Catal. Today.* **38**, 205, (1997).

[154] A. Corma, M. E. Domine, S. Valencia. *J. Catal.* **215**, 294, (2003).

[155] M. Renz, T. Blasco, A. Corma, V. Formes, R. Jensen, L. Nemeth. *Chem. Eur. J.* **8**, 4708, (2002).

[156] G. Valerio, A. Goursot, R. Vetrivel, O. Malkina, V. Malkina, D. R. Salahub, *J. Am. Chem. Soc.* **120**, 11426, (1998).

[157] J. C. van der Waal, H. v. Bekkum. *J. Mol. Catal.* A **124**, 137, (1997).

[158] A. Corma, L.T. Nemeth, M. Renz, S. Valencia. *Nature* **412**, 423, (2001).

[159] A. Corma, M. E. Domine, L. T. Nemeth, S. Valencia. *J. Am. Chem. Soc.* **124**, 3194, (2002).

[160] N. K. Mal, A. V. Ramaswamy. *Chem. Commun.* 425, (1997).

[161] G. Sastre, A. Corma. *Chem. Phys. Lett.* **302**, 447, (1999).

[162] X. Rozanska, Th. Demuth, F. Hutschka, J. Hafner, R. A. van Santen, *J. Phys. Chem.* B **106**, 3248, (2002).

List of Publications

1. *Inter-cluster reactivity of Metallo-aromatic and anti-aromatic Compounds and Their Applications in Molecular Electronics: A Theoretical Investigation*,
   S. Shetty, R. Kar, S. Pal and D. G. Kanhere.
   J. Am. Chem. Soc. *submitted*

2. *Structural, electronic and bonding properties of zeolite Sn-Beta: A periodic density functional theory study*
   S. Shetty, S. Pal, D. G. Kanhere, A. Goursot
   Chem. Eur. J. *In press.*

3. *A quantitative and a qualitative study of the resonance assisted double proton transfer in formic acid dimer*,
   S. Shetty, S. Pal, D. G. Kanhere and A. Goursot
   I. J. Chem. A *In press.*

4. *Metallo–antiaromatic Al_4Na_4 and $Al_4Na_3^-$ compounds: A theoretical investigation*,
   S. Shetty, S. Pal and D. G. Kanhere
   J. Phys. Chem. A **108**, 628, (2004).

5. *Aromaticity and antiaromaticity of Li_xAl_4 clusters: Ring current patterns versus electron counting*,
   R. W. A. Havenith, P. W. Fowler, E. Steiner, **S. Shetty**, D. G. Kanhere and S. Pal
   Phys. Chem. Chem. Phys. **6**, 285, (2004).

6. *A study of electronic and bonding properties of Sn doped Li_n clusters and aluminum based binary clusters through electron localization function*,
   S. Shetty, S. Pal and D. G. Kanhere.
   J. Chem. Phys. **118**, 7288, (2003).